AN EXPERIMENTAL STUDY ON ENHANCEMENT OF HEAT TRANSFER IN A SOLAR AIR HEATER COLLECTOR BY USING POROUS MEDIUM

A Thesis Submitted to
the Graduate School of Engineering and Sciences of
İzmir Institute of Technology
in Partial Fulfillment of the Requirements for the Degree of

MASTER OF SCIENCE

in Energy Engineering

by
Gizem MARABA

October 2012
İZMİR

We approve the thesis of **Gizem MARABA**

Examining Committee Members:

_____

Prof. Dr. M. Barış ÖZERDEM
Department of Energy Engineering Systems
Bahçeşehir University

_____

Assoc. Prof. Dr. Serhan KÜÇÜKA
Department of Mechanical Engineering, DEU

_____

Assist. Prof. Dr. Ünver ÖZKOL
Department of Mechanical Engineering, IZTECH

12 October 2012

_____ _____

Prof. Dr. M. Barış ÖZERDEM
Supervisor, Department of Energy Engineering Systems, BAU

Assoc. Prof. Dr. Moghtada MOBEDİ
Co-supervisor, Department of Mechanical Engineering, IZTECH

_____ _____

P**rof. Dr. Gülden GÖKÇEN AKKURT**
Head of the Department of Energy Engineering

Prof. Dr. R. Tuğrul SENGER
Dean of the Graduate School of Engineering and Sciences

ACKNOWLEDGEMENTS

I would like to thank to my advisors, Prof. Dr. M. Barış Özerdem and Assist. Prof. Dr. Moghtada Mobedi for their supervision, guidance and support during this study.

I would like to thank to Mechanical Engineer Ali Dönmez to his valuable recommendations, contributions and support during this study.

I would like to thank and indicate gratitude to Zeynep Elvan Yıldırım and Gamze Gediz İliş for their helps and supports.

Lastly, I would like to thank to my dear family for their endless encouragement and support during my master thesis study.

ABSTRACT

AN EXPERIMENTAL STUDY ON ENHANCEMENT OF HEAT TRANSFER IN A SOLAR AIR HEATER COLLECTOR BY USING POROUS MEDIUM

The aim of this thesis is to enhance the heat transfer of a solar air heater by using porous material. A comprehensive literature survey has been carried out to learn the previous researches. Depending on this literature survey, some design parameters were determined and a solar air heater was constructed to the Solar & Wind Energies Laboratory according to this parameters.

In order to obtain the optimum design parameters and maximum efficiency of solar air heater, several studies have been carried out including clear and porous material assisted channels. For this purpose different configurations and designs were investigated and tested. Temperature data along the collector, average velocity of air inside the channel, pressure drop due to the porous material, power that fan and electrical heater consumes were measured and tabulated regularly. Related graphs were drawn according to the experimental results. The effect of porous material on the heat transfer and collector efficiency was discussed based on these graphs.

ÖZET

GÖZENEKLİ ORTAM KULLANILARAK HAVA ISITICILI GÜNEŞ KOLLEKTÖRLERİNDE ISI GEÇİŞİNİN ARTTIRILMASI ÜZERİNE DENEYSEL BİR ÇALIŞMA

Bu tezin amacı bir güneşli hava ısıtıcısında gözenekli yapı kullanarak ısı transferinin arttırılmasıdır. Daha önceki araştırmaları öğrenmek için kapsamlı bir literatür taraması yapılmıştır. Bu literature taramasına dayanarak bazı tasarım parametreleri belirlenmiş ve bu parametrelere gore Güneş & Rüzgar Enerjileri Laboratuvarına bir Güneşli Hava Istıcısı kurulmuştur.

Güneşli hava ısıtıcısın, optimum tasarım parametrelerini ve maksimum verimini elde edebilmek için, içi boş ve içinde gözenekli yapı bulunan kanalların deneylerini içeren bir çok çalışma yapılmıştır. Bu amaç için değişik konfigürasyon ve tasarımlar incelenmiş ve test edilmiştir. Kollektör boyunca sıcaklık değişimi, kanal içindeki havanın ortalama hızı, yüzey sıcaklıklarının gözenekli yapıya gore değişimi, gözenekli yapıdan kaynaklanan basınç düşümü, fan ve elektrikli ısıtıcının harcadıgı güç değerleri düzenli olarak ölçülmüş ve tablolanmıştır. Deneysel sonuçlara göre ilgili grafikler çizilmiştir. Gözenekli yapının ısı transferine ve kollektör verimin olan etkisi bu grafikler üzerinden tartışılmıştır.

TABLE OF CONTENTS

APPENDICES

LIST OF FIGURES

Figure **Page**

CHAPTER 1

INTRODUCTION

As the population around the world and the demand for energy increases, the consumption of conventional fuels also increases. The limited sources of conventional fuels have directed researchers' attention to renewable energies in recent years. The total solar energy absorbed by the Earth's atmosphere, oceans and land masses is approximately 3,850,000 exajoules (EJ) per year (Smil, 2006). In 2002, this represented greater energy consumption in one hour than the world used in one year (Morton, 2006). The amount of solar energy reaching the surface of the planet is so vast that in one year it is about twice as much as will ever be obtained from all of the Earth's non-renewable resources of coal, oil, natural gas, and mined uranium combined (Hermann, 2006). This is a huge source of energy and many applications that use solar energy, which is an abundant, clean and safe source, have been investigated.

Solar technologies can be classified into two groups; passive and active heating. Passive solar techniques include designing spaces according to natural circulation, locating buildings with reference to the Sun or selecting high thermal conductive materials. On the other hand, active solar techniques include using solar panels, pumps or fans to convert solar energy into useful outputs.

Solar air heaters are devices that utilize solar radiation for a variety of purposes. These devices are simple and can be constructed inexpensively. Mainly, solar air heaters consist of a transparent cover, an absorber plate and insulation material. The air flow enters through the channel that is formed by the absorber plate and the transparent cover. Solar radiation absorbed by the absorber plate. The absorbed heat transferred to the air as it flows along the channel increases its temperature. This heated air can be used in several applications such as drying agricultural products, space heating and air conditioning, water heating and industrial process heating.

There are many advantages of solar air heater systems. Firstly, they are simple to maintain and design. After the set-up cost, a solar air heater system has no fuel expenditure. There is less leakage and corrosion when compared to the systems that use liquid. It is also an eco-friendly system which has zero greenhouse gas emissions.

The primary disadvantage of these systems is the low heat transfer coefficient compared to systems that use liquid as the working fluid. This is the result of low heat transfer coefficient between the absorber plate and the air. Low heat transfer coefficients lead to low thermal efficiency of solar air heaters. For many years researchers have studied the enhancement of heat transfer coefficients of solar air heaters. To increase the efficiency of such a system, various configurations and designs have been proposed.

The efficiency of solar air heaters can be affected by various parameters such as collector length, number of channels, depth of channels, type of absorber plate, number and material of glass covers, air inlet temperature and air velocity. All of these parameters and their effects on the efficiency of solar air heaters will be discussed below.

In this thesis, porous material was placed in a solar air heater which was constructed for this study and the effect of this material on the collector efficiency and heat transfer was investigated. A literature survey was conducted to specify the design parameters of solar air heaters and based on this survey a collector was designed specially in order to obtain maximum efficiency and minimum heat loss from the collector and its channels. Air passing through the channel was supplied by a radial fan.

In Chapter 2 of this thesis brief information is given about solar air heaters. A total of 45 published papers were reviewed for this study. The literature classifies solar air heaters into two main groups and each group classified into four subtitles depending on their design and flow configurations. The general designs parameters and the working principles for every design are explained in this chapter. The schematic figures of each type of solar air heater are also illustrated.

The studies conducted on solar air heaters were reviewed in literature and are presented in Chapter 3. The 45 papers reviewed were classified according to the groups explained in Chapter 2. Each paper was summarized with its conclusions under the related title. A table prepared for an easy comparison of research conclusions is also given in Chapter 3.

In Chapter 4, the experimental setup and its components are explained in detail. The components of the experimental setup and measurements devices with their working principles are presented in this chapter.

The experimental procedure and the procedure of heat transfer calculations of this study are given in Chapter 5. The methodology of experiments is explained step by

step. The data collected with this explained methodology during the experimental period. Based on this data, all the calculations are performed and graphs plotted such as;

- The velocity profile in 3D
- Change of temperature longitudinally and transversely inside the collector
- Change of air inlet and outlet temperature for each experiment.
- Change of absorber plate temperature according to the porous layer number.

With the help of this graphs, the effect of porous layers are discussed better.

Many problems occurred during the experimental period. Because of the problems which occurred during the experiments some changes were necessary on the constructed setup. The improved setup, the problems that have been faced are explained in Chapter 6.

Chapter 7 includes results and discussions for the experiments performed during the study. The effect of porous material identified in the experimental results is discussed. The plotted graphs are also discussed in this chapter.

In Chapter 8 the conclusions of the studies performed. The evaluations and comments are also given in this chapter.

CHAPTER 2

SOLAR AIR HEATERS

Solar air heaters are simple devices that utilize incident solar radiation to obtain clean energy for a wide usage. The solar air heater device intercepts solar radiation, converts this radiation to the heat in air and delivers the air for use.

The main components of a solar air heater is an absorber plate, one or more channels for the flowing air, insulation for the bottom and lateral sides of the solar collector and one or more transparent covers. The use of a blower is optional for the air supply. Detailed information is given below.

2.1. Types of Solar Air Heaters

Solar air heaters may be divided into two main categories. The first category is related to the air channel flow configuration. To increase the system efficiency various air channel flow configurations will be constructed. The various configurations may be expressed in four sub-titles under this category. The sub-categories are; single flow single pass, double flow single pass, single flow double pass and single flow recycled double pass

The second category is related to the air channel design. The air channel design affects the system efficiency significantly. For that reason different design configurations can be used in solar collectors. The second category can also be expressed in three sub-categories such as; flat plate, extended surface assisted, porous media assisted. All main and sub categories are explained below.

Other studies exist that cannot be explained under any of these categories. These studies are categorized as special designs.

2.1.1. Classification According to Air Channel Flow Configuration

The first category in solar air heater studies is “Classification according to air channel flow configuration”. This category is classified into four different configurations. Since air flow channel configuration is an important parameter that affects the efficiency and outlet temperature of the solar air heater, researchers studied many different kinds of air flow channel configurations. In this part of this thesis, the purpose and methods of achieving different air channel flow configurations are explained.

2.1.1.1. Single Flow Single Pass

Single flow single pass is the most common and simplest type of solar air heater. This type of solar air heater mainly consists of an air flow channel, a transparent cover, an absorber, and insulation material in the bottom of the absorber as shown in Figure 1. Ann absorber plate is placed at the bottom of the air flow channel, and the top of the channel is covered by a transparent sheet with one or more layers, such as glass. The absorber is made from a high conductive material such as aluminum with high solar absorptivity values. Generally, a black plate is used for a high rate of solar absorption and as a selective absorber plate. The air flow channel is insulated on the bottom and lateral sides to prevent heat loss to the surroundings. The insulation materials can be glass wool, rock wool or polyurethane. The solar radiation passes through the transparent cover and is absorbed by the absorber plate. The temperature of the absorber plate increases since its bottom is insulated. Heat is transferred from the heated absorber plate to the air flowing through the channel. In the single flow single pass solar collector, there is an inlet and outlet for the air to enter and leaved the channel directly. That is why this kind of solar air heater is named as “single flow single pass” in this study.

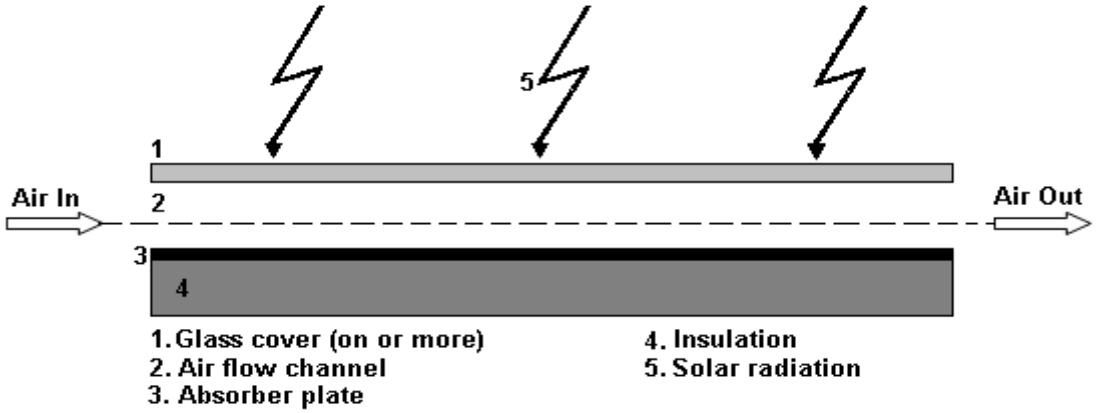

Figure 2.1. A schematic view of single flow single pass

2.1.1.2. Double Flow Single Pass

The double flow single pass solar air heater is very similar to the single flow single pass heater. The main difference between them is the number of air flow channels. In a double flow single pass solar air heater, there are two air channels as illustrated in Figure 2. The top channel consists of a solar absorber and a cover glass. The second channel which is located on the bottom of the first channel consists of the same absorber plate (on top) and insulated plate (on bottom). The air entering the collector is divided; half passes through the upper channel while the remainder flows through the bottom channel. For both channels, the airflow enters the channel and directly leaves it. That is why this kind of solar air hearer is called a "double flow single pass". Using a double flow single pass solar air heater increases the heat transfer area and the thermal performance of the system may be higher than a single flow single pass model for the same mass flow rate.

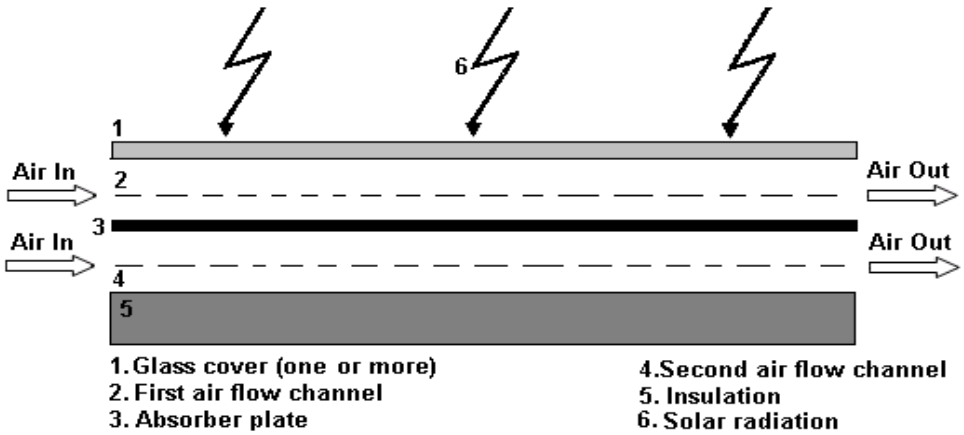

Figure 2.2. A schematic view of double flow single pass

2.1.1.3. Single Flow Double Pass

There are two overlapping air flow channels in a single flow double pass solar air heater. Air flows from the upper channel, changes direction at the channel end and enters the lower channel. It flows straight through the bottom channel. That is why this type of solar air heater is named a "single flow double pass". Two different constructions of a single flow double pass solar air heater are reported in literature. Figure 3(a) illustrates one of them. As can be seen, there are two overlapping air flow channels. These channels are separated from each other by a glass (or transparent sheet) and an absorber is placed at the bottom side of the lower channel. Air flows from the first and the second transparent sheet and is received by the absorber. The bottom side of the absorber is insulated. In the second design, the absorber plate is placed as a separator between the upper and lower channels as illustrated in Figure 4. The upper air flow channel is formed by the glass cover and the absorber plate where the lower air flow channel is located between the same absorber plate and the insulated lower plate.

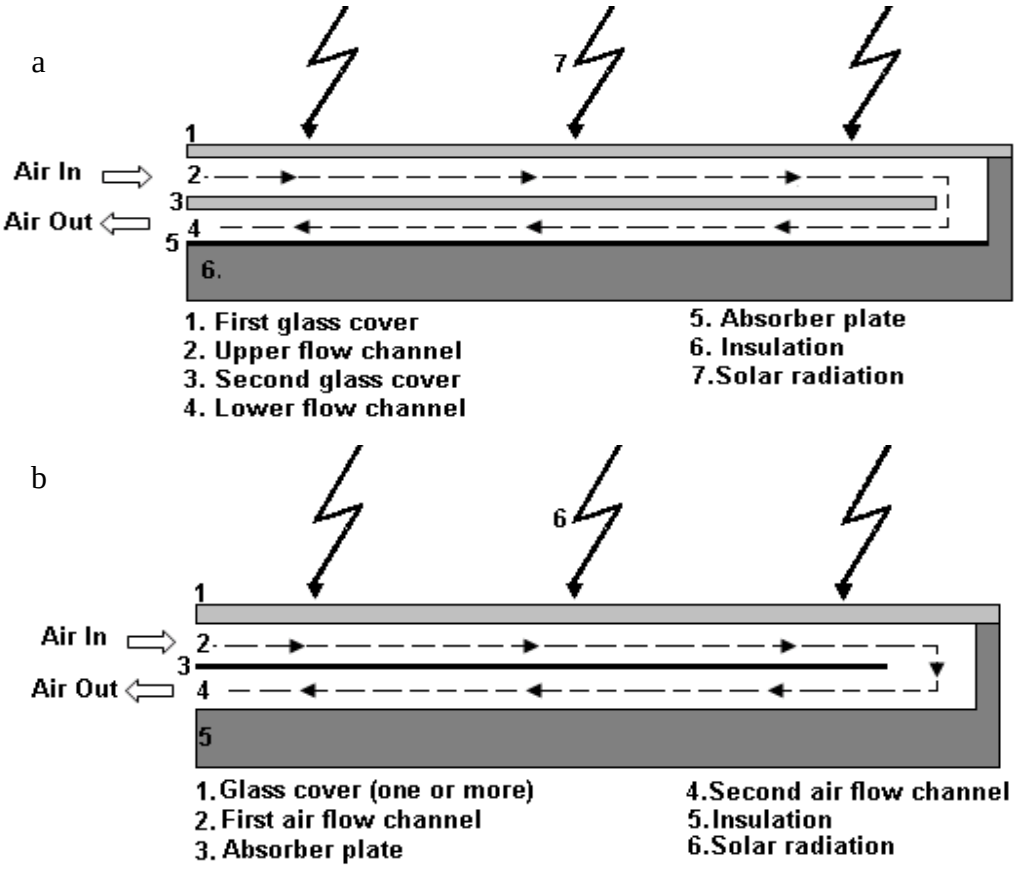

Figure 2.3. A schematic view of a single flow double pass with absorber plate, a) solar air heater with glass separator b) solar air heater with absorber separator

2.1.1.4. Single Flow Recycled Double Pass

Using recycled heated air in the design of a solar air heater may improve its efficiency and adjust the air outlet temperature. The partial circulation of heated air can provide the desired air temperature at the air flow exit if the outlet temperature is different than the desired temperature. As illustrated in Figure 4, the solar air heater consists of two channels. The upper channel is formed by the glass cover (on top) and the absorber plate (underneath). The walls of the other channel are insulated. A portion of heated air is transferred to the bottom channel and then it flows into the main air flow channel. There is a single inlet and outlet in the system and that is why this type of solar air heater is called a "Single flow recycled double pass solar air heater.

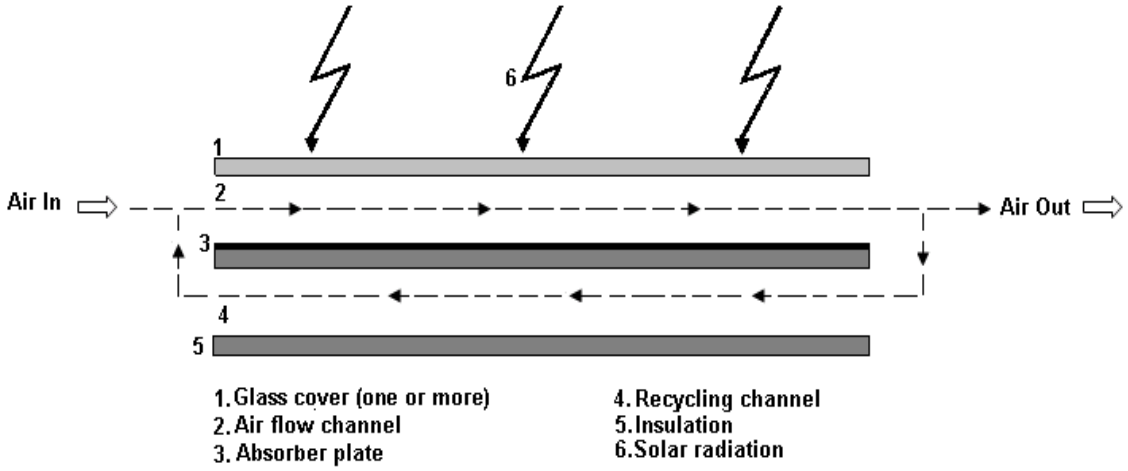

Figure 2.4. A schematic view of a single flow recycled double pass.

2.1.2. Classification According to Air Channel Design

The solar air heaters in the study can also be classified according to air channel design. The channel design of the solar air heater can be classified into four different configurations. By changing the air channel design, the efficiency of a solar air heater can be enhanced significantly. In this part of this review, different air channel designs are briefly explained.

2.1.2.1. Flat Plate

Flat plate type is the simplest form of solar air heater. This type of solar air heater includes one or more glass covers and an absorber plate (Figure 5). All sides of the solar air heater except the glass cover should be well insulated to prevent heat loss. Air can flow either over or under the absorber plate. Flat plate solar air heaters can be designed as single pass, double pass, double flow or recycled. The absorber plate is generally a smooth plate and it does not contain a fin, obstacle or roughness element. That is why this type of solar air heater is called a "Flat Air Channel". The construction of a Flat Air Channel solar air heater is simple; hence it has a low cost. Since no mechanism or method is used to enhance heat transfer in the channel, the efficiency of this kind of solar air heater is lower than other types.

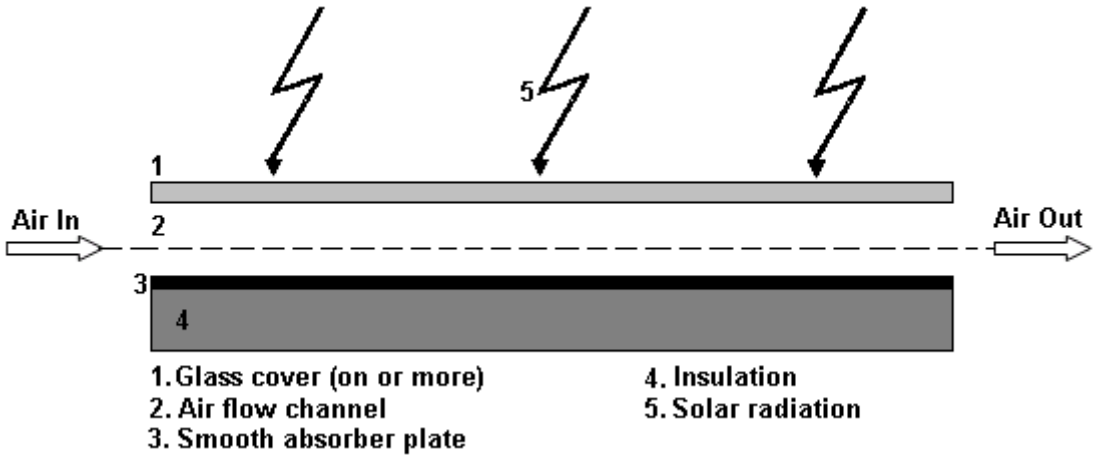

Figure 2.5. A schematic view of a flat plate solar air heater

2.1.2.2. Extended Surface Assisted

Several designs have investigated how to increase the low thermal efficiency of flat air channel solar air heaters. Since the type of absorber plate is one of the most important parameter that affects the thermal efficiency of solar air heaters, many absorber modifications were studied. The extension of the surface area of the absorber plate can be an efficient way to improve the performance of solar air heaters. Attaching fins, ribs, obstacles or any other roughness element (any element that causes roughness on the absorber plate) on the absorber plate could extend the surface area of the solar air

heater. A solar air heater assisted by an extended surface of air channel has a transparent cover, insulation material and a roughened absorber plate that absorbs the solar radiation. The roughness element or fins mounted on the absorber plate not only extend the area of absorption but also provides the mixing of air flowing in the channel and consequently increases the heat transfer coefficient. A solar air heater collector whose channel is assisted by an extended surface can be designed as a single pass, double pass, double flow or recycled model. Although the use of roughness elements or fins increases the surface area and heat transfer coefficient, the pressure drop through the channel will be increased at the same time. An increase in the pressure drop of the channel will result, as an increase in the required power of the fan or blower that supplies the air to the heater is also required. That is why a lot of research has involved designing the roughness element or fin geometries.

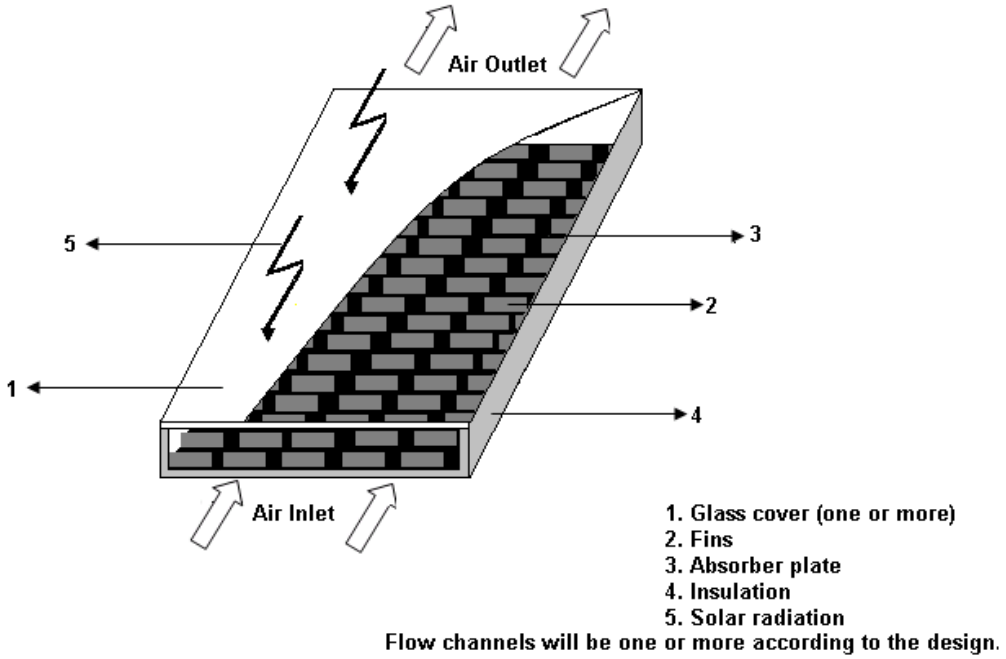

Figure 2.6. A schematic view of a fin assisted absorber plate

2.1.2.3. Porous Media Assisted

Assisting the air channel of a solar air heater with a porous medium might be a useful way to increase the air outlet temperature and thermal efficiency. The use of porous media in the flow channel of a solar air heater increases both the mixing of the air stream and the heat transfer area. These solar heaters consist of a transparent cover,

insulating material, an absorber plate and porous media (Figure 7). The porous media is inserted in the flow channel of the solar air heater. The air flows in the channel in contact with the porous media which is in contact with the absorber. Porous media assisted heaters can be designed as single pass, double pass or recycled but they are generally single flow double pass systems The porous media can be chosen from high conductive materials to accelerate heat transfer between the porous media and the air flows through the channel. The porosity of the porous media is a very important parameter for indicating pressure drop through the channel. Although the decrease of porosity increases the effective heat transfer coefficient, it also increases the pressure drop in the channel. That is why studies have been performed on the characteristics of porous media required for designing a system with high heat transfer rate but low pressure drop. There is no doubt that with the optimum porosity, thickness and position, the heat transfer between absorber and air flow in the channel can be enhanced considerably.

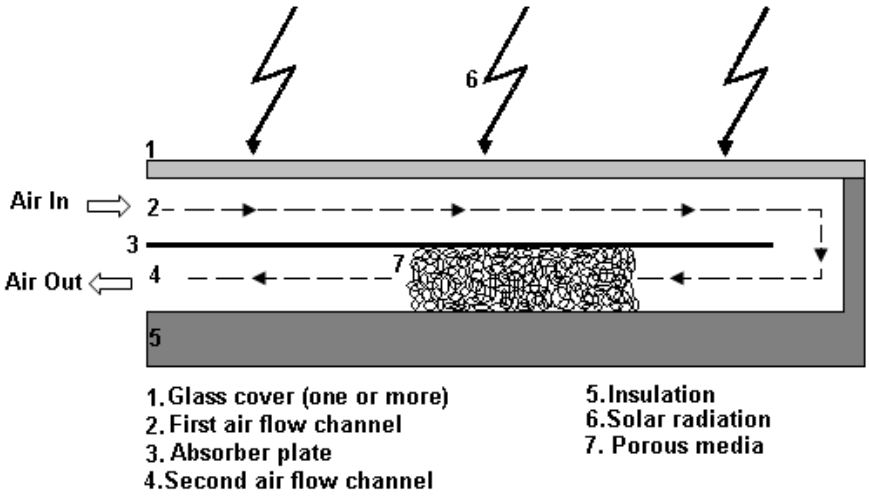

Figure 2.7. A schematic view of a porous assisted solar air heater

CHAPTER 3

LITERATURE SURVEY

A comprehensive literature survey on solar air heaters has been in accordance with the main categories and their classifications referred to in previous sections. A summary of the findings is presented in this chapter.

3.1. Studies According to Air channel Flow Configuration

3.1.1. Single Flow Single Pass Studies

Varshney et al. (1998) investigated the heat transfer and fluid characteristics of a solar air heater whose duct is packed with wire mesh screen matrices. The experiments were conducted using a wide range of geometrical parameters of wire mesh screen matrices such as wire diameter, pitch and number of layers (Fig. 3.1). The solar air heater collector dimensions were 2390 x 25 mm. Double glasses with a distance of 20 mm were used as glazing and the wire mesh packing was placed between the second glass cover and the back plate. In the study, the heat transfer was represented by employing Colburn-j factor. Generalized correlations were developed based on the data,. It was concluded that the heat transfer coefficient and friction factor were depending on wire mesh geometry such as wire diameter, pitch and number of layers of the matrix.

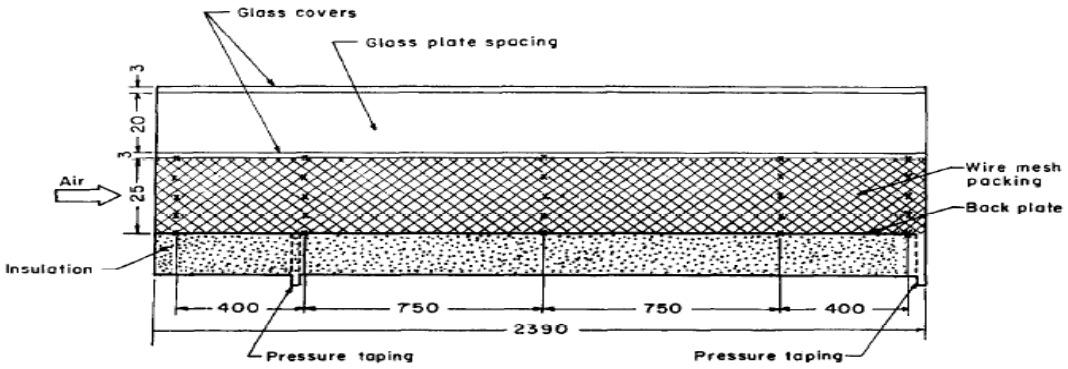

Figure 3.1. Details of packed bed collector
(Source: Varshney et al.1998)

Pakdaman et al. (2011) evaluated the performance of a natural convection solar air heater with a rectangular finned absorber plate. It aimed to achieve an empirical model which predicts various significant parameters for natural convection solar air heaters. The Nusselt number correlations for such finned devices were also obtained in the study. The exergy analysis and the conditions that give the maximum efficiency for the system were also determined. The collector frame dimensions were 2000 x 1000 x 150 mm (Figure 3.2). A black painted galvanized-iron plate was used as an absorber plate with a thickness of 1 mm. A total of 46 rectangular fins were attached to the absorber plate which was 20 mm apart from each other. The attached fins were 2000x10mm with a thickness of 1 mm. A single glass cover with a thickness of 4 mm was used as glazing. It was concluded that a longitudinal rectangular fin arrangement enhanced the heat transfer of solar air heaters. In this study the heat transfer area was increased by 66% whereas heat transfer was increased by 20% approximately.

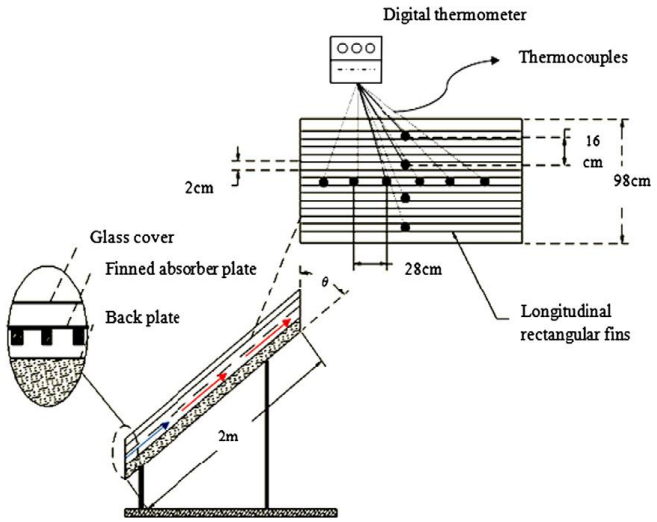

Figure 3.2. Experimental setup and location of thermocouples on the absorber plate.(Source: Pakdaman et al. 2011)

Karmare et al. (2009) experimentally investigated the effect of roughness of rib grits on the thermohydraulic performance of solar air heaters. The metal rib grits were placed on the absorber plate with a 60° angle of attack to the air flow direction. On the basis of thermohydraulic considerations, the optimum design and operating conditions were determined and an experimental setup was constructed (Fig. 3.3). The setup consisted of two identical collectors, each with dimensions of 1500 x 250 x 25 mm. Three different absorber plates with different roughness parameters and a smooth

absorber plate were tested (Table 1). The experimental data obtained from these four absorber plates under optimum operating conditions were compared. It was concluded that the thermal efficiency could be increased between a range of 10–35% by using metal rib roughness on the absorber plate in place of a smooth absorber plate. As the thermal efficiency was enhanced the power required for the blower increased due to increase in the friction factor. It was also found that the Reynolds number range must be specified to obtain better thermohydraulic performance and that this depended upon the insulation. To achieve optimum performance for a solar air heater, an empirical relation was developed which included the system and operating parameters.

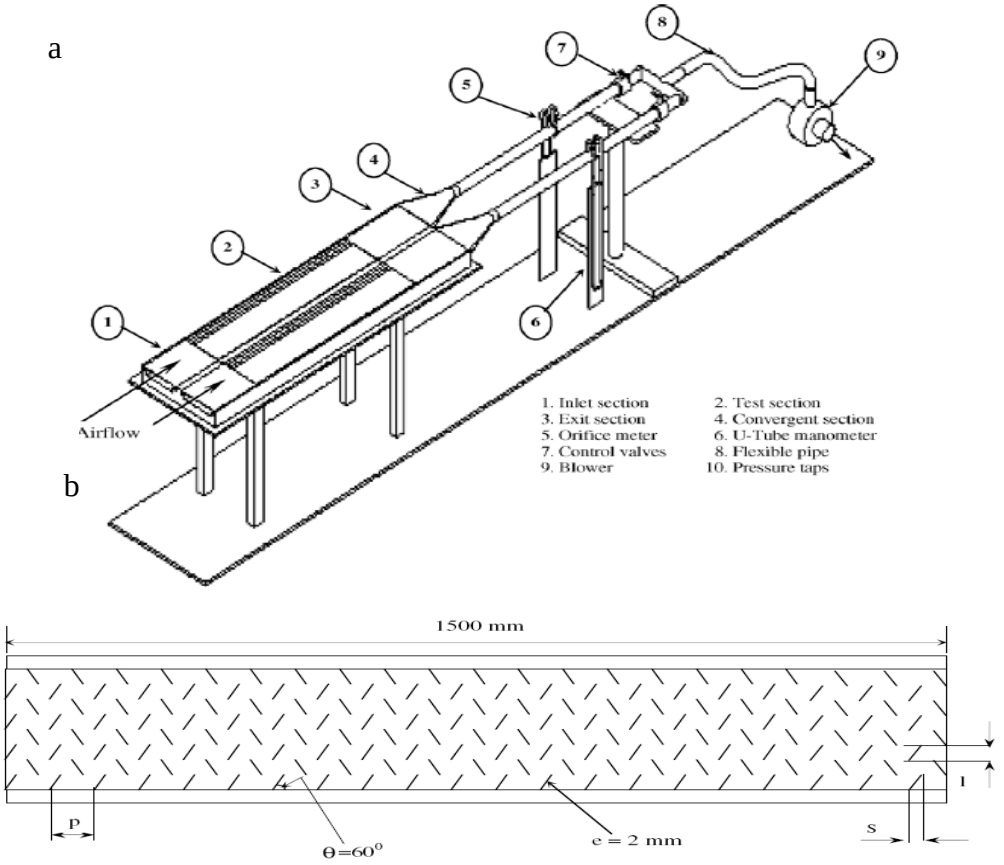

Figure 3.3. a.Schematic layout of the experimental setup, b.Layout of roughness surface.(Source : Karmare et al. 2009)

Moheseni-Languri et al. (2009) investigated the energy and exergy analysis of a solar air heater. A solar air heater was designed, manufactured and connected to a room to investigate the applicability and feasibility of such a system (Fig. 3.4). The absorber plate was made of carbon steel and painted black with dimensions of 1800 x 1000 x 4 mm. Single glazing was used with a thickness of 3 mm. A small fan with the power of

40 W was used to circulate the air through the collector and room. To protect the collector from the shadow of neighboring buildings, it was installed 2500 mm vertically above the ground. Two aluminum ducts with an insulation of 20 mm thick glass wool were used to connect the collector inlet and exit to the testing room. The testing room's dimensions were 4 x 3 x 3 m. In order to find the optimum mass flow rate which produces the maximum energy, the experimental data obtained by the measurements during winter were analyzed using energy and exergy analysis. This study concluded that the optimum mass flow rate which leads to the highest second law efficiency was 0.0011 kg/s.

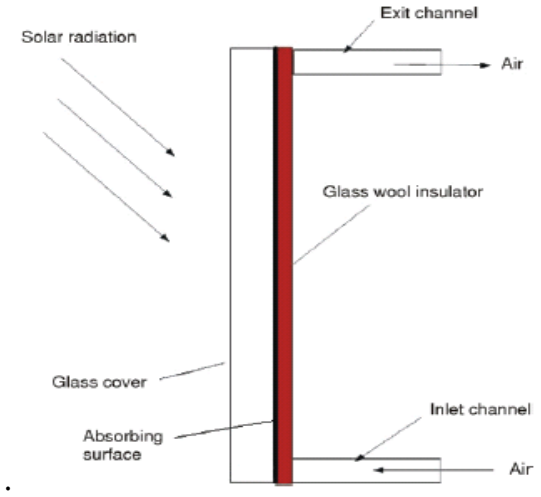

Figure 3.4. A schematic of the designed collector
(Source: Moheseni-Languri et al. 2009)

Moummi et al. (2004) theoretically and experimentally analyzed the energy of a solar air collector with rows of rectangular plate fins inserted perpendicular to the flow. The aim of the study was to improve the thermal performance of the solar air collector by generating turbulent flow between the absorber and the back wooden plate via obstacles. In order to achieve this goal, a solar collector 1.6 m in length and 0.8m in width was constructed (Fig 3.5). The transparent cover was alveolar polycarbonate sheets with 10 mm thickness and the gap between the cover and the absorber plate was 25 mm. Two types of absorber plates were used in the collector; black-painted aluminum sheets (nonselective absorber plate) and coopersun plates (selective absorber plate). The results achieved were compared with experimental results of a solar air collector without fins. It was concluded that the rectangular fins increased the temperature of the absorber plate and enhanced the heat transfer.

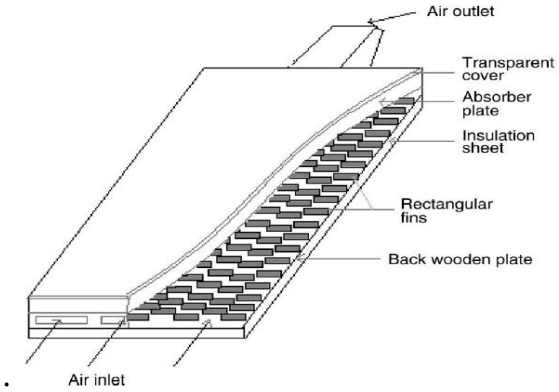

Figure 3.5. Schematic view of the collector with fins
(Source: Moummi et al. 2004)

Ozturk et al. (2004) experimentally investigated the thermal performance of a solar air heater with a packed flow channel. The Raschig rings made of black polyvinyl chloride (PVC). were used as the packing material. The heater was of 1900 x 900 mm in dimension. The absorber plate was an aluminum plate with black paint coating. Single glass of 4 mm thickness was used as glazing, and the distance between the absorber plate and glazing was 50 mm (Figure 3.6). The depth of the packed bed in the flow channel was 60mm. The Raschig rings type of packing was used to improve heat transfer from the plates to the airflow underneath the absorber plate. In addition to the experiments, the heaters energy and exergy analysis were performed to evaluate the efficiencies of the packed bed solar air heater. The ratio of the recovered energy delivered by the solar air heater to the total solar energy passing through the heater was defined as the energy efficiency. It was concluded that selecting, sizing and optimizing the components of solar air heating systems should be performed using exergy analysis for the highest possible efficiencies.

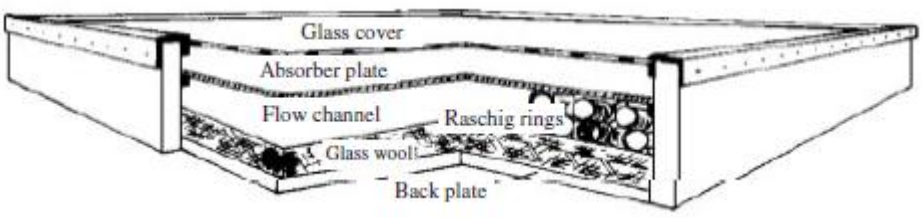

Figure 3.6. Section view of experimental the packed-bed solar air heaters.
(Source: Ozturk et al. 2004)

Peng et al. (2010) theoretically and experimentally analyzed the performance of a solar air heater with fins attached to the absorber plate both. They aimed to enhance

the thermal performance of the solar air heater with a cheap and accessible collector design that has a long durability. For this purpose an experimental setup was installed (Figure 3.7). In this study 25 pin-finned collectors and a flat plate clear collector were discussed. The pin-fins were 10, 20, 30, 40, 45 mm in length and 12, 16, 20, 24, 28 mm in width. 4 mm thick single glazing with dimensions of 1100 x 580 mm was used above the finned absorbers. The absorber plate used was black painted stainless steel. A mathematical model was developed to evaluate the performance of pin-finned collector in theory. Thus with theoretical calculations, the mathematical formulations of thermal efficiencies of a total of 26 collectors were obtained. It was concluded that, with 19 m3/h air flow rate, the pin-fin arrangement in a solar air collector could increase the heat transfer coefficient up to three times when compared with flat-plate collector.

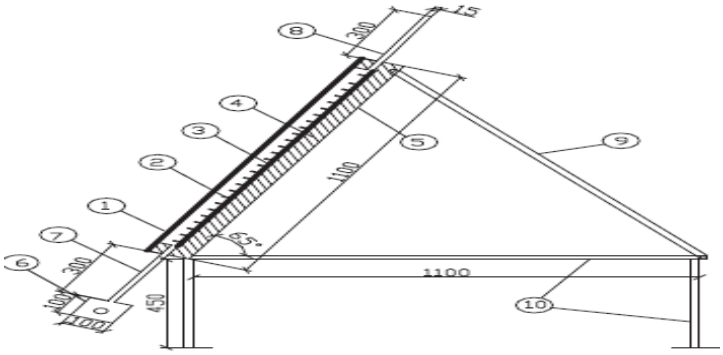

Figure 3.7. Configuration of pin-fin arrays solar air collector.
(Source: Peng et al. 2010)

Sahu et al. (2005) experimentally investigated the heat transfer coefficient of a solar air heater with 90° broken transverse ribs on the absorber plate. The study aimed to discuss the effect of various flow and roughness parameters on heat transfer characteristics for flow of air in rectangular ducts of different pitch. The experimental setup was constructed with a length of 1500 mm and an aspect ratio (aspect ratio, W/H, is the proportional relationship between the collector's width and length) of 8.0. The absorber plate was made of galvanized iron with 1.5 mm diameter wires in different pitch dimensions pasted over one side of the plate (Figure 3.8). For comparison of the results, four types of absorber plates were used; one smooth and three artificially roughened with roughness pitch of 10, 20 and 30mm. During the experiments, the roughened wall was heated while the other three walls were insulated. The pressure drop, Reynolds and Nusselt numbers, heat transfer coefficients and the efficiencies were

calculated based on the experimental results obtained. The comparison of the smooth and roughened three collectors revealed that the plate having a roughness pitch of 20 mm provided the highest efficiency of 83.5% and the roughened absorber plates increased the heat transfer coefficient 1.25 - 1.4 times under similar operating conditions. The maximum enhancement of heat transfer coefficient occurred at a pitch approximately 20 mm.

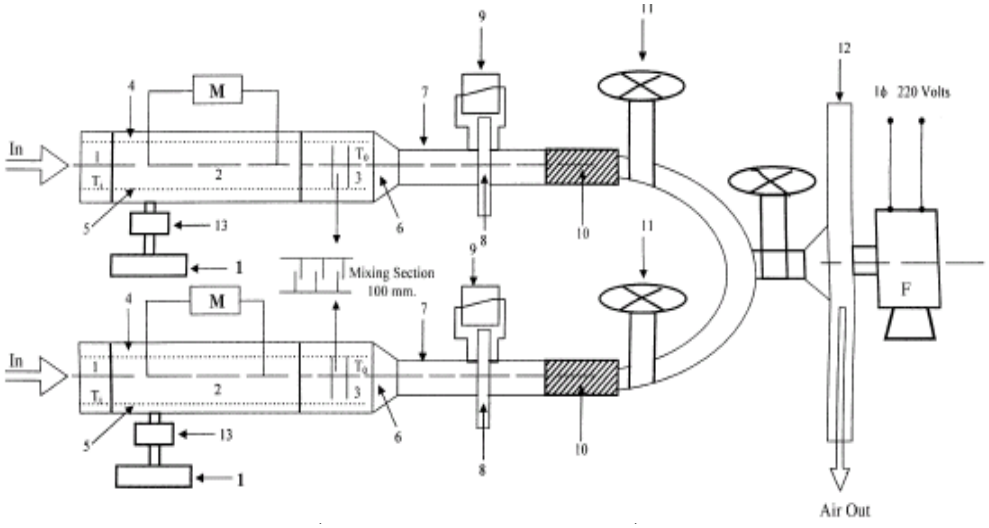

Hachemi (1999) compared the thermal performances of solar air heater collectors with selective and nonselective absorber plates. The use of selective absorber plates in a solar air heater reduces the heat losses to the environment. The aim of the study was to show that using selective absorber plates was not the only way to increase the thermal performance of a solar air heater as this method is very expensive. The heat loss by radiation from the absorber to the environment was lowered by reducing the temperature of the absorber plate. The fins created a turbulent flow and a high thermal heat transfer coefficient resulted in lowering the absorber temperature while at the same time to reducing the thermal heat loss. For the experiments a single glazed flat plate fin consolidated solar air collector was constructed which could be dismantled (Figure 3.9). Two types of absorber plates were used in the experiments; a black painted aluminum sheet as a nonselective absorber plate and a copper-sun plate as a selective absorber plate. Fins created a turbulent air flow and the thermal heat transfer coefficient increased while the absorber plate temperature decreased. The thermal heat losses were reduced and high thermal performance was achieved. It was observed that the efficiency had reached the value of 38.53% and 45.87% for the flat plate collector using a nonselective and a selective absorber, respectively, for a mass flow rate fixed at 50

kg/hm2. For the same mass flow rate, values of 69.72% and 76.15% thermal performances were attained when the finned system collector was used with the nonselective absorber and with the selective absorber, respectively.

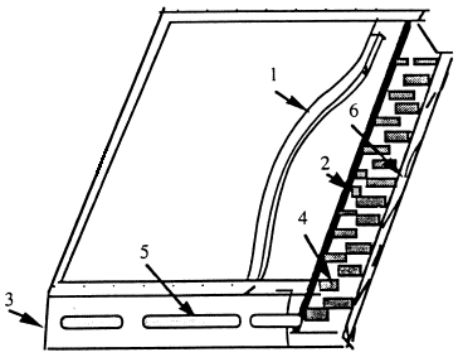

Figure 3.9. Dismantled collector with finned system on the back side.
(Source: Hachemi 1999).

Akpinar et al. (2010) experimentally investigated the performance of a new flat plate solar air heater with different obstacles on the absorber plate,. Four types of absorber plates which had dimensions of 1200 x 700 mm with a thickness of 120 mm were tested in this study (Figure 3.10). All types of absorbers had different type of obstacles at different angles. Type I had triangular shaped obstacles with 50 x 50 mm dimensions, Type II had leaf shaped obstacles with same dimensions. Type III had rectangular shaped obstacles with dimensions of 100 x 100 mm. and Type IV absorber had no obstacles in its design. Each absorber plate was made of stainless steel with black chrome selective coating. Normal window glass of 5 mm thickness was used as glazing. The energy and exergy analysis of the solar air collectors were also evaluated in the study. Solar air collectors were compared on the basis of energy and exergy efficiencies. It was concluded that the highest efficiencies were observed for the Type II solar air heater while the lowest values were obtained for the solar air heater without obstacles. It was also shown that the efficiency of the solar air collectors significantly depended on the inlet solar radiation, surface geometry of the collectors and extension of the air flow line

$$\eta_I = \frac{\dot{m} C_p (T_{a,out} - T_{a,in})}{(IA_C)}$$

$$\eta_{II} = \frac{\dot{E}x_{out}}{\dot{E}x_{in}} = \frac{\dot{m}[h_{out} - h_{in} - T_e(s_{out} - s_{in})]}{\left(1 - \frac{T_e}{T_s}\right)\dot{Q}_s}$$

Figure 3.10. Photograph of the experimental set-up
(Source: Akpinar et al. 2010)

Alta et al. (2010) investigated and compared three different types of designed flat plate solar air heaters at different mass flow rates of 25, 50 and 100 m3/m2h and different tilt angles of 0, 15 and 30°. A Type I solar air heater was designed without fins and had double glass covers. A Type II solar air heater was designed with fins and had double glass covers. Finally, a Type III solar air heater was designed with fins and had a single glass cover. Three solar air heaters were constructed with dimensions of 630x315x150 mm and an absorber plate made of dull black painted sinusoidal corrugated iron sheet with a thickness of 0.5 mm. The experiments found that the air was much more heated at lower flow rates, as more air was needed to raise the temperature inside the collector. Also it seemed that glass covers decreased the heat losses and fins resulted in more heat due to an increase in the heating time required by the air circulating inside the channel. However, it was also found that the circulation time of air inside the heater played a more important role than the number of transparent sheets. The efficiencies of the finned collectors were higher than that of the collector without fin. Thus, it was concluded that attaching fins to absorber surfaces increases the efficiency of the solar collector. In this study, energy and exergy analysis of the solar air heaters was performed. . It was found that the air heater with double glass covers and fins was more effective and the difference between the input and output air temperatures was higher than the others.

Hans et al. (2010) investigated the effect of multiple v-ribs on the heat transfer coefficient and friction factor in an artificially roughened solar air heater duct. The artificial roughness was obtained by pasting the v-ribs along the width of heat exchanging surface. The experimental setup consisted of a wooden rectangular duct of 2400 x 300 x 25 mm dimensions (Figure 3.11). The absorber plate was black painted galvanized iron sheet with dimensions of 1925 x 300 mm. Simulation of solar radiation was achieved with an electrical heating element which supplied a uniform heat flux of

1000 W/m2. The electrical heating element made of six loops of nichrome wires with dimensions of 1525 x 300 mm which were connected in series and parallel. The wires were fixed on 4 mm thick asbestos sheet covered with strips of mica to keep the uniform distance between the wires. 38 roughened absorber plates with different roughness parameters were used in this experiment. To compare the results, a smooth absorber plate was also tested under same conditions. Each roughened absorber plate experimented with ten different flows rate values with Reynolds Number values ranging from 2000 to 20000. It was concluded that by changing the roughness and flow parameters of such a system, considerable enhancement in heat transfer could be obtained. Nusselt number and friction factor correlations in terms of roughness geometry and flow parameters were developed using experimental data. It was seen that such an artificial roughness could enhance the Nusselt number and friction factor by a maximum 6 and 5 times, respectively, when compared to the smooth channel.

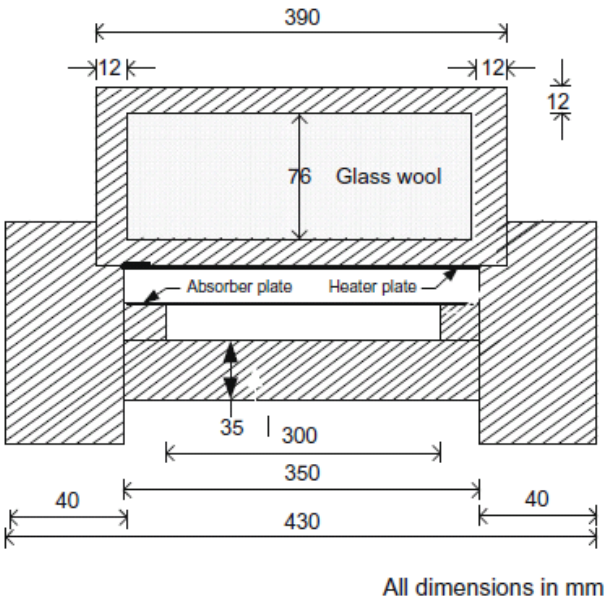

Figure 3.11. Experimental set-up of the solar air collector.
(Source: Hans et al. 2010)

Prasad et al. (2009) presented details of heat transfer and friction characteristics of a packed bed solar air heater as a function of bed geometry and operating parameters. The packing material was wire mesh and the tests were conducted for a low porosity range from 0.599 to 0.816. The air flow rate varied between 0.0159 to 0.0347 kg/m^{2}s with eight different wire mesh designs. A conventional solar air heater also experimented under similar operating conditions to compare the performance of the

packed bed solar air heater. For this purpose the set-up consisted of two identical solar air heaters; the first designed with a clear channel and the second with a packed bed channel (Figure 3.12). The channels were made from 20 mm thick plywood with identical dimensions of 1650 x 400 x 25 mm. An aluminum plate with 2 mm thickness was used as the absorber plate. In the design of the packed bed solar air heater two glass covers placed 20 mm apart from each other were used. The wire screen matrices were placed between the absorber plate and the lower glass cover for this type. A single glass cover was used in the design of the conventional solar air heater which was placed 25 mm apart from the absorber. It was concluded that the mass flow rate and the porosity of the bed influences the efficiency. It was found that the heat transfer coefficient increases with a decrease in porosity and with an increase of mass flow rate. The best efficiency results which varied between 53.3 - 68.5 % could be obtained with the lowest porosity value of 0.599. At the maximum flow rate with this porosity value, the range of efficiency enhancement could be 89.5 to 76.9 %. In this study the Colburn Jh factor and the friction factor was developed as a function of geometrical ad operating parameters. These correlations and the experimental results were found to be in agreement with each other.

a

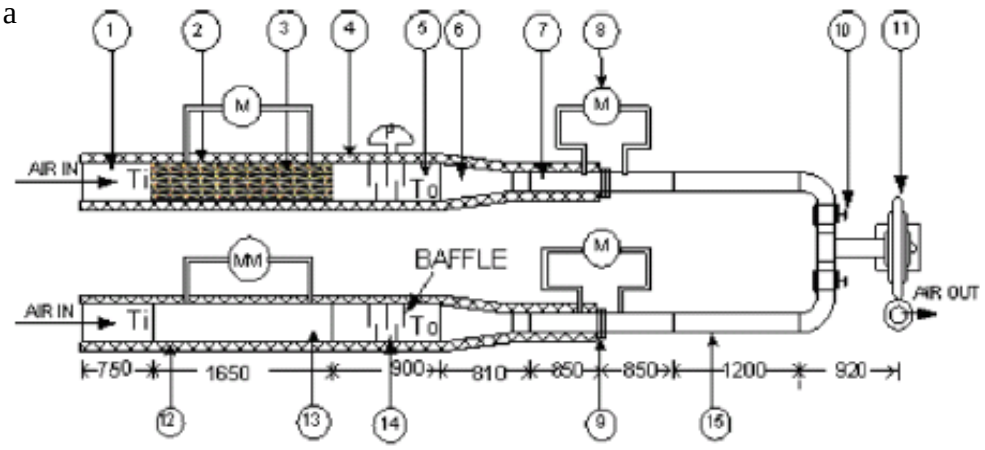

Figure. 3.12. a.Schematic diagram of the experimental set-up b.Details of wire-mesh packing of the packed bed solar air heater.(Source : Prasad et al.2009)

(cont. on next page)

b

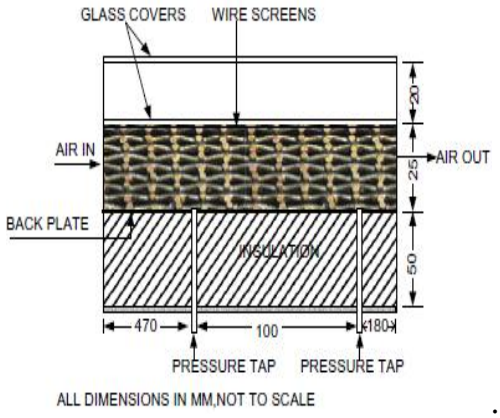

Figure. 3.12. (cont.)

Kumar et al. (2009) experimentally investigated the heat transfer and friction characteristics of a solar air heater which was artificially roughened with W-shaped ribs. The test section of the setup was in dimensions of 1500 x 200 x 25 mm (Figure 3.13). An amount of 900 W/m^2 constant heat flux was supplied to the absorber with an electrical heater. The electrical heater was constructed by combining serial and parallel loops of heating wire on asbestos sheets. The absorber plate was galvanized iron with 1 mm thickness. The maximum height of the W-shaped ribs was 1.5 mm. Twenty W-shaped ribs with varying geometries were tested for the study. During the testing procedure, only the roughened wall was heated. Additionally, a smooth duct was tested under similar conditions for the comparison purposes. The Nusselt number and friction correlations were derived based on roughness and flow parameters for both the roughened and smooth ducts. It was concluded that, with an increase in the Reynolds and the Nusselt numbers were also increased while the friction factor was decreased. The roughened solar air heaters were produced better results when compared with smooth ducted types. With the use of artificial roughness the Nusselt number and friction factor could be enhanced a maximum of 2.16 and 2.75 times according to the smooth duct.

a

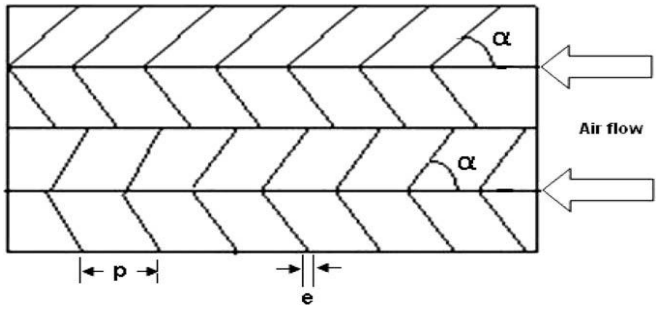

b

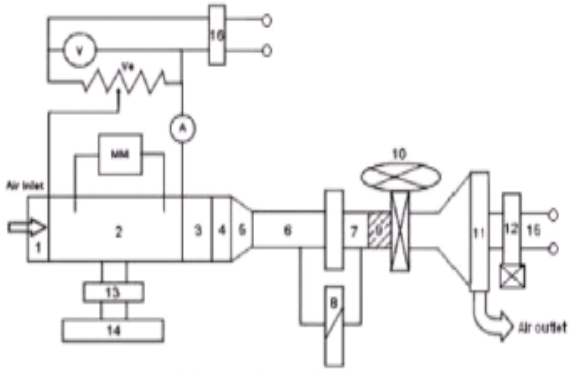

c

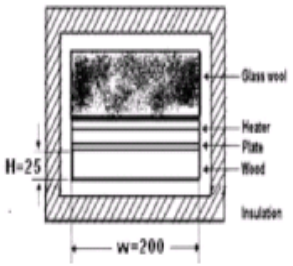

1.Inlet section(177x200)	11.Blower
2.Test section(1500x200)	12.Electric motor
3.Mixing section(200x200)	13.Selector Switch
4.Outlet section(153x200)	14.Millivoltmeter
5.Transition section	15.Power source
6.G.I Pipe(53 inner diameter)	16.Voltage Stabilizer
7.Orificemeter	MM Micromanometer
8.Inclined manometer	V Voltmeter
9.Flexible pipe(L=1000)	A Ammeter
10.Control valve	Ve Variac

All dimensions in mm

Figure 3.13. a.Roughness geometry b.Schematic diagram of experimental setup c.Enlarged wiev of the test cross section.(Source Kumar et al. 2009)

Bopche et al. (2009) investigated the heat transfer and flow characteristics of an artificially roughened solar air heater. The roughness was obtained by using u-shaped turbulators on the absorber plate of the solar air heater. During the experiments the roughened wall was heated while the remainder was insulated. The collector was of 1850 x 130 x 22 mm in dimensions and made from acrylic sheet of 10 mm in thickness (Figure 3.14). The solar radiation was simulated with an electrical heater. The heater was made from stainless steel (Grade 304) with a thickness of 0.05 mm of 1000 x 136 mm in dimensions and provided uniform heat flux to the system. In order to minimize the heat loss, the top of the collector was made of bakelite plate with a thickness of 16 mm. A mica sheet was fixed between the bakelite plate and the electrical heater to improve the accuracy of the temperature measurement. The tests were conducted under same operating conditions with a heat flux of six different flow rate values. The researchers studied the effect of the Reynolds number, relative roughness pitch and relative roughness height on the heat transfer coefficient and friction factor using the experimental setup. The results of the experiments were compared with the results of the smooth duct. It was concluded that the u-shaped turbulator roughness enhanced the heat transfer and friction factor by a factor of 2.82 and 3.72 times, respectively. This roughness geometry was also effective at low Reynolds number.

a

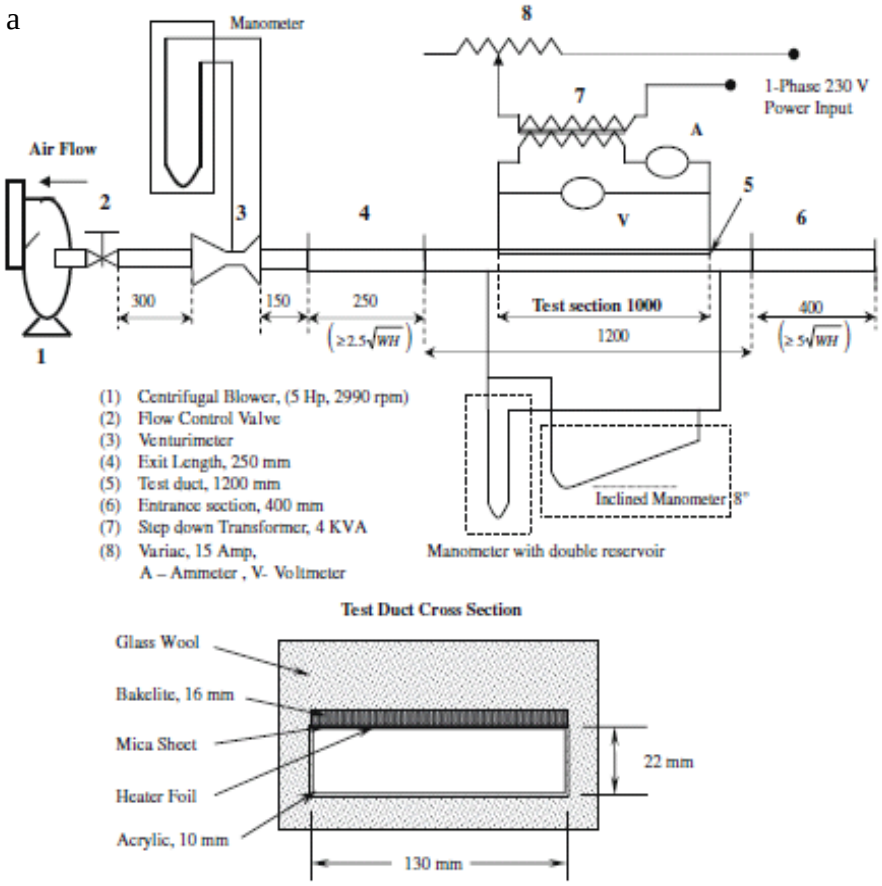

b

Figure 3.14. a.Schematic diagram of experimental set-up with test duct cross-section b.Photograph of turbulator roughened absorber plate. (Source: Bopche et al. 2009)

Al-Kamil et al. (1996) theoretically and experimentally studied the performance of a flat plate solar air heater. The researchers investigated the effect of thermal radiation inside the heaters and the blackening of the collector rear plate. The constructed solar air heater was of 1690 x 1030 x 60 mm in dimensions and made of galvanized steel with 1.1 mm thickness The absorber was a dull, matt and blackened plate. A single glass cover with a thickness of 4 mm was used as glazing. The temperature distribution inside the solar air heater was also evaluated numerically. It was concluded that blackening the rear plate could enhance the heat transfer up to 10%. It was also found that the sectioning method was suitable for solving solar air heater problems and could be used for future studies.

Bhagoria et al. (2002) investigated the heat transfer and friction factor correlations for the flow of air in a rectangular shaped duct with one roughened wall and three insulated walls. The roughness was obtained by using transverse shaped wedge ribs inside the duct. The roughened wall was subjected to a uniform heat flux during the experiments. The experimental setup was of 2600 ×150 x 30 mm in dimension (Figure 3.15). The setup was examined in laboratory conditions so the solar radiation was simulated by an electrical heater. The electrical heater was of 1650 ×150 mm in dimensions and constructed by combining the heating wire in serial and parallel loops on a 5 mm thick asbestos sheet. A variac was used to adjust the heat flux between 0 and 1000 W/m2. The absorber plate was 6 mm thick aluminum. Between the electrical heater and the absorber plate, a 1 mm thick mica sheet was placed which acted as an insulator. The experiments were conducted under quasi-steady state conditions with eight different flow rate values at a fixed heat flux. During the experiments heat transfer and friction factor data were collected. The results were compared with the results of smooth duct to investigate the effect of roughness on heat transfer and the friction factor. It was concluded that the presence of roughness enhanced the heat transfer and friction factor 2.4 and 5.3 times in comparison to the smooth duct. The maximum heat transfer occurred with a relative roughness pitch (p/e which is the ratio of pitch to the roughness height in meters) of about 7.57 and with a wedge angle about 10°C. Also, Nusselt number and friction factor correlations performed well in terms of roughness parameters such as rib spacing, rib height, rib wedge angle and Reynolds number.

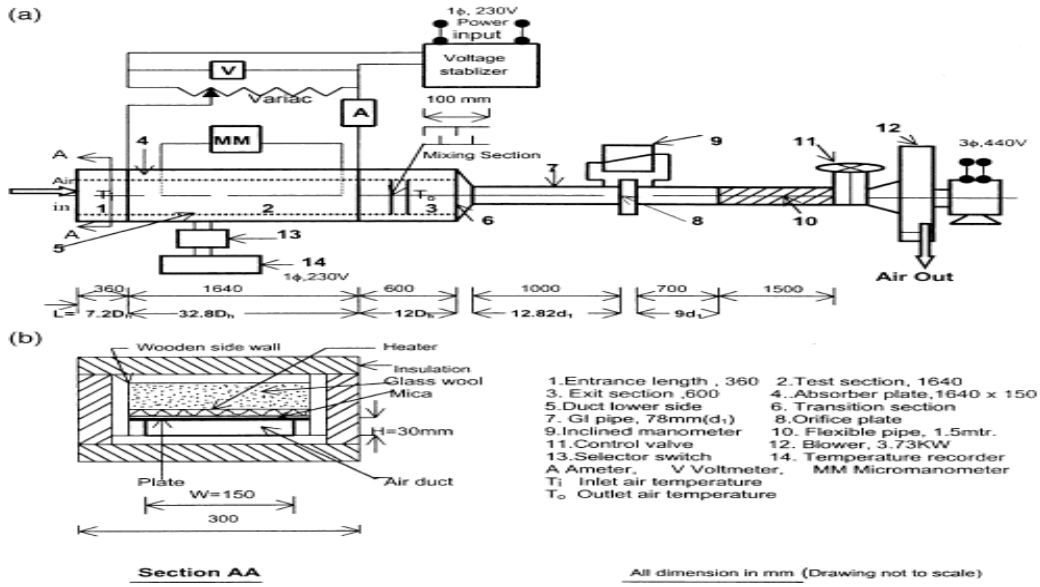

Figure 3.15. a. Schematic diagram of experimental set-up. b. Enlarged view of the duct. (Source: Bhagoria et al.2002)

Layek et al. (2009) investigated the flow in a rectangular shaped solar air heater with a chamfered rib-groove roughened absorber plate. The researchers studied the effects of integral transverse chamfered rib-groove roughness and the angle of roughness on heat transfer and friction characteristics of solar air heaters. The experimental setup was of 2600 x 150 x 30 mm in dimension with a collector length of 1200 mm (Figure 3.16). A heating wire was combined in series and parallel to construct the electrical heater part of the solar air heating system. The absorber was an aluminum plate with a thickness of 6 mm. The integral rib-groove roughness was performed on the bottom of the absorber plate which was the upper side of the duct.The tests were conducted using six roughened plates with a 60° V groove placed at the center between two consecutive chamfered ribs. For each plate, eight different flow rate values were examined. To investigate the increase in the heat transfer, the results were compared with the square rib grooved and smooth duct results. It was concluded that the Nusselt number and friction factor was enhanced approximately 2.6 and 3.35 times when compared to the smooth duct. The maximum increase in the Nusselt number could be obtained with a chamfer angle of 18°. On the other hand as the chamfer angle increases the friction factor increases. It was also found that, when the performance parameter value (a parameter that facilitates the simultaneous consideration of thermal and hydraulic performance) was between the range of 1.4 and 1.76, the thermo-hydraulic performance was substantially improved. (Performance parameter value: $\eta = (Nu/Nu_s)/(f/f_s)$.

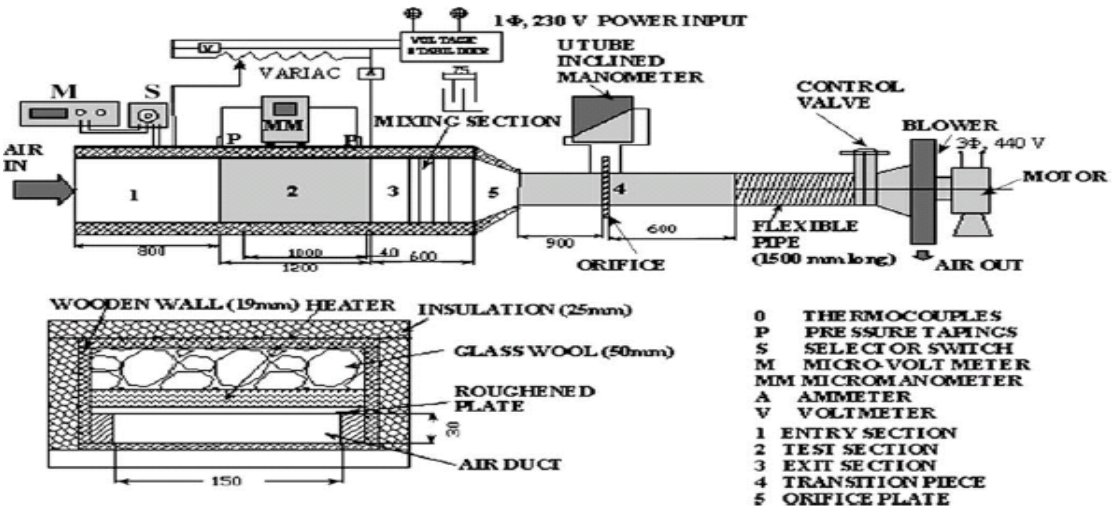

Figure 3.16. a.Experimental set-up and duct section.b.Roughness geometry.
(Source: Layek. et al.2009) (cont.on next page)

b

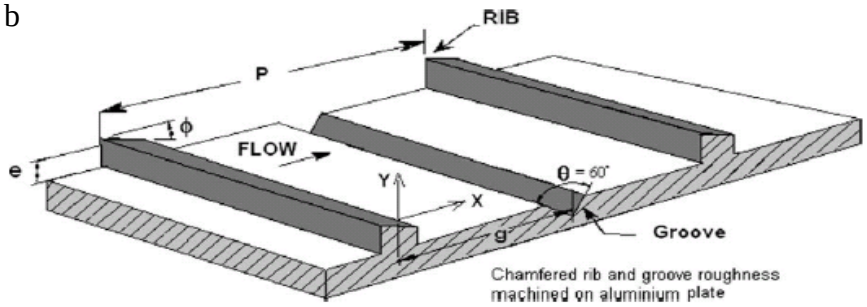

Figure 3.16 (cont.)

Jaurker et al.(2006) investigated the heat transfer and friction characteristics of a rectangular shaped duct with a roughened absorber plate. The roughness was achieved by repeated rib-grooves. The roughened wall of the solar air heater was heated constantly while the other three walls were insulated. The experimental setup was of 2420 x 156 x 22 mm in dimensions and consisted of a test section of 1200 mm (Figure 3.17). The absorber was a 3 mm thick aluminum plate. The bottom of the absorber was the rough surface at the top side of the air flow channel. An electrical heater was used to supply a constant heat flux to the system. The electrical heater was constructed by combining a heating wire in series and parallel on an asbestos sheet. The intensity of the heat flux between 0 and 1200 W/m2 was adjusted with the help of a variac. Based on the roughness parameters, the Nusselt number and friction factor correlations were developed. It was concluded that the existence of roughness increased the Nusselt number and friction factor up to 2.7 and 3.6 times, respectively. To obtain the maximum heat transfer, the relative roughness pitch value should be about 6.0. The Nusselt number and friction factor correlations developed were found to predict the experimental values with a deviation of 2.73 and 3.16% respectively.

a

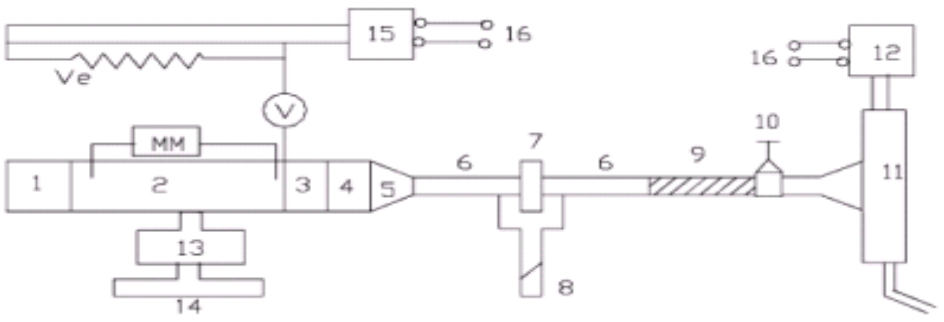

Figure 3.17. a.Experimental set-up, b.Enlarged view of the test cross section, c. Rib roughness geometry. (Source: Jaurker et al.2006)

(cont.on next page)

b

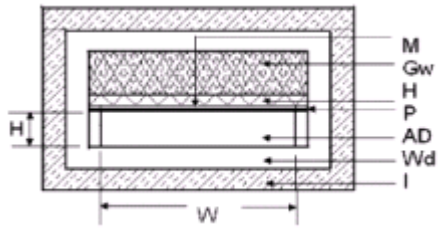

c

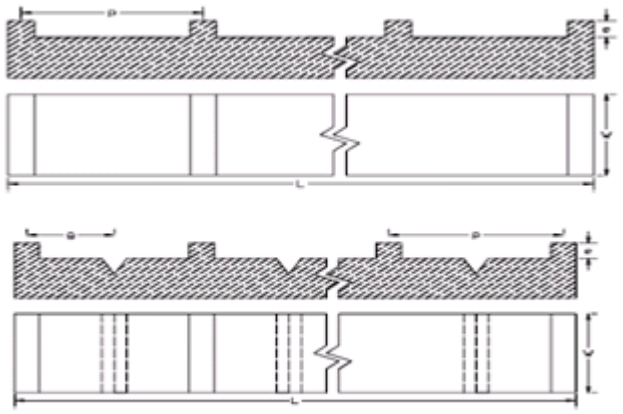

Figure 3.17 (cont.)

Karwa et al. (2001) investigated the performance of a solar air heater with chamfered rib roughness on an absorber plate. Two identical rectangular ducts were constructed for the study. Each duct was of 2640 x 150 mm in dimensions with a variable depth from 16.5 to 21.8 mm (Figure 3.18). One of the ducts has its absorber roughened and the other three walls of it were smooth, while the other duct was completely smooth. Three roughened absorber plates and for comparison the smooth absorber plate. were experimented during the study. The roughness of the absorber plates was obtained by machining. The transverse grooves were machined on the plates. which were prepared in three or two pieces. A single glass cover with a thickness of 3.25 mm was used in both ducts and the airflow rates were varied between 0.024 to 0.102 kg/sm^2. It was concluded that, compared to the smooth duct the thermal efficiency and Nusselt number of roughened absorber plates increased about 10 to 40% and 50 to 120%, respectively. The friction factor was also increased about 1.8 to 3.9 times with the roughness element. As it was found that enhancement in the efficiency was a function of the relative roughness height (e/Dh which is rib height over hydraulic diameter), the maximum increase occurred with the highest relative roughness height. The mathematical model for chamfered rib roughened solar air heaters was also investigated in the study. It was shown that the theoretical and experimental studies agreed within a deviation of ±5.8%

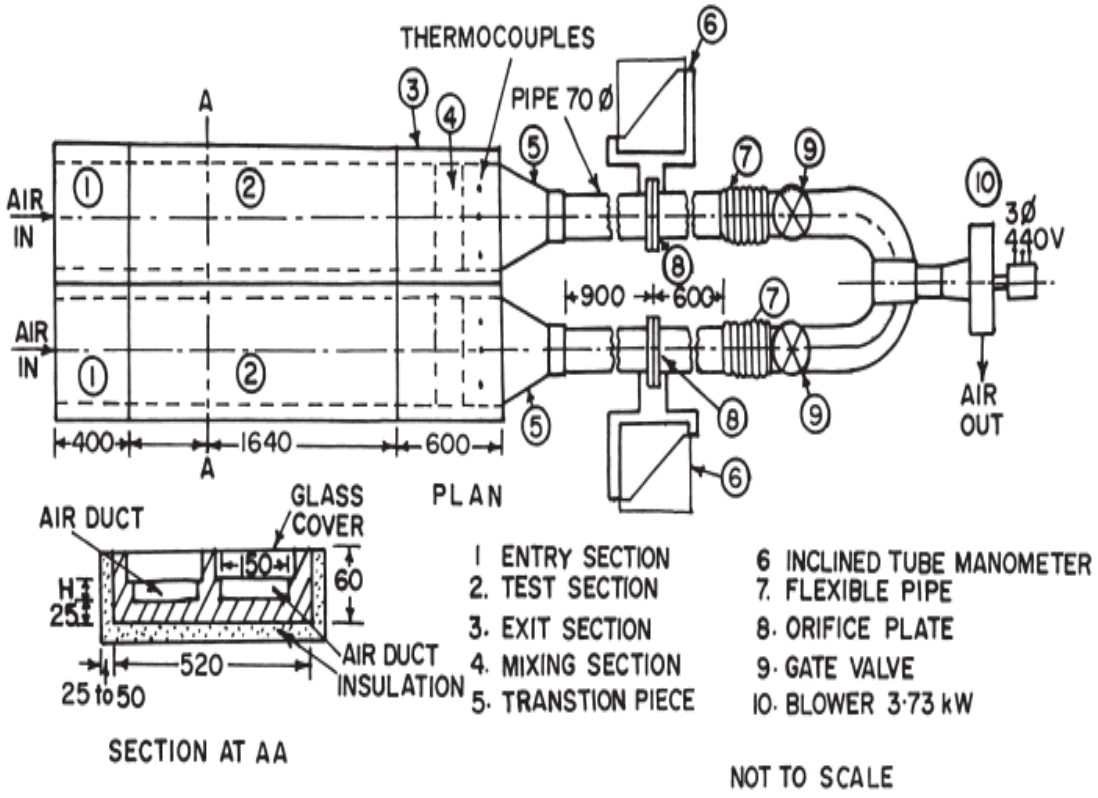

Figure 3.18. Schematic diagram of experimental setup.
(Source: Karwa et al. 2001)

Momin. et al. (2002) investigated the effects of V-shaped roughness elements on the heat transfer and flow characteristic of a solar air heater. Their setup had a rectangular shaped duct with v-shaped ribs on its absorber plate. The experimental duct was of 2800 x 200 m in dimensions and was made of aluminum (Figure 3.19). The absorber plate was also an aluminum sheet of 22 ASWG with dimensions of 1500 x 200 m2. The artificial roughness was achieved with V-shaped copper wires on the lower side of the absorber plate. Seventeen plates were tested in this study. The roughened plates had different roughness geometries. The ribs were at different gauges with angles of 30° and 60°. Uniform heat flux up to 1500 W/m2 was supplied to the absorber plate with an electrical heater. A variac was used to control the intensity of the flux. Fourteen runs with different mass flow rates corresponding to the Reynolds number range 2500–18000 were examined. The experiments were repeated with smooth absorber plates under similar flow conditions to compare the results. Nusselt number and friction factor correlations were performed and the results were discussed with the results of experimented setup. It was concluded that, when the Reynolds number increased, the Nusselt number was also increased with a decrease in the friction factor. The roughness

elements increased the Nusselt number and the friction factor. The Nusselt number and friction factor enhanced about 2.30 and 2.83 times compared to the smooth absorber duct for an angle of attack of 60°. As the relative roughness and the angle of attack increased, thermo-hydraulic performance was improved. It was also found that the experimental results and the predicted results from the correlations agreed with each other with a maximum deviation of ±10%.

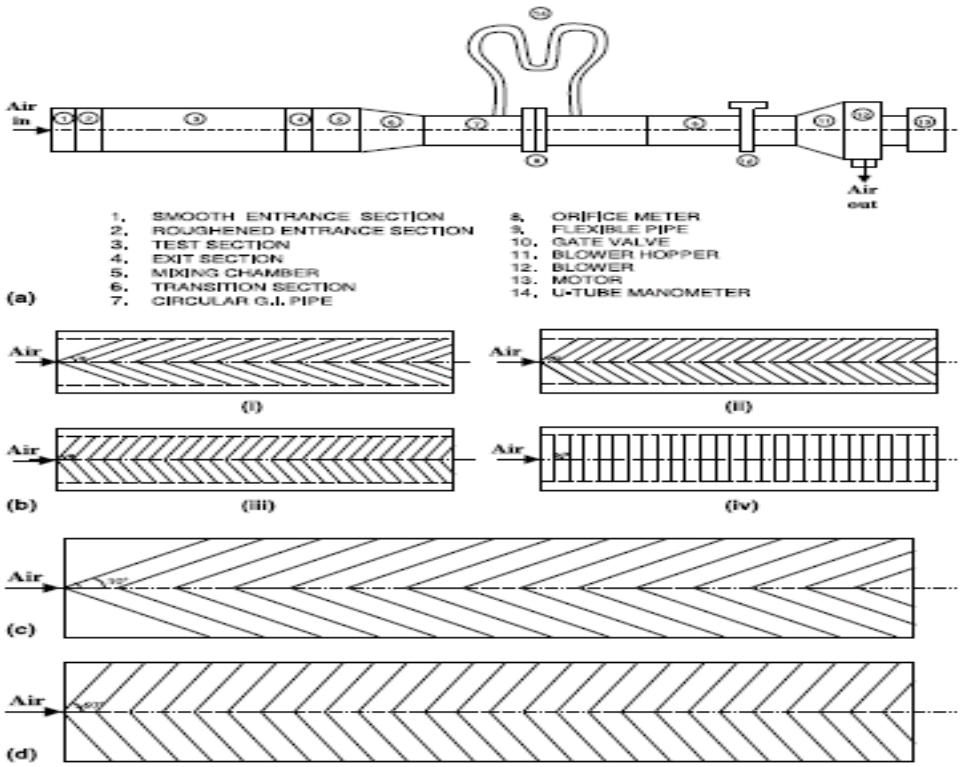

Figure 3.19. (a) Schematic diagram of experimental set-up. (b) Roughness elements on absorber plate. (c) Schematic diagram of 30° V shaped ribs. (d) Schematic diagram of 60° V-shaped ribs. (Source: Momin et al. 2002)

Aharwal et al. (2008) investigated the heat transfer and friction characteristics of a solar air heater duct with an absorber plate having integral inclined square rib roughness. An experimental setup was constructed with dimensions of 2600 x 181 x 31 mm and a test section of 1200 mm (Figure 3.20). An aluminum plate with a thickness of 6 mm was used as the absorber of the system and located at the top wall of the test section. Constant heat flux was supplied to the absorber plate from its top with the help of an electrical heater. The artificial roughness was achieved by machining the absorber plate. To investigate the effects of the rib parameters (rib gap, rib position. etc.) on the heat transfer and friction factors, the rib height was varied between 1 to 2 mm while the

rib width was held constant at 2 mm. It was concluded that the Nusselt number and the friction factor increased approximately 2.83 and 3.60 times respectively according to the smooth absorber. To obtain maximum enhancement in solar air heaters, the relative gap position, the relative gap width, the relative roughness pitch and the relative roughness height of the ribs should be 0.25, 1.0, 8.0 and 0.037, respectively. The maximum friction factor was observed for the transverse ribs with a relative roughness pitch of 8.0,. The Nusselt number and friction factor correlations were calculated based on the experimental results and found to predict them with a small deviation

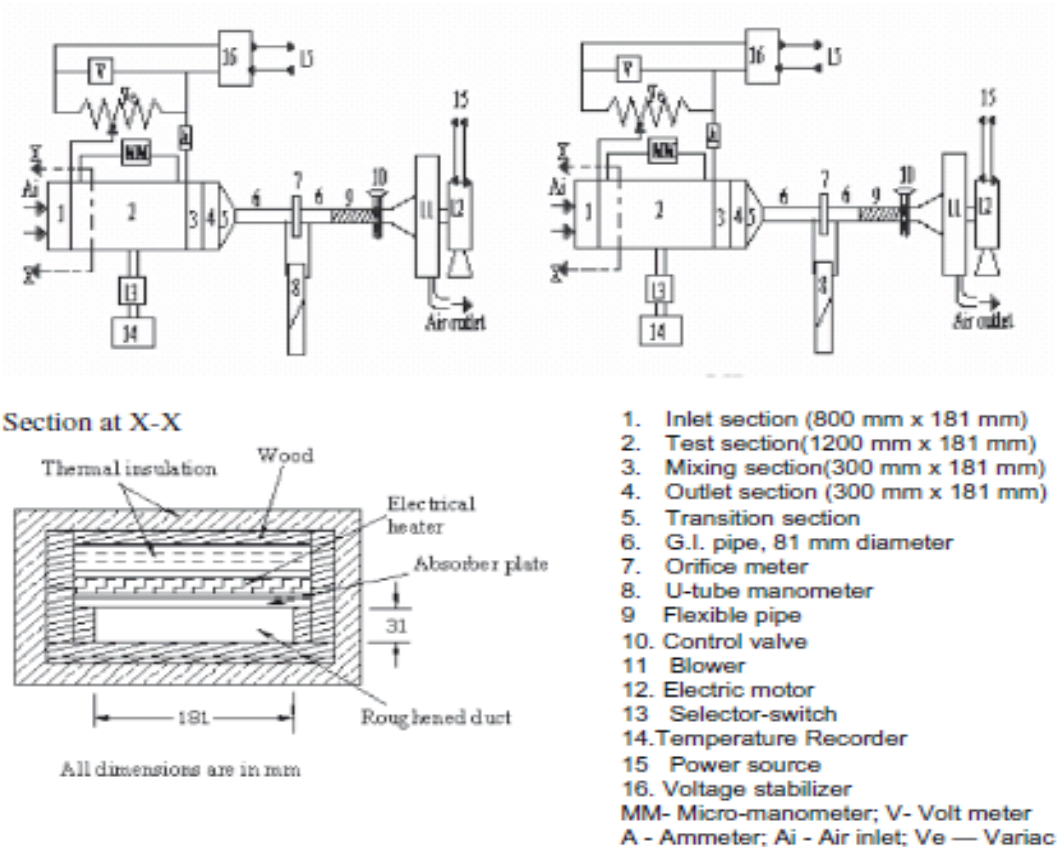

Figure 3.20. Schematic diagram of experimental set-up.
(Source: Aharwal et al. 2008)

Aharwal et al. (2009) investigated the heat transfer and friction factor characteristics of a rectangular duct solar air heater with a roughened absorber plate. The roughness was obtained by square inclined repeated ribs. It aimed to determine the optimum location, width and gap size of ribs in a solar air heater duct. The rectangular duct was in dimensions of 2600 x 182 x 31 mm with a test section of 1200 mm (Figure 3.21). Following test, three baffles were added to the system for mixing the air. The

absorber was an aluminum plate with a thickness of 6 mm. The experiments were performed on the range of Reynolds numbers between 3000 and18000. In order to observe the variations in heat transfer and friction characteristics, the results were compared with the smooth duct under similar conditions. It was concluded that the 60° inclined square ribs enhanced the heat transfer and friction factor by approximately 1.48-2.59 times and 2.26-2.9, respectively. For the maximum values of heat transfer and thermohydraulic performance, the relative gap position and relative gap width should be 0.25 and 1.0, respectively.

a

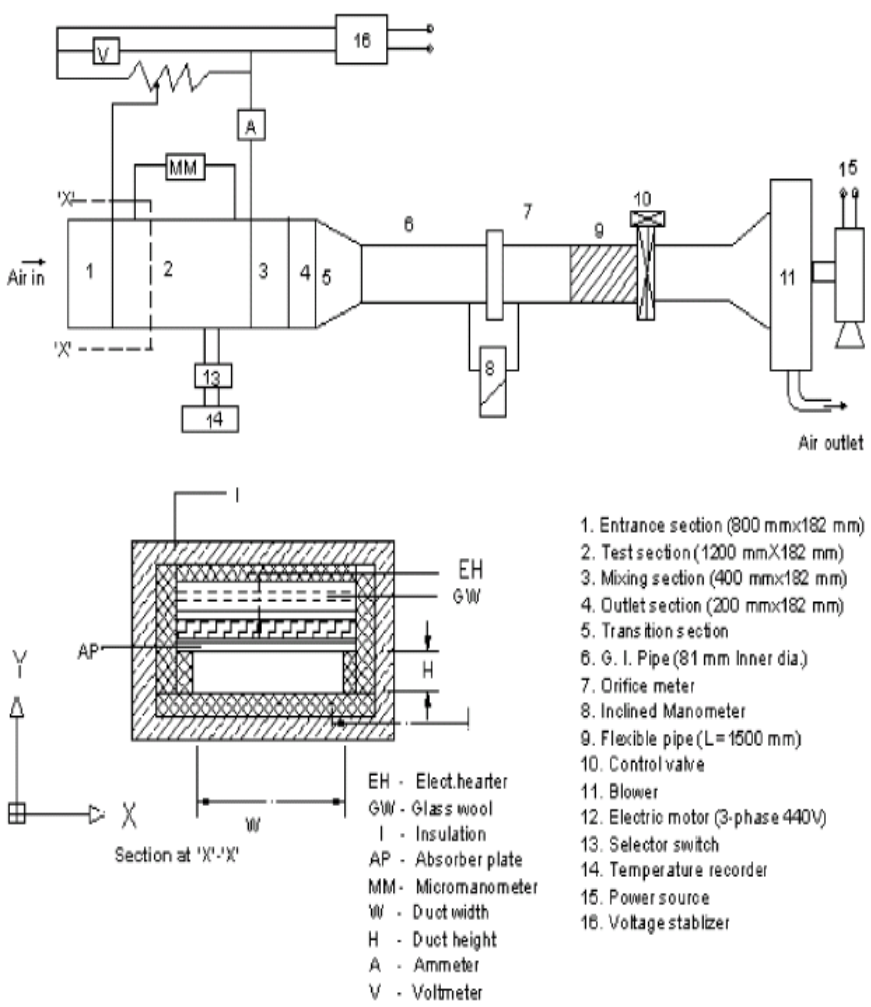

Figure 3.21. a.Schematic diagram of experimental set-up. b. Flow pattern of secondary flow for inclined continuous rib c.Flow pattern of secondary flow for inclined discrete rib.(Source: Aharwal et al.2009) (cont.on next page)

b

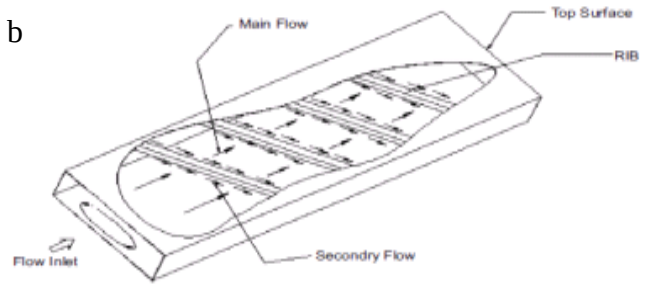

c

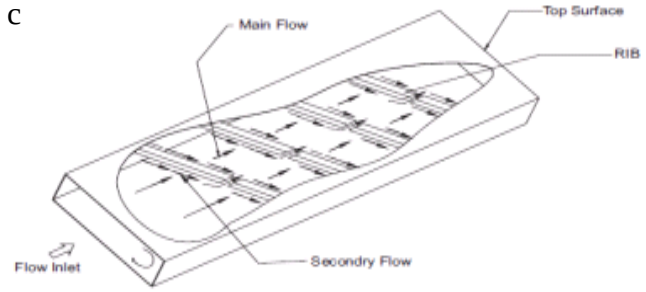

Figure 3.21 (cont.)

3.1.2. Double Flow Single Pass Studies

Madhlopa et al. (2002) designed a single glazed solar air heater with an integrated flat-plate collector which had composite–absorber systems (a removable mild steel screen absorber and a fixed wooden plate) in one collector frame. Several removable absorber plates, made from materials (such as metals and plastics) with different thermal and other characteristics could be used interchangeably in the same collector system to achieve the desired temperature and rate of air heating under the prevailing meteorological conditions. The collector could convert solar radiation to thermal power in the absence of the removable absorber plates. The solar collector heater was combined with a drying chamber for food dehydration (Figure 3.22). The aim of this study was to preserve fruit spoilage using a simple solar dryer which utilizes solar radiation. The collector was in dimensions of 810 x 625 mm. The performance of the dryer was determined based on the moisture content, pH and ascorbic acid of fresh and dried mango samples. It was found that the air heater raised the temperature of the drying air from approximately 31.7 to 40°C around noon, and reduced the moisture content of sliced fresh mangoes from about 85 to 13% on wet basis, while the ascorbic acid percent was retained at 74%. The designed air heater had achieved efficient drying of fresh mangoes slices and relatively high retention of ascorbic acid.

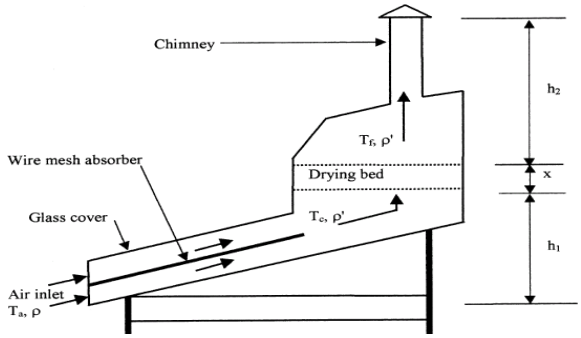

Figure 3.22. Cross-section of solar dryer showing collector, drying chamber and chimney.(Source: Madhlopa et al. 2002)

Potdukhe et al. (2007) developed and tested a solar dryer including a drying chamber and a solar air heater with thermal storage. It is aimed to reduce the drying period and enhance the quality of dried agro products. The dimensions of the solar air heater were 850 x 790 x 135 mm (Figure 3.23). A box shaped blackened, corrugated, galvanized iron sheet was used as the absorber plate and this box shaped absorber was filled with storage material. The storage material used was thermic oil. Single glass cover was used as glazing. The experiments were performed with chilies and fenugreek leaves and their drying periods were observed. The mathematical modeling of such a solar drying system was also performed in this study. It was concluded that, by using a solar air heater which was connected to a drying chamber, the desired air temperature (65±3°C) for drying the agro products could be achieved. The efficiency of the dryer and the quality of the products in terms of color enhanced with this method when compared with open sun drying. The use of thermic oil increased the cost of setup 10% but reduced the drying period by 40 % approximately.

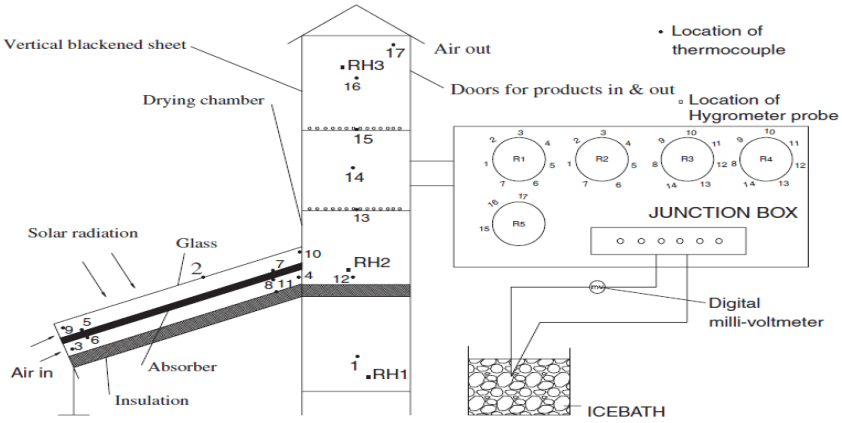

Figure 3.23. Schematic of experimental set-up.
(Source: Potdukhe et al. 2007)

Yeh et al. (2002) developed a design to investigate the collector efficiency of a double flow solar air heater with fins attached over and under the absorbing plate. The investigation was evaluated both experimentally and analytically. The artificial simulation including an indoor solar simulator was used to carry out the experiments for steady operations. The collector was of 300 x 300 x 27.5 mm in dimension (Figure 3.24). Double normal glass was used to cover the air channel. The equations for the theoretical prediction of collector efficiency in double-flow solar air heaters with fins attached on both surfaces of the absorbing plate were derived from energy balances with the ratio of airflow rate as the parameter. The theoretical predictions were confirmed by the experimental results. It was found that the collector efficiency could be improved by attaching fins to the collector. It was concluded that fins attached on the absorber would increase the fan power while it might not increase operating cost. Consequently, the application of a double-flow in the design of a solar air heater with fins attached was technically and economically feasible

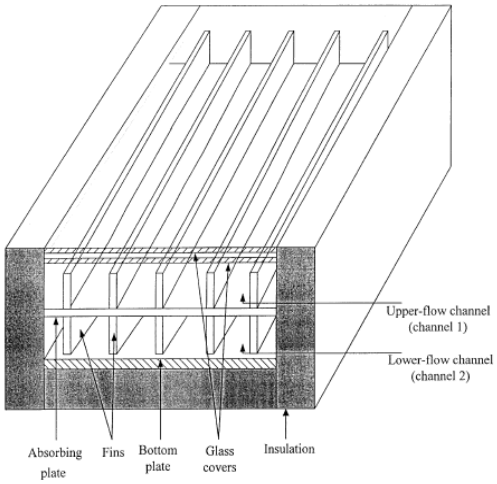

$$\eta = \frac{Q_u / A_c}{S_0} = (M / S_0)[rT_{1,0} + (1-r)T_{2,0} - T_{in}]$$

Figure 3.24. Schematic view of the experimental setup.
(Source: Yeh et al. 2002)

Esen (2008) experimentally investigated the energy and exergy analysis for a double-flow flat plate solar air heater with and without obstacles. Four types of absorber plates made of stainless steel with black chrome selective coatings were used (Figure 3.25). The dimensions and plate thickness for all four collectors were 1250 x 800 mm and 1mm, respectively. Single glazing with 5 mm thickness was used. It was observed that the obstacles created the turbulence and reduced the dead zones. The shapes of tested obstacles were presented in the study. Following analysis of the results, the

optimal value of efficiency was found to be when the absorbing plate was in the middle level of flow channel for all operating conditions. It was also found that the double-flow collector equipped with obstacles appeared significantly better than that without obstacles. It was shown that the Type III (the one which was staggered with leaf shaped obstacles) absorber plate always yielded higher efficiency than the Type I (flat plate) (Figure 8). An exergy analysis for the experimented collector was also performed. The results showed that the largest irreversibility occurred at the flat plate (without obstacles) collector in which collector efficiency is the smallest.

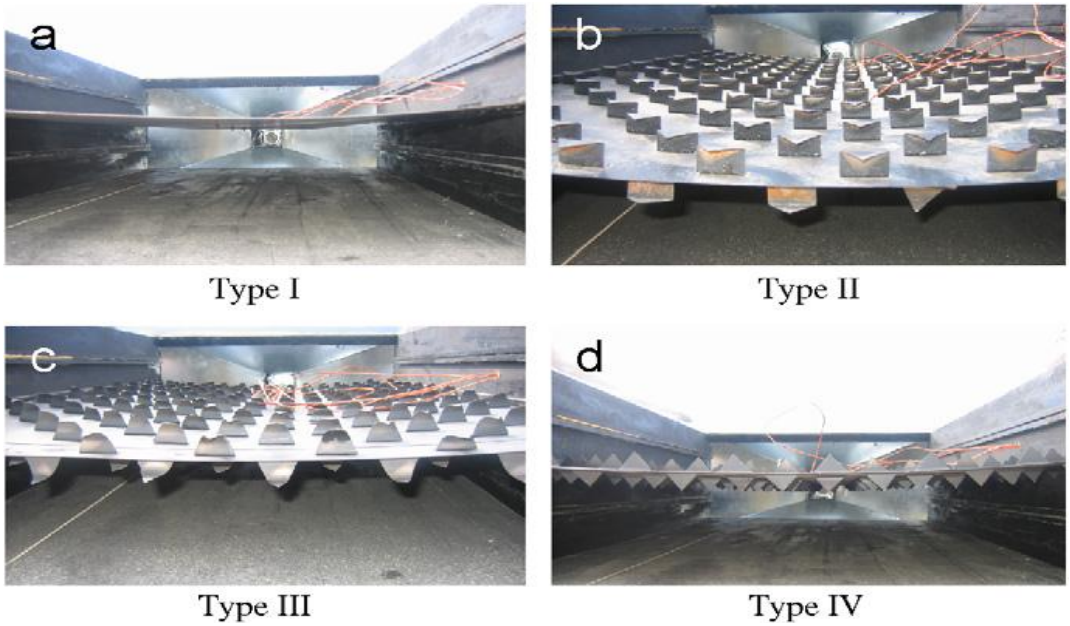

Figure 3.25. Types of absorber plates
(Source: Esen 2008)

Ozgen et al. (2009) experimentally evaluated the energy efficiencies of three types of double flow solar air heaters with aluminum cans. Three types of absorber plates were used which were made of stainless steel with black chrome selective coating (Figure 3.26). The dimensions and plate thickness for three collectors were 2140 m x 840 m and 1 mm, respectively. Normal window glass of 5 mm thickness was used as glazing. Single cover glass was used in all three collectors. The cans were staggered as zigzag on the absorber plate in the first type (Type I), while they were arranged in order in Type II. Type III was a flat plate without cans. It was observed that the heat transfer area was enhanced for the collector with cans, and consequently, the efficiency of the solar collector was increased. At the end of the experiments, the highest efficiency was

obtained for Type I (Fig 10) at 0.05 kg/s mass flow rate. The testing results always yielded higher efficiency values for the Type I (non-arranged cans) model than that for the Type III (without cans) flat-plate collector.

Figure 3.26. Photograph of Type I absorber plate
(Source: Ozgen et al.2009)

Midilli et al. (1999) investigated the drying periods for mushrooms and pollens of honey. The drying experiments were carried out both in the laboratory and in outdoor atmospheric conditions. An experimental drying set-up connected to a solar air collector (Figure 3.27) was established to dry mushrooms and pollen under laboratory conditions. Double glass covers were used as glazing. The pipe of the heater in the system was directly connected to the inlet of the drying cupboard. The temperature of the drying cupboard was set at 45°C during the drying experiment by an auxiliary heater. The mass of the samples were measured before and after the experiments to obtain the mass loss due to the drying process. Based on the results obtained, drying curves, variation of the mass change ratio, moisture ratio and temperatures of the shelves with respect to drying time were presented in the study. It was concluded that mushrooms could be dried in the cupboards by using hot air at 50°C in a time period of 5-6 hours, and that pollen also must be dried at temperatures between 40 and 45°C in a time period of 2.5-3 hours without losing their color, flavor, smell and structure.

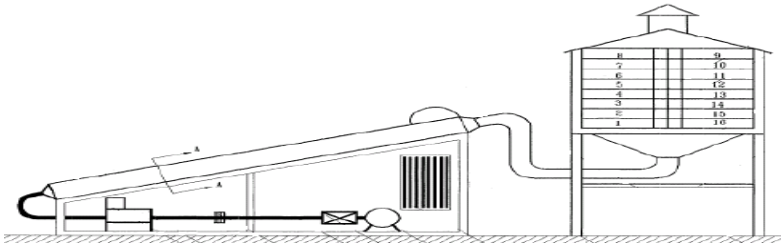

Figure 3.27. Solar assisted drying cupboard
(Source: Midilli et al.1999)

Forson et al. (2003) experimentally studied the single pass double duct solar air heater,. A mathematical model was investigated and described to predict the performance and the design properties of a solar air heater. The validation of the model was performed by comparing its results with the results of a small scale laboratory model and a full scale conventional type (Figure 3.28). Two sets of experiments were conducted; one of them with a small scale laboratory model and the other one with a full scale conventional model. The small scale model was 400 x 740 x 75 mm in dimension. Solar radiation for the laboratory model was provided by ten infrared laps, each rated 100 W. The full scale model was of 6750 x 1260 x 280 mm in dimension and connected to a commercial size drying chamber. The absorber plate was placed at the centerline and divided the collector into two rectangular flow channels for both scales. Air could flow both over and under the absorber plate. The two hot air streams were mixed in the plenum. The collectors were made of plywood and a single glass cover which was used at the top. It was concluded that the developed mathematical model's results were in good agreement with the experimental results and could be used as a design tool for future works. The collector performance could be enhanced if the number of parameters were chosen correctly and carefully. The air mass flow rate significantly affected the efficiency of the collector

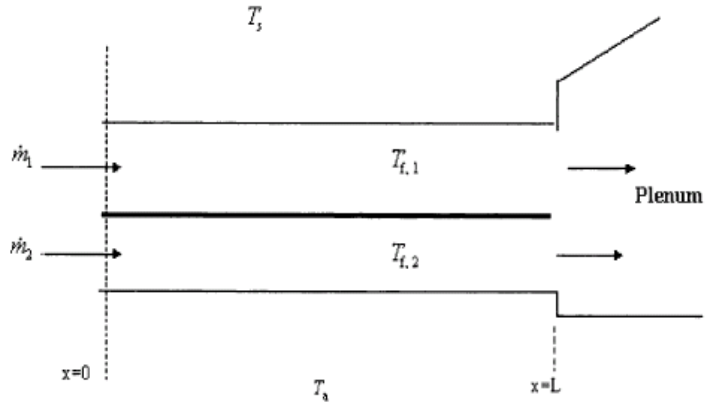

Figure 3.28. Schematic diagram of a single pass double duct solar air heater.
(Source: Forson et al. 2003)

Alvarez et al. (2004) studied the performance of a solar air collector with an absorber plate that was made of recyclable aluminum cans (RAC). A simulation model was examined to achieve the design parameters of the experimental setup. Also, numerical studies were conducted for the flow characteristics. The solar air collector

was of 2000 x 700 x 180 mm in dimension and made of a steel frame (Figure 3.29). A total of 128 recyclable aluminum cans were used in the experimental setup. The recycled aluminum cans were sanded and then glued to the absorber surface before being painted black. The cans formed eight circular cross sectional flow channels in the solar collector and for each channel 16 blackened recyclable aluminum cans were used. Single glass with a thickness of 4 mm was used to cover the system. It was concluded that enhancement in the efficiency of a solar collector by using recyclable aluminum cans was achievable. The maximum efficiency that was obtained by using RAC ‘s was 74 %.

a

b

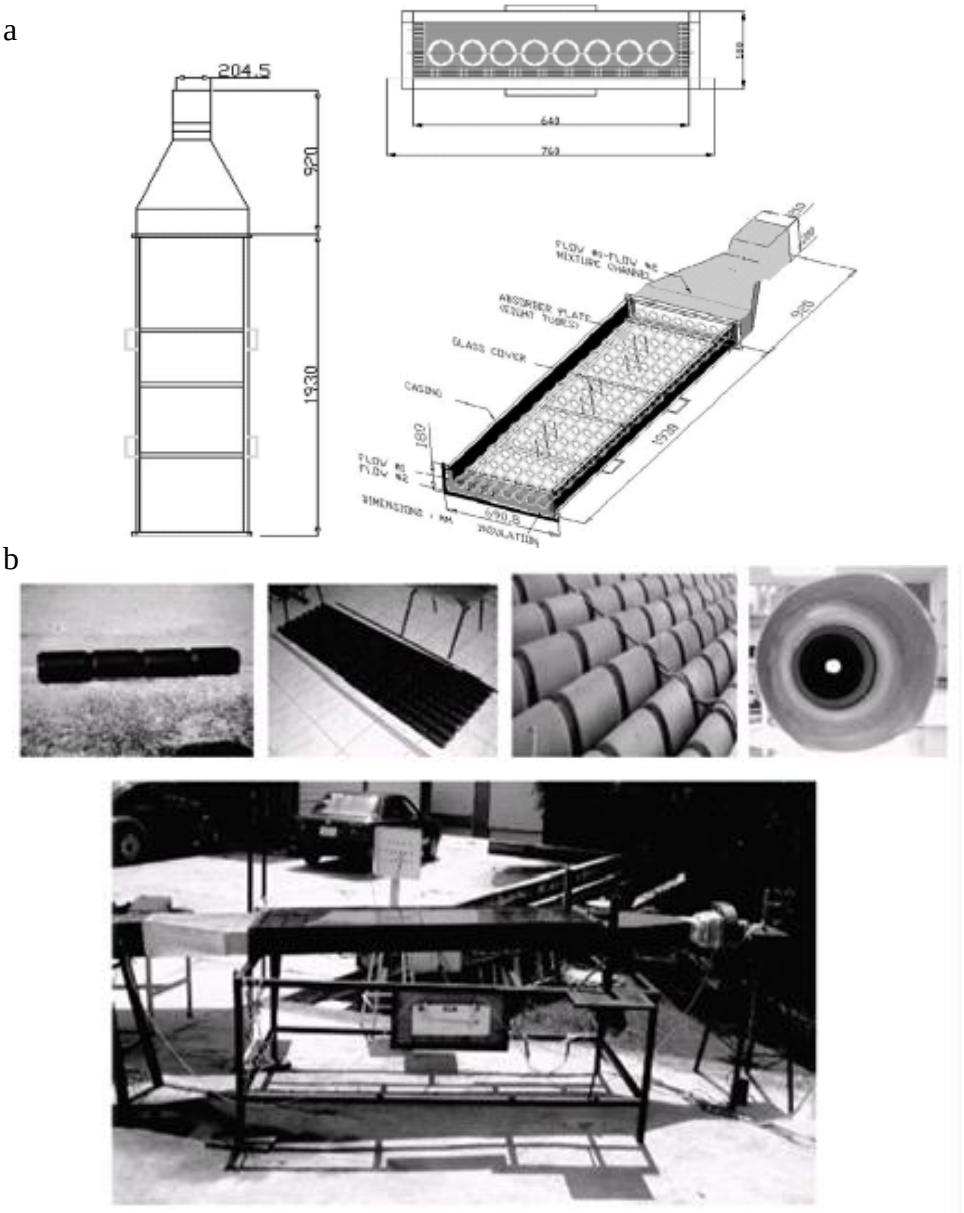

Figure 3.29. a.Schematic diagram of the air solar collector b.Test facility of the air solar collector. (Source: Alvarez et al.2004)

3.1.3. Single Flow Double Pass Studies

Ramani et al. (2010) theoretically and experimentally investigated the performance of a double pass solar air collector with and without porous material. The effects of parameters on the efficiency and on the pressure drop of solar air heater were also discussed. Two glass covers were used with a thickness of 4 mm in the collector. There were two air flow passages in the collector (Figure 3.30). The first one was formed by the gap between the first and second glass covers while the second air passage was formed by the second glass cover and the absorber plate. Two solar air collectors were constructed in order to compare the results. One of them had two clear air flow channels while collector's second air flow channel of the other was filled with porous material. Black painted wire mesh was used as porous material. The two passages were of 2100 x 540 x 21 mm in dimension. A black painted aluminum sheet with a thickness of 1mm was used as the absorber plate in both collectors. In addition to the experiments a mathematical model was developed on the basis of volumetric heat transfer coefficient in order to describe the heat transfer characteristics of such a solar air heater. It was concluded that using a double pass solar air heater with porous material improved the thermal performance significantly. The thermal efficiency of a double pass solar air collector with porous media was 20-25% higher than a double pass solar air collector without porous media and also 30-35% higher than single pass collector.

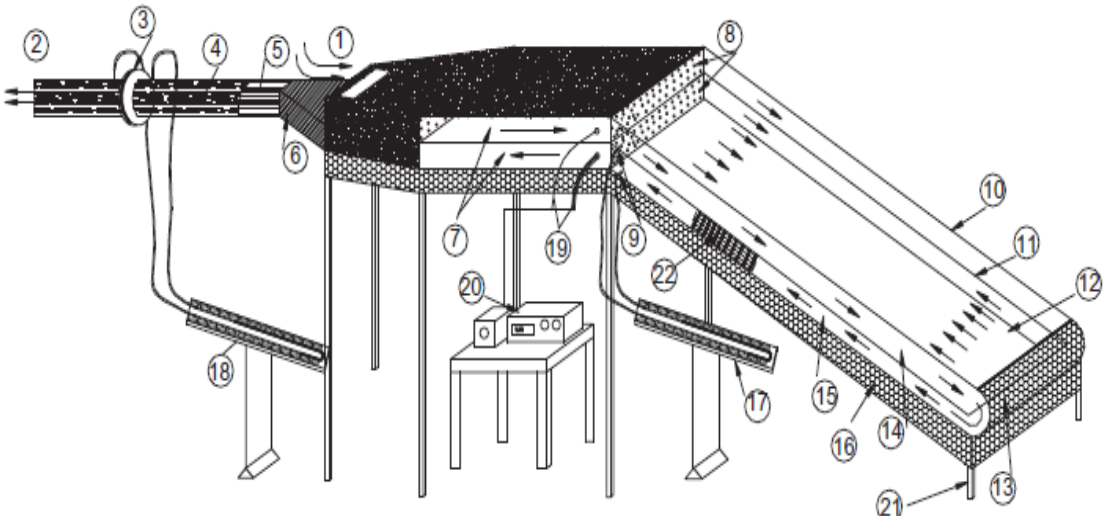

Figure 3.30. The schematic diagram of experimental set up.
(Source: Ramani et al. 2010)

Sopian et al. (2009) theoretically and experimentally evaluated the thermal efficiency of a double pass solar collector with porous and nonporous media. The testing facility consisted of a solar collector and a solar simulator (Figure 3.31). The simulator used 45 halogen lamps, each with a rated power of 300W. A maximum average radiation of 642 W/m2 could be reached with this simulator. The collector was of 2400 x 1200 mm in dimension. In the design of the collector, a single glass cover and a black painted aluminum plate were used. The solar collector was operated at varying inlet temperature and radiation conditions. The airflow rate was between 0.03 - 0.07kg/s, the upper channel depth was between 35-105 mm, and the lower channel depth was between 70-140 mm. The results of theoretical and experimental studies were compared based on the outlet temperatures and the thermal efficiencies of the solar collector. The study concluded that the presence of porous media in the second channel increased the outlet temperature. This also caused the thermal efficiency of the system to be increased.

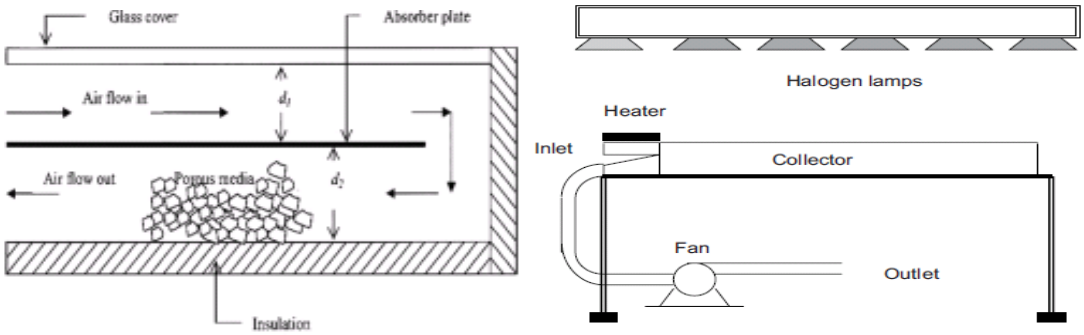

Figure 3.31. a.Schematic of double pass solar collector with porous media. b. Schematic of exp. set-up with solar simulator. (Source: Sopian et al. 2009)

Omojaro et al. (2010) investigated the thermal performance of single and double pass solar air heaters with fins attached (Figure 3.32). The lower channel of the double pass solar air heater filled with porous media acted as the absorber plate. The porous media was created by seven black painted steel wire mesh layers, each placed at 1 cm distance from the bottom to the top. The frame of the collector was made from 2 mm thick black painted plywood with dimensions of 1500 x 1000 mm. Double glass was used to cover the collector. The distance between the lower and upper glass was 30 mm. The distance between the lower glass and the bottom of the collector was 70 mm. By removing the upper glass cover, the system tested as a single pass solar air heater. Black painted metallic fins were used to increase the heat transfer area and were

installed longitudinally along the lower and upper channels. The fins were 1500 mm in length for both channels with heights of 70 and 30 mm for lower and upper channels, respectively. In this arrangement, both channels were divided into five equal sections for air passage. The mass flow rate varied between 0.012 and 0.038 kg/s. It was concluded that the flow rate of air affects the efficiency significantly. The efficiency of the system was enhanced with the increased flow rate of air. For the same flow rate, the efficiency of the double pass was found to be higher than the single pass. When the flow rate was 0.038kg/s, the efficiency of a single and double pass solar air heater was 59.62 and 63.74%, respectively. As a result, fin consolidated single or double pass air heater using steel wire mesh layers as absorber was found to be much more efficient when compared with conventional type heaters. It was found that a double pass solar air heater was about 7-19.4% more efficient than single pass solar air heater depending on the air mass flow rate. Furthermore, for a double pass solar air heater, increasing the height of the first pass decreased the thermal efficiency of the system.

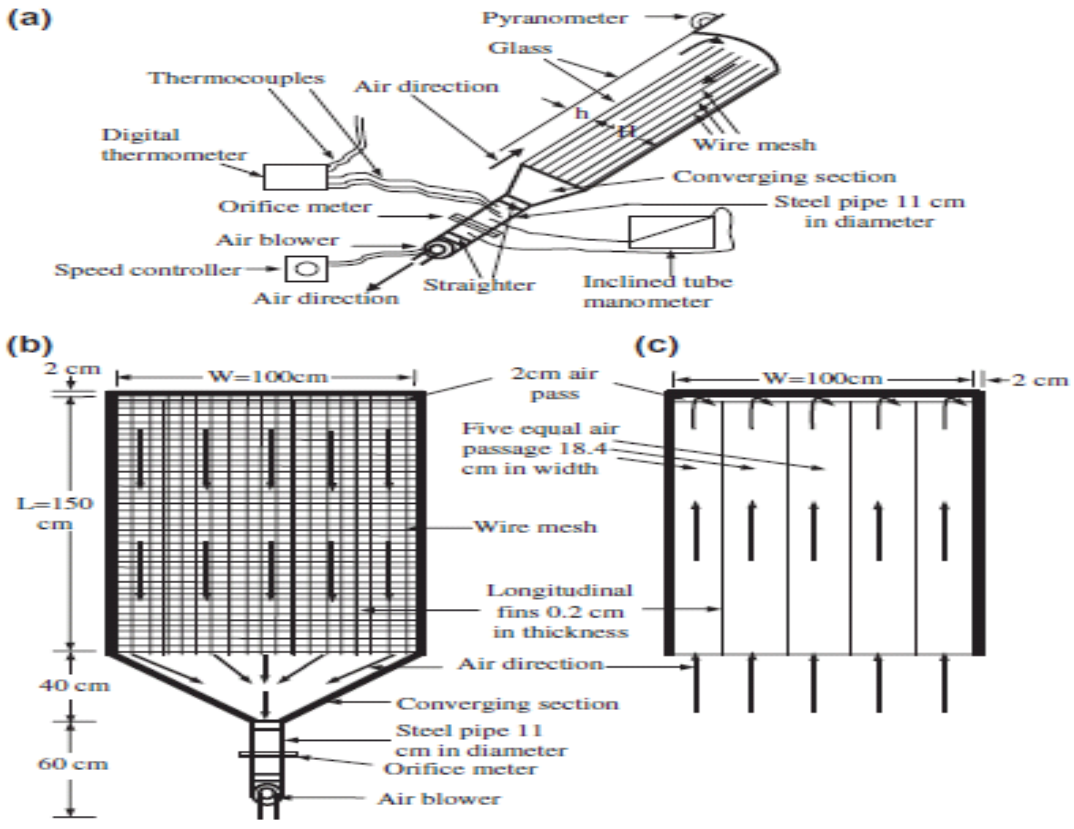

Figure 3.32. Single and double pass solar air heater showing: a. Schematic diagram of the experimental setup, b. lower pass channel, and c. upper pass channel. (Source: Omojaro et al. 2010)

Aldabbagh et al. (2010) experimentally investigated the performance of single and double pass solar air heaters with steel wire mesh layers. The set-up was constructed from 20 mm thick, black painted plywood with dimensions of 1500 x 1000 mm (Figure 3.33). Two normal window glasses with 4 mm thickness were used in the design of solar air heater. The distance between the upper and lower glass covers was 50 mm and the distance between the lower glass and the wire mesh layers was 100 mm. By removing the upper glass cover, the setup could be used as a single pass solar air heater. Ten black painted steel wire meshes were placed in the second channel of the collector. The wires were 2 x 2 mm in cross section and placed with a distance of 10 mm from each other. With this arrangement, the layers acted like an absorber so it was not necessary to install hence no another absorber plate in the solar air heater. During the experiments mass flow rate of the air was varied between 0.012 to 0.038 kg/s in order to observe the effect of mass flow rate on the efficiency of the system. It was concluded that by using steel wire mesh layers as the absorber plate, the efficiency of the collector could be enhanced when compared to the conventional type. Also, for both cases the efficiency of the system was enhanced with the increasing flow rate. For the mass flow rate of 0.038 kg/s, the maximum efficiencies for the single and double pass solar air heaters were 45.93 and 83.65% respectively

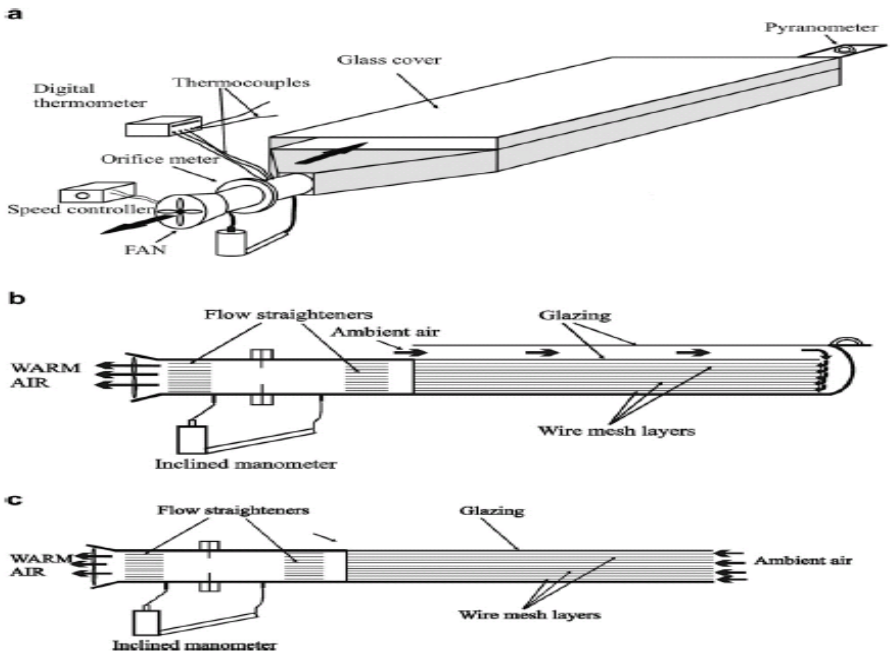

Figure 3.33. Schematic assembly of the a. double pass SAH, b. side view of the double pass SAH and c. side view of the single pass SAH.(Source: Aldabbagh et al.2010)

3.1.4. Single Flow Recycled Double Pass Studies

Ho et al. (2005) theoretically and experimentally investigated the performance of a double pass recycled solar air heater. The velocity of air was increased to enhance the efficiency of the solar air heater. They aimed to investigate the effect of recycling on collector efficiency based on the recycle ratio and to perform mathematical formulation of the recycled double pass solar air heater. In addition, the effect of the height of absorbing plates in the channel was investigated. An experimental set-up with two glass covers was used (Figure 3.34). It was of 300 x 300 x 50 mm in dimension. The blackened absorbing plate was inserted at the center of the collector, resulting in equal heights (50 mm) for each channel. It was found that the added recycle unit improved the efficiency of the double pass solar air heater. The performance of the double pass solar collector was enhanced as a result of the increased air velocity and the heat transfer coefficient by the recycling operation or by decreasing the equivalent diameter of the channel. The external recycling enhanced the efficiency of the collector by approximately 28-95% compared with the arrangements of sub-collectors connected in series. Although the recycle operation enhanced the convective heat transfer it reduced log mean temperature difference between the absorbing plate and the air stream.

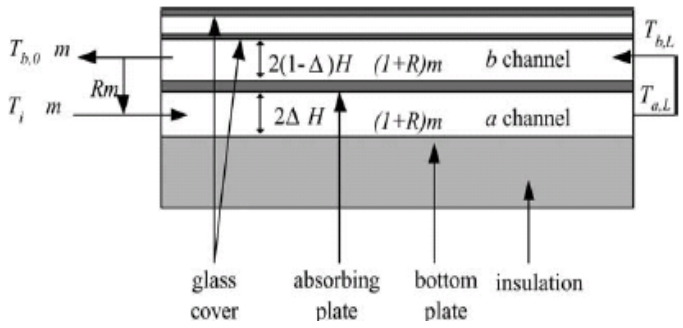

Figure 3.34. Double pass flat solar air heater with recycle.
(Source: Ho et al. 2005)

Ho. et al. (2009) theoretically and experimentally investigated the effect of recycling on baffled double pass solar air heaters with attached internal fins. The study was carried out with artificial simulation. An experimental setup was constructed from stainless steel with a thickness of 0.07 mm (Figure 3.35). The system was insulated with 60 mm thick Styrofoam. The system was of 300 x 300 x 50 mm in dimensions. Two

glass covers were used as glazing. The absorber plate was blackened and finned on both sides. At the same time, the system included baffles which were welded on fins. The air inlet temperature was controlled by a preheater and fixed at 30°C. Three different mass flow rates were used in the experiment; 38.52, 57.96 and 77.04 kg/h. The results were compared with the results of a single pass solar air heater without a recycle. It was concluded that the collector efficiency was significantly enhanced with baffled double pass solar air heaters with recycle. The collector efficiency increased with the increased mass flow rate and the recycle flow.

a

b

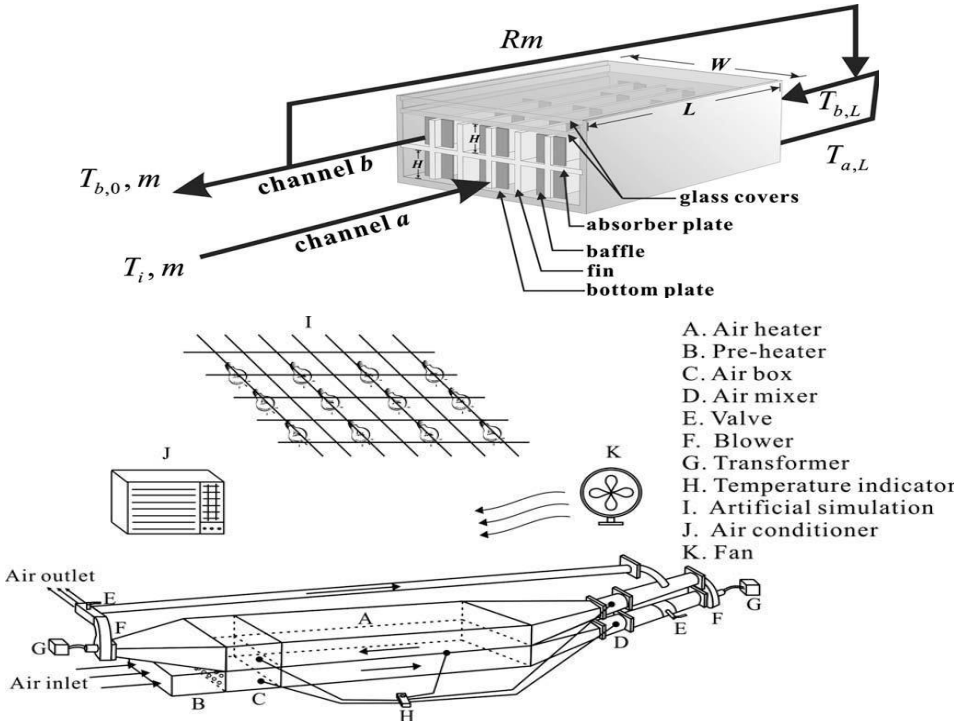

Figure 3.35. a.The baffled solar air heater with internal fins attached and external recycle b.Schematic diagram of a solar air heater with artificial simulation. (Source: Ho et al. 2009)

3.2. Studies According to Air Channel Design

There are two classifications performed in this study. The 45 reviewed papers are classified according to the two titles explained above. Some of the papers referred to above can also be classified under this title. For simplicity, their reference numbers and author names only are given.

3.2.1. Flat Plate Studies

The publications of Mohseni-Languri et al.(2009) and Al-Kamil et al.(1996) that were reviewed above are also examples of flat plate solar air heaters.

3.2.2. Extended Surface Assisted Studies

The publications of Peng et al.(2010), Pakdaman et al.(2011), Sahu et al.(2005), Yeh et al.(2002), Hachemi (1999), Akpınar et al.(2010), Esen (2008), Hans et al.(2010), Karmare et al.(2009), Moummi et al.(2004), Kumar et al.(2009), Bopche et al.(2009), Bhagoria et al. (2002), Layek et al. (2009), Jaurker et al.(2006), Karwa et al.(2001), Momin et al. (2002), Aharwal et al.(2009), Aharwal et al. (2008) that were reviewed above are also examples of extended surface assisted solar air heaters.

3.2.3. Porous Media Assisted Studies Studies

The publications of Sopian et al. (20099, Varshney et al.(1998), Ramani et al.(2010), Prasad et al.(2009), Omojaro et al.(2010), Aldabbagh et al.(2010) that were reviewed above are also examples of porous assisted solar air heaters.

3.3. Studies on Special Designs

Kiatsiriroat et al. (2007) experimentally studied the heat transfer enhancement of a flat plate solar air heater using an electric field. The aim of the study was to investigate the effect of electrode spacing and Reynolds number on the performance of the solar air heater. The experiments were conducted with and without electric field under steady state conditions with a solar radiation range between 840-1100 W/m2. An experimental setup was designed and constructed as shown in Figure 3.36. The dimensions of the flat plate solar air heater were 1200 x 1800 x 50 mm with a collector area of 2.16 m2. The flow channel was positioned at the back of the absorbing plate. Nine electrodes with diameters of 0.5 mm were installed and used in the experimental setup. The electrodes were tested with three different spacing arrangements; 50, 100 and

150 mm. The electric field was generated by a high-voltage generator so each electrode wire operated with 0–25 kV voltage. The enhanced ratio of the solar air heater to the use of electric field was calculated using the Equation 3 below where QEHD is the heat transfer rate of solar air heater under the electric field, while QNON-EHD is the heat transfer rate of solar air heater without the electric field and P is the energy consumption of the high voltage supply. It was concluded that the electric field enhanced the heat transfer rate significantly at low Reynolds numbers

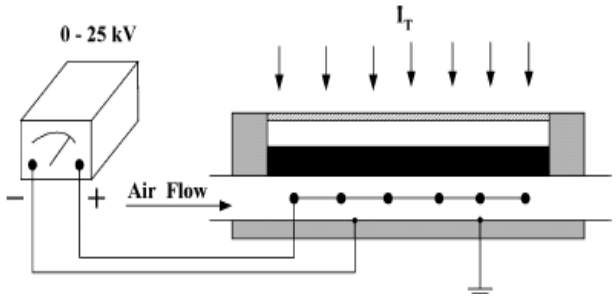

$$Enhanced\ ratio = \frac{Q_{EHD} - P}{Q_{NON\_EHD}}$$

Figure 3.36. The schematic sketch of the solar air heater operating under an electric field (Source: Kiatsiriroat et al. 2007)

Othman et al. (2006) theoretically and experimentally studied a hybrid photovoltaic-thermal (PV/T) solar air heater. The solar air heater was a double pass system with monocrystalline silicon cells pasted on the absorber plate with fins attached on the other side of the absorber plate in the second channel (Figure 3.37). The collector was 850 mm in width and 1220 mm in length. The upper channel was 165 mm in height and the lower channel height varied between 30 to 120 mm. The installed solar cells were 110 mm in both width and length. The absorber plate was a black painted aluminum sheet with an emissivity of 0.9. The experiments were conducted under a solar simulator which included 23 tungsten halogen lamps each rated at 500 W. The air flow rate varied from 0.027 to 0.181 kg/ s which were in the turbulent flow region. The system generated electricity and heat energy simultaneously. It was concluded that using fins in the design of the hybrid PV/T collector improved both thermal and electrical efficiencies. A steady-state solution was obtained to determine the outlet and mean photovoltaic temperature. The comparisons between theoretical and experimental studies were in a good agreement with each other

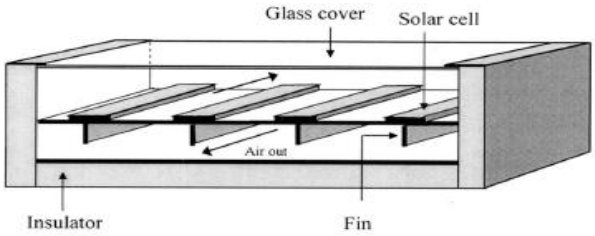

Figure. 3.37. Schematic model of a finned double-pass photovoltaic-thermal solar air heater. (Source: Othman et al. 2006)

Gao et al. (2007) experimentally analyzed the thermal performance of cross-corrugated and flat-plate solar air heaters. Both absorbing and bottom plates of the analyzed solar air heaters were cross-corrugated to enhance the turbulence and consequently the heat transfer rate inside the air flow channel. Three solar air heaters with different designs were investigated in their study. In the first type of collector, the wavelike absorber was fixed along the air flow direction while the wavelike bottom plate was fixed perpendicular to the flow direction (Figure 3.38). In the second type of collector, both plates were fixed in opposite directions to the first collector. The third type of collector had flat absorbing lower plates. The comparison of these three collectors was considered necessary in order to achieve improved efficiencies. In all collectors, single normal glass cover was used. The collector dimensions were 2000 x 1000 x 80 mm. The efficiencies of the first and second corrugated solar air heaters and the flat plate-type heater were obtained as 58.9%, 60.3% and 48.6%, respectively. The efficiency calculations were performed using Equation 4 below. The study indicated that use of the cross-corrugated wavelike absorption and bottom plates improves the efficiency of solar air-heaters. The convective heat-transfer coefficients on the absorbing plates were found to be 28.6 W/m2K for corrugated type collectors, and 8.8 W/m2K for flat plate type collectors. In addition, the effects of selective coatings on the solar air heaters were investigated and it was found that the selective coatings increase thermal performance of the heaters and its use was strongly recommended for practical applications.

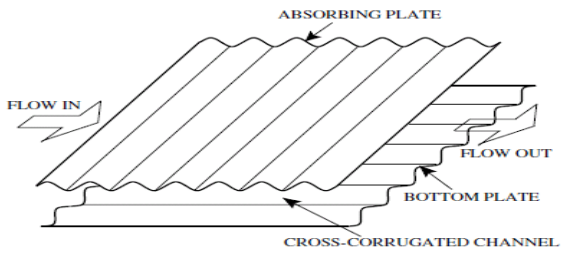

Efficiency :

$$\eta = \frac{q_u}{I} = \frac{c_p * \dot{m}_f * (T_{fo} - T_{fi})}{I} =$$

$$\eta = \frac{2 * c_p * \dot{m}_f * (T_{fo} - T_{fi})}{I}$$

Figure 3.38. Schematic description of the cross-corrugated absorbing plate and bottom plate (Source: Gao et al. 2007)

Enibe (2002) produced a single pass flat plate solar air heater integrated with phase change material (PCM) heat storage system. He used paraffin type prepared in modules. The solar collector heater was single-glazed with dimensions of 1635 x 945 mm. The absorber plate was made of steel with a non-selective coating. The modules were placed through the collector as shown in Figure 3.39. The modules behaved like fins and the spaces between them behaved like air heating channels. The experiments were conducted over the ambient temperature range of 19-41°C and a daily global irradiation range of 4.9-19.9 MJ/m^2 for 14 different days in May and June usually between the hours of 6:30 and 18:30. The efficiency of the collector was calculated using Equation 5 below. It was found that for solar collectors with storage, when the cumulative efficiency includes the time integral of energy it was a more useful measure of performance than the instantaneous efficiency. Peak temperature rise of the heated air was about 15K, while peak cumulative useful efficiency was about 50%.

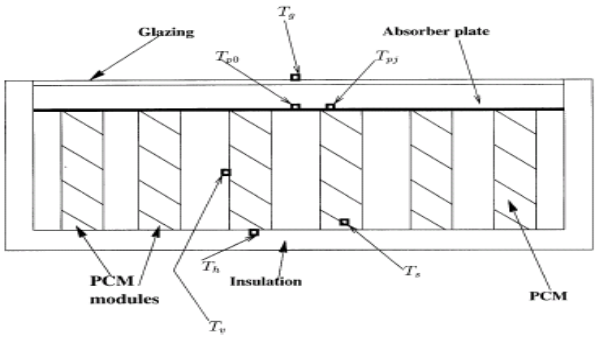

$$\eta_{uc} = \frac{\int_0^t \dot{m}_a c_a (T_3 - T_a)\, dt}{A_c \int_0^t G_T\, dt}$$

Figure 3.39. Cross-sectional view of the collector assembly.
(Source: Enibe 2002)

Koyuncu (2006) experimentally and theoretically studied the performance of various design of solar air heaters for crop drying applications, (Figure 3.40). He aimed to determine a cheap an easily manufactured and a high efficiency solar air collector for low temperature crop drying applications. The first model was a single plastic glazing, black painted hardboard absorber and front-pass (i.e., air flows between absorber and glazing plates). The second model was a single plastic glazing, black painted flat plate absorber on hardboard and front-pass. The third model was a single plastic glazing and front-pass, but with a black painted zigzag plate absorber. The fourth model was identical to the second model (single plastic glazing and black painted flat plate absorber) however air is allowed to flow in the channel between the back side of the absorber and the hardboard insulator (i.e. back pass). Similarly, the fifth model had the same structure as the third model collector except for the back pass flow arrangement.

Finally, the sixth model mainly consisted of double plastic glazing, a black painted flat plate absorber and a back-pass flow arrangement. The absorber plates were made of black coated aluminum sheet. A clear plastic glazing made of polyethylene with a thickness of 0.15mm was also used. The experimental results indicated that the most efficient collector was the second model whose efficiency was approximately 9% greater than the least efficient one which was the sixth model. Additionally, it was concluded that the effect of the shape of absorbing surface on performance was considerably less than the number of glazing sheets and the air pass arrangement.

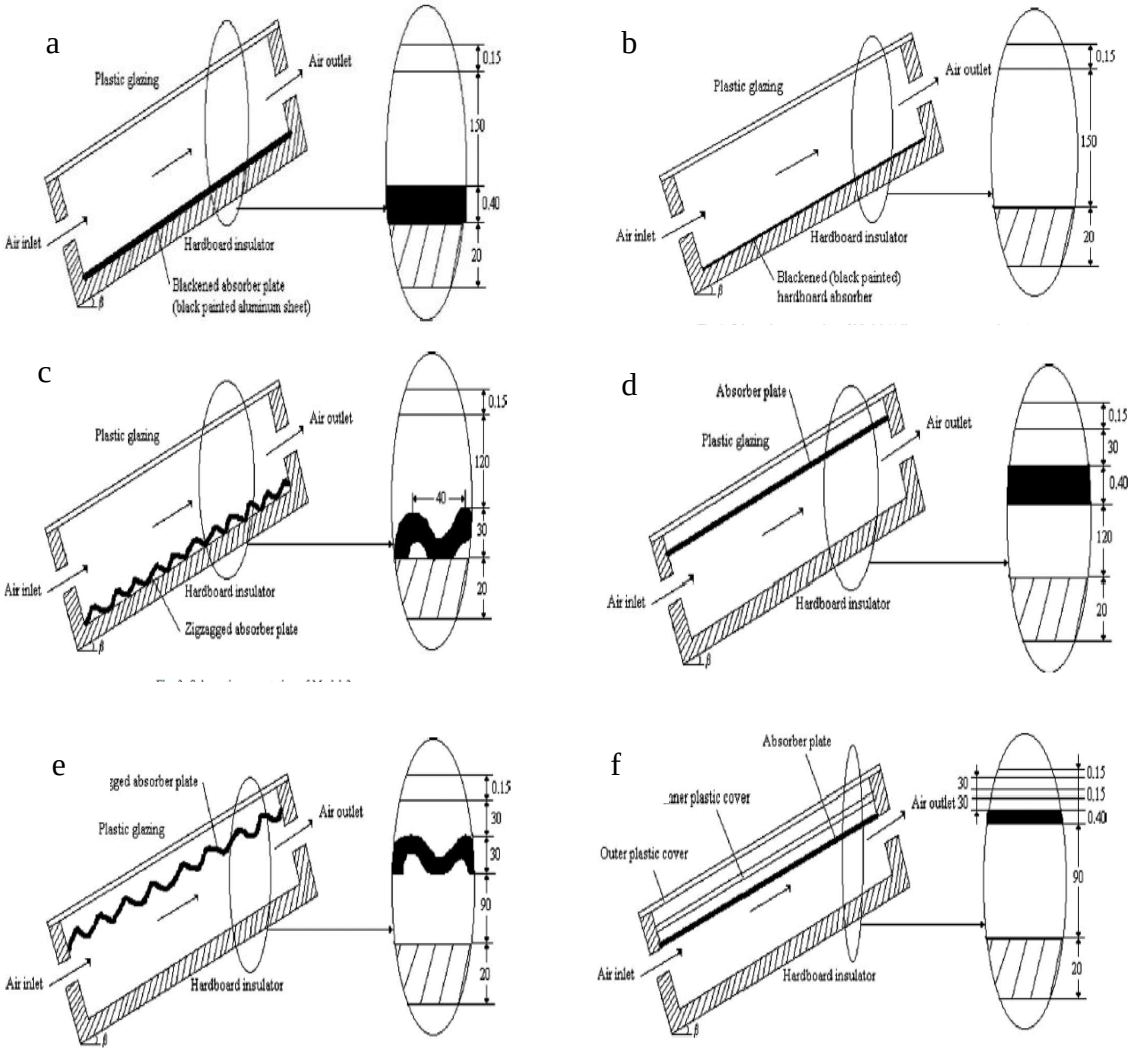

Figure 3.40. a.Schematic presentation of Model 1 b.Schematic presentation of Model 2 c.Schematic presentation of Model 3 d.Schematic presentation of Model 4. e.Schematic presentation of Model 5 f.Schematic presentation of Model 6. (Source: Koyuncu 2006)

Karim et al. (2004) conducted an experimental study to evaluate the thermal performances of three types of solar air heaters; a simple flat plate, finned and V-

corrugated solar air heaters. The aim of their study was to achieve the most efficient design of solar air collector suitable for solar drying. Three types of collectors were designed, constructed and tested (Figure 3.41). In order to avoid construction of several solar air collectors for different absorber plate configurations, a collector frame with interchangeable absorber plates was designed. The absorber plate of each collector was 1800 m in length and 700 m in width, and made of stainless steel with black chrome coating. The flat plate and finned collectors had 25 mm channel height and the V-corrugated collector had 50 mm V-height. The flow passage area was 0.0175 m2 for all three collectors. Single window glass was used as the glazing for all the collectors. The results showed that the V -corrugated collector was the most efficient collector and the flat plate collector had the least efficiency. The efficiency of the V -corrugated collector was 7-12% higher than that of the flat plate collectors. The constructed collectors were also tested in double pass mode to investigate the improvement in efficiency. As expected, a significant improvement of efficiency was achieved in the collectors with double pass operation when compared to the single pass operation. Consequently, the V -corrugated collector showed better efficiency in both single and double passes operations. It was also structurally stable and predominantly useful for drying applications.

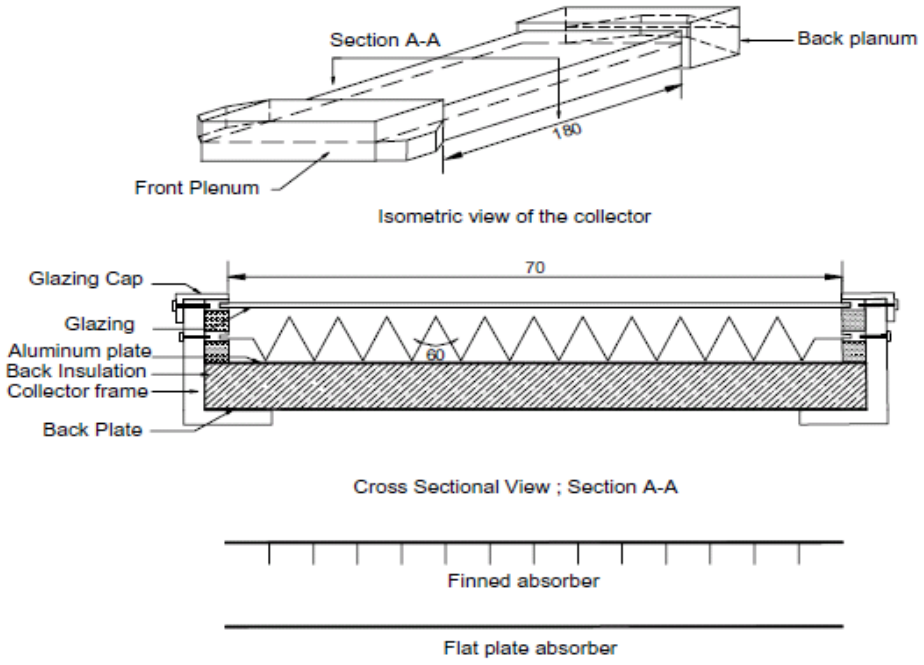

Figure 3.41. Collector frame and three types of absorbers.
(Source: Karim et al. 2004)

Kurtbas et al. (2004) analyzed the efficiency and exergy of a solar air heater. In order to investigate the effect of flow line dimensions of a solar collector on its performance, an absorber was designed with four different plates. The absorber of 900 x 400 mm was in dimension and the plates were in different flow line dimensions (narrowed-extended) and surface geometries (Figure 3.42). The absorber material was a black painted galvanized sheet with 0.8 mm thickness. In the Type I plate, the fluid passed through a narrowed-extended gap. The dimension of the gap was between 25 to 180 mm. The upper surface of the Type II plate had a wavely profile while the bottom surface had a flat profile. The Type III plate had a wavely profile plate with a gap of 25 mm between the plates. Finally, the Type IV had a flat absorber with a gap of 25 mm between the plates. During the experiments five slices were placed perpendicular to the flow direction in dimensions of 1000 x 2000 mm inside the collector. Single glass was used as glazing and air flow was supplied with a radial fan up to 0,31 m3/s. It was concluded that, with an increase in the mass flow rate the efficiency of the collector increased. The efficiency of the collector significantly depends on the surface geometry of the collector. The pressure loss and the heat transfer increased as the roughness of the absorber surface increases.

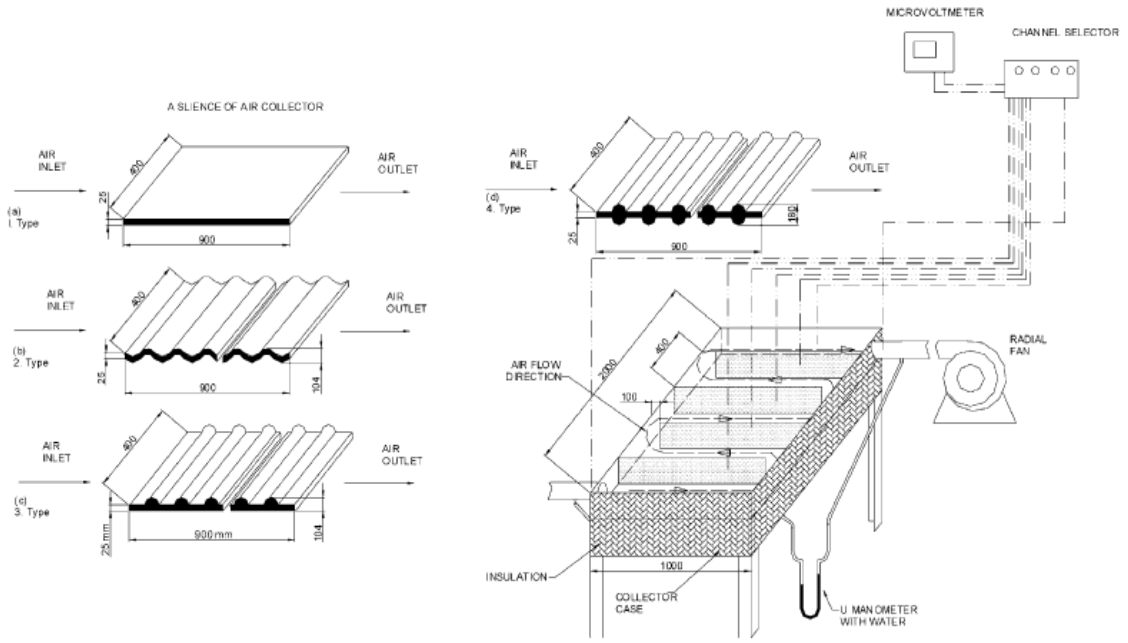

Figure 3.42. Experimental set-up.
(Source: Kurtbas et al. 2004)

Togrul et al. (2004) , studied the performance of a solar air heater with a cylindrical absorber which is fixed to the center of a conical concentrator. They aimed

to enhance the air outlet temperature of solar air heater when compared to a flat plate collector. The solar air heater system they examined included a conical concentrator, a cylindrical absorber, a movable main air tube, a 1-D sun-tracking system, an electronic control device and a temperature-recording unit (Figure 3.43). The conical concentrator was made from stainless steel and painted black on the outer side. The absorber was a copper tube mounted at the center of the conical concentrator. The absorber was a two pass heat exchanger rounded with a glass tube. The copper absorber tube was tested with both a selective and a nonselective paint. The experiments were conducted with a mass flow rate of 7.5 kg/s. In order to ensure sunshine for the entire duration of the experiment two motors rotated the system according to the sun. The movements of the motors were achieved with two photocells which were fixed on top of absorber. These two motors worked alternatively. It was concluded that, with a conical concentrator, the efficiency and air temperature were increased to 12% and 150°C respectively.

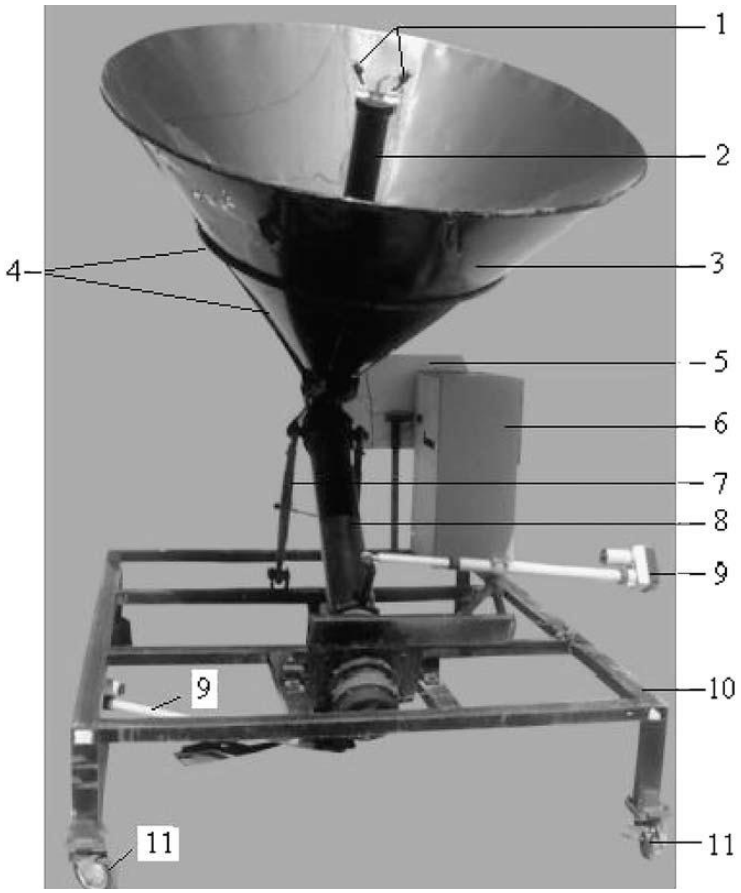

Figure. 3.43. Solar air heater with conical concentrator. 1, Photocells; 2, absorber; 3, conical concentrator; 4, conical concentrator supporting frame; 5, tracking unit; 6, temperature measurement unit; 7, the ars for setting tilting; 8, main air flow tube; 9, moving arm and driving system for tracking; 10, collector table; 11, wheel.(Source: Togrul et al.(2004)

As a result of this literature survey, the researches' that are investigated in recent years, studied carefully in a detail way. The construction choices, the purposes of other researches', the results of such approaches are determined. Some items about the experimental setups like the dimensions, the materials, the testing procedures are investigated clearly. Based on this data from all these searched papers, the experimental setup that will be constructed and tested for this thesis is took its shape of configuration.

CHAPTER 4

EXPERIMENTAL SETUP

A *"Solar Air Heater"* was constructed to determine and compare the efficiencies of solar air heater systems with or without porous material. The experimental setup was located at Solar & Wind Laboratory in the Mechanical Engineering department of İzmir Institute of Technology. The experiments were conducted between November 2011 and August 2012. The experiments were carried between the hours of 08:30 and 17:00 or 20:00 each day.

All parts of this experimental setup are made from galvanized steel. The system is insulated from all sides to prevent heat losses through the surroundings. Air is supplied to the system with the help of a radial fan with forced convection. The flow rate of the fan is controlled and manipulated by a control panel. Solar radiation is simulated by a jacket type electrical heater placed under the solar air collector. The temperature profile of the air across the channel is observed by k-type thermocouples. The data taken by the thermocouples is transferred to a computer with the help of a data logger. Each part will be discussed separately and in detail in the next section.

Figure 4.1. Photograph of the Experimental Setup

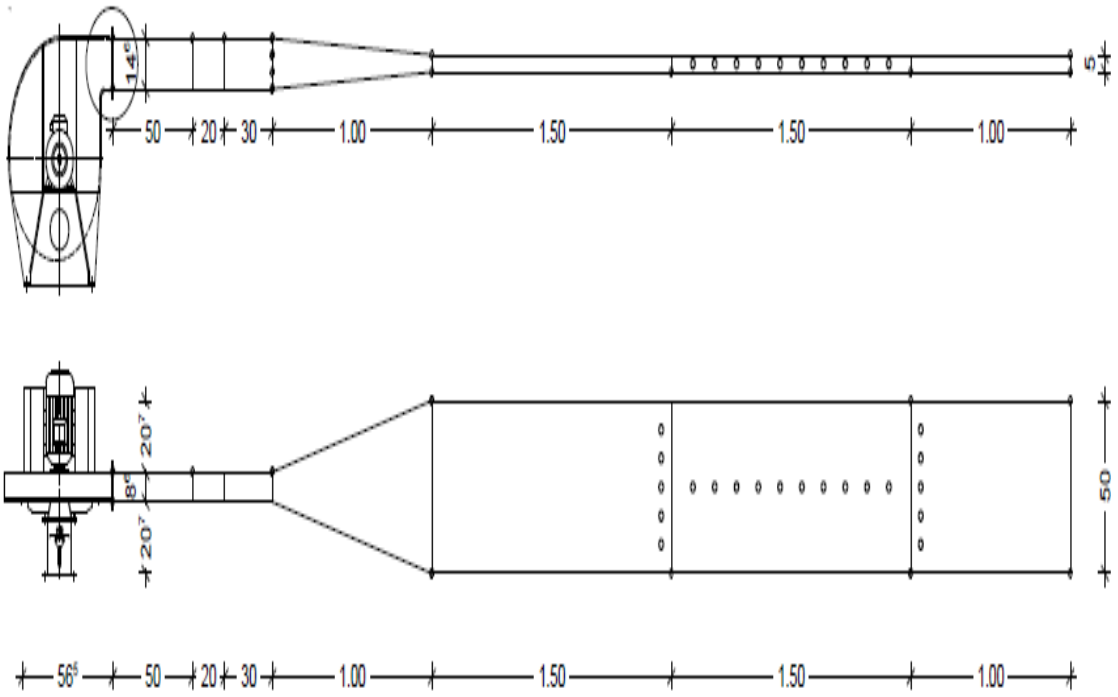

Figure 4.2. Side and Top View of Experimental Setup Schematically.

4.1. Components of Experimental Setup

All parts of this experimental solar air heater are made from steel. The system is insulated from all of its sides to prevent heat losses through the surroundings. Each part is explained below.

4.1.1. Radial Fan

Air is supplied by a radial fan to the experimental setup. The volumetric flow rate and the pressure drop of the fan are 600 m^3/h and 1.5 kPa(150 mmSS), respectively. Two silencers are fixed at both sucking and exhaust sides of the fan to reduce the noise. The technical dimensions and a photograph of the radial fan are given in Figure 4.3. The flow rate is varied between 0-600 m^3/h with the help of a control box during the experiments in order to observe the effect of mass flow rate on the efficiency of a solar air heater.

a

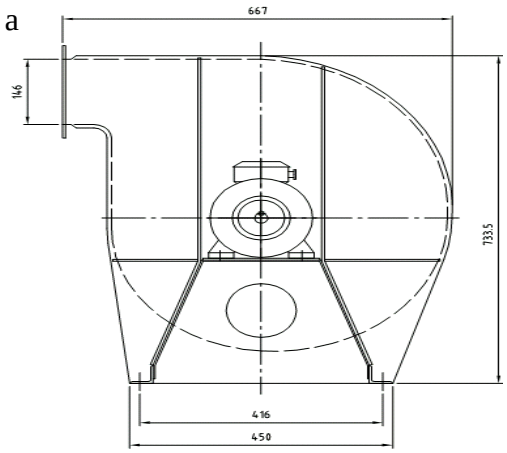

b

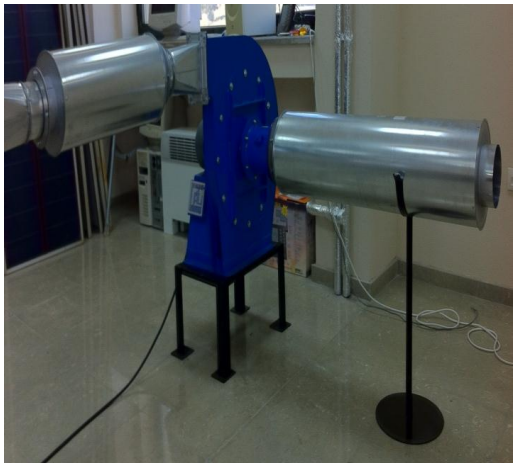

Figure 4.3. a. Technical dimensions of the radial fan, b. Photograph of the radial fan

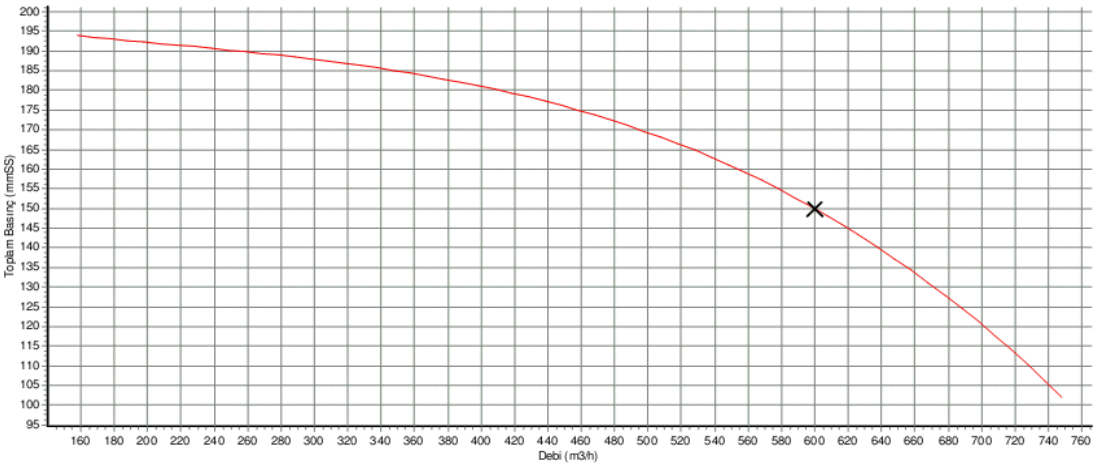

Figure 4.4. Characteristic Trend line of the Radial Fan

4.1.2. Preheater

If it is possible experiments should be done under same operating conditions for an accurate measurement and comparison of the experimental results. By adding this equipment to the system, it was aimed to feed the air to the collector at the same temperature for each experiment. In this system a preheater is located after the radial fan. As air flows through the duct which the preheater was fixed, its temperature could be maintained to a fixed temperature before it enters the collector. But unfortunately, this part of the system cannot be used during the experiments. Because, controlling this part manually cannot be possible; the temperature change cannot be controlled efficiently.

Figure 4.5. Photograph of the preheater.

4.1.3. Flow Straightening & Exhaust Type Duct

The flow straightening duct is a clear channel which enables a fully developed flow for air for dimensions of 1500 x 500 x 50 mm (Figure 4.6.a) Until air reaches the solar collector it passes from various dimensioned ducts. This makes the flow turbulent. As the velocity data are collected from this part of the solar air heater, the flow must be fully developed in every part of the duct. For this purpose the flow straightening duct could be considered as the distance that is left for air to become laminar for the accuracy of measurements.

The exhaust type duct was constructed just before the flow straightening duct and used to provide the dimensional changeover between the flow straightening duct and the duct that includes the preheater. The preheater was fixed after to the fan outlet side so the duct that includes the preheater was in the same dimensions of the fan's outlet. The flow straightening duct was placed just before the main solar collector so this duct is of the same dimensions as the collector. Here, the exhaust type ducts provides this pass (Figure 4.6.b).

Figure 4.6 a. Flow straightening duct, b. Exhaust type duct

Flow straightener equipment was added to the inlet section of this duct as seen in Figure 4.7. The aim was to balance the forces between the front and back of this material and obtain a uniform air flow. The velocity profile is be similar in all domains of collector.

Figure 4.7. The flow straightener

4.1.4. Solar Collector

The solar collector is of 1500 x 500 x 50 mm in dimension (Figure 4.8). It is a laboratory simulation model so the upper side is made from steel, not from a transparent cover. Basically, the collector is a rectangular duct where the temperature of air increases as it flows through. The underside of the collector is the absorber plate. It can be made from different materials, but in this case it was made from the same material as the collector itself. Since the system was constructed in a laboratory, the solar radiation is simulated by an electrical heater. The electrical heater could supply a maximum power of 15 kW and is fixed to the bottom of the absorber plate of the collector. The flux of the electrical heater could be manipulated from the control panel according to experimental conditions. The temperature of air is measured along the length and width of the collector during the experiments.

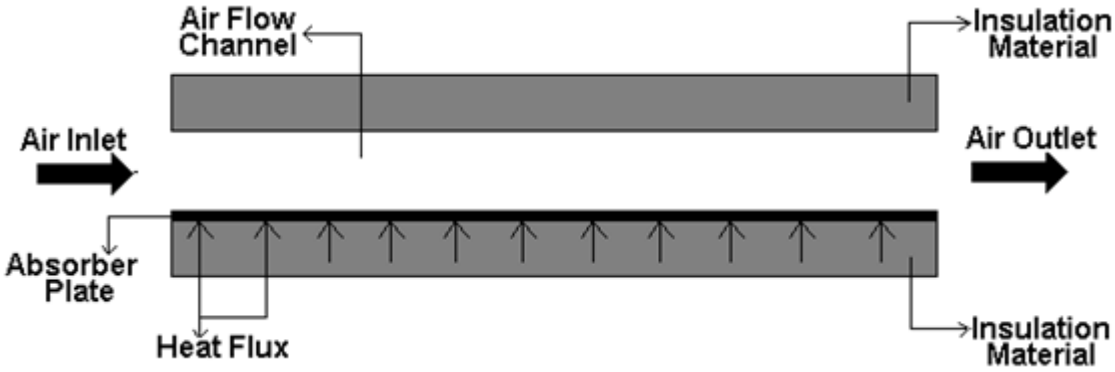

Figure 4.8. The schematic view of the collector

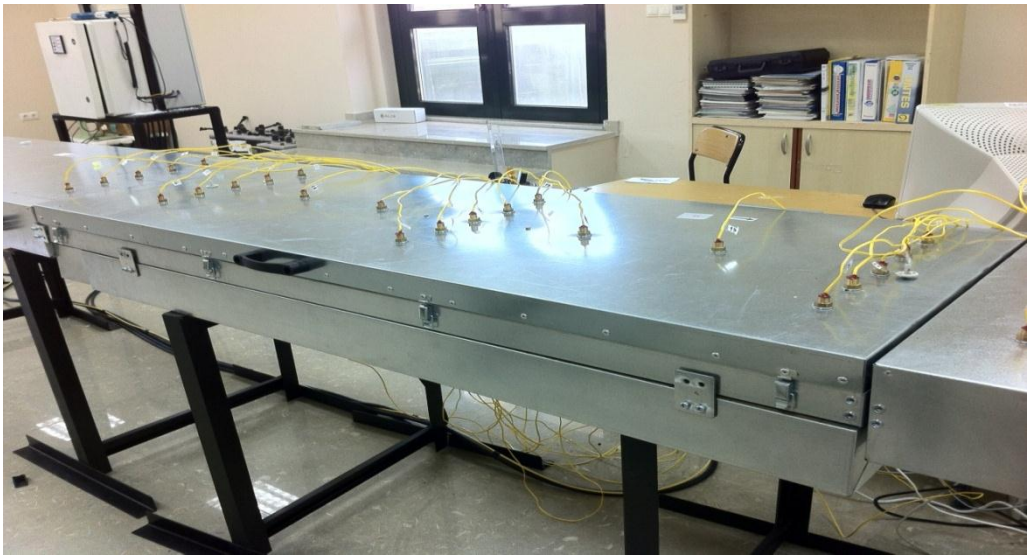

Figure 4.9. Photograph of the Solar Collector

4.1.5. Porous Material

The porous material, which is like a wire mesh with 50 x 50 mm square dimensions, is illustrated in Figure 4.10 below. The porous material was placed in the collector after the reference experiments were completed with a clear solar air collector channel to enable comparison of results with and without porous material. When air enters the collector, it encounters the porous material and flows over and under it. This method increases the heat transfer area and forms a turbulent flow. The collector was tested with different porosities to reach the optimum heat transfer and collector efficiency.

Figure 4.10. Photograph of porous material

4.1.6. Exit Duct

The dimensions of this part are 1000 x 500 x 50 mm (Figure 4.11). This is the last part of the solar air heater system. Air enters the solar collector and exits with a significant increase in its temperature. Then air enters the exit duct and is released outside. At the beginning of the exit duct there were 5 thermocouples to control the temperature change of the air as it exits the electrical heater. Because of the accuracy of these measurements, the duct's length is kept at 1000 mm to prevent probes from the conditions of the outlet.

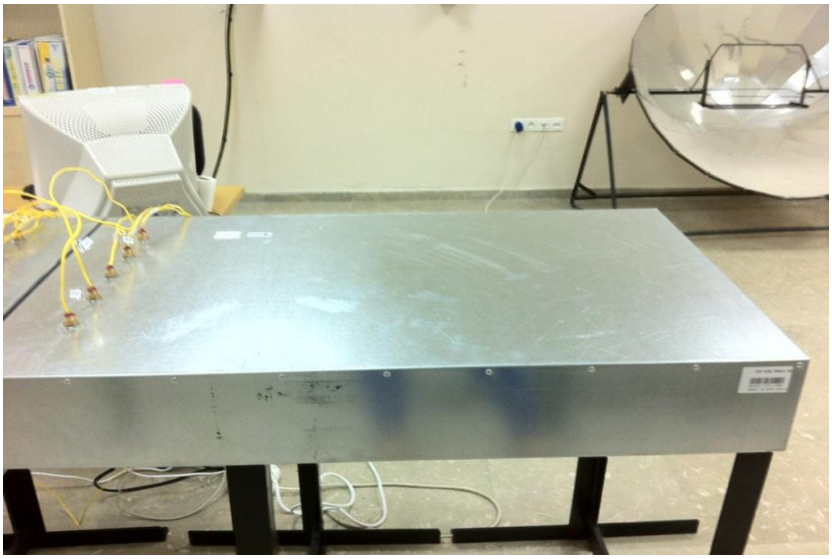

Figure 4.11. Photograph of the Exit Duct

4.2. Measurement Equipment

4.2.1. Data Logger

In this study, an ELİMKO E-380 model data logger is used. This data logger has 32 channels which are used to measure temperature data. With the help of this device the temperature values along the collector are saved during the experiments. The data logger is connected to a computer and a software program was installed to store the temperature values for each part of the experiment separately. For each experiment the data was initially taken during time intervals of 30 minutes then, in order to collect more data, this was shortened to 5 minutes intervals.

Figure 4.12. Photographs of the data logger

4.2.2. Temperature Sensors / Thermocouples

The temperature profile during the experiments is achieved by the thermocouples which are located along the length and width of the collector. K type thermocouples are used in the setup. The k-type thermocouples are composed of a positive portion, which is approximately 90% nickel and 10 chromium and a negative portion, which is approximately 95% nickel, 2% aluminum, 2% manganese and 1% silicon. The negative portion is colored red and the positive portion is colored yellow.

The k-type thermocouple wire used is a 1000 ft long roll. The roll is shortened to obtain 32 thermocouples according to the needs of the experimental setup. The thermocouples can read values between -200 to 1350 °C with an error of ±2. One side

of each thermocouple is plunged into the duct while the other side is connected to the data logger. A total of 29 thermocouples are used to measure the air temperature while the other 3 are used to measure the absorber plate temperature. The data taken with the help of k-type thermocouples are transmitted to the computer by means of a data logger.

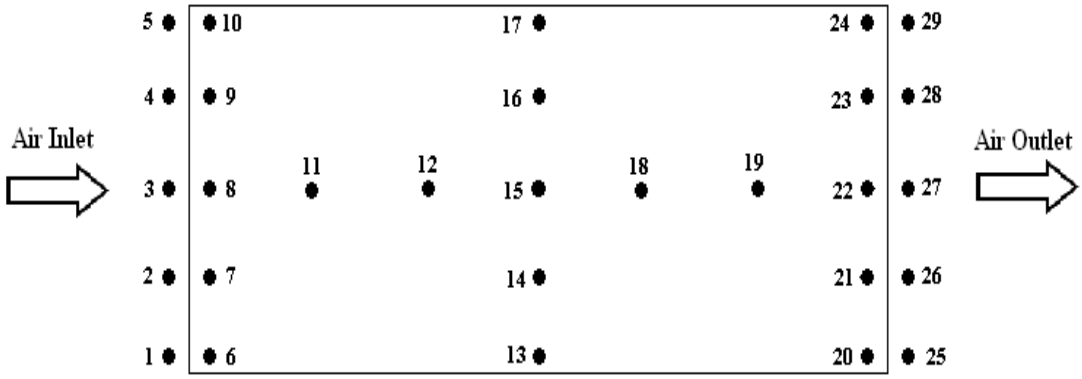

Figure 4.13. Location of Thermocouples which were used to measure the air temp.

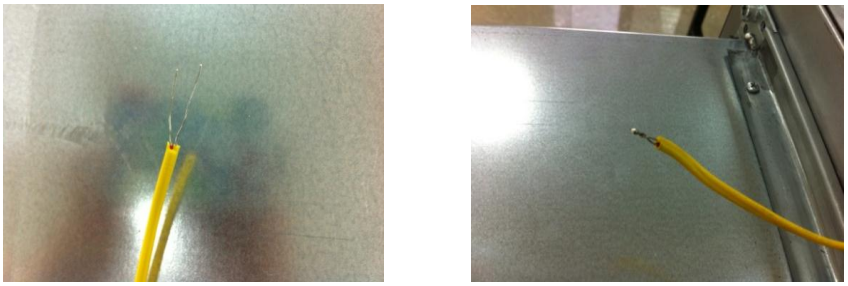

Figure 4.14. Photograph of the thermocouples (original and welded tip)

4.2.3. Velocity Calculator

The velocity measurement is performed using a TSI 8386-M Velocity Calc Plus device as illustrated in Figure 4.15 below. For an accurate measurement, 5 velocity measurement holes are opened on the top side of the flow straightening duct of the solar air heater system (Figure 58.a). The probe of the velocity calculator device is plunged into the flow duct from each of these holes sequentially. The velocity data are taken vertically from 6 different heights for each five holes. By this method, 30 velocity values are obtained along the duct, horizontally and vertically. Each velocity value is multiplied by the differential area that it measured in the collector. These multiplications were added to each other and then divided by the total cross sectional

area of the collector to find an average velocity value for the flowing air. The average velocity was then used in the power and efficiency calculations.

a 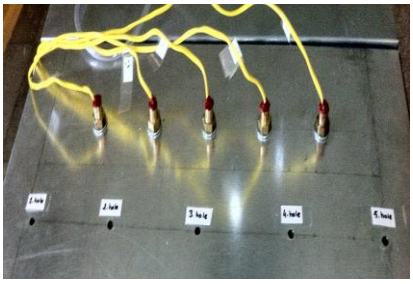 b 

Figure 4.15. a.The measurement holes b. Velocity Calculator

4.2.4. Control Panel and Network Analyzer

The control panel of the solar air heater system is constructed to manipulate the flow rate of the fan, the power of the preheater and the panel electrical heater which simulates solar radiation. There is an on-off switch on the control panel box that provides the main electricity supply to the system and the control panel. There are three buttons that help to manipulate the working efficiencies of these three parts between zero and a hundred percent efficiency (Figure 4.16.a).

The network analyzer device is used to measure the power that the panel electrical heater consumes during the experiments. But, because of the discontinuous working of the electrical heaters which was caused by the P.I.D control, the consumption cannot be measured accurately. The network analyzer shown in Figure 4.16.b was found to be suitable for this purpose and was connected to the system. This device measures the electricity consumed during the experiment hours in kWh unit. Then by multiplying the value which was taken from this device at the end of the each experiment by the total experiment hours, the heat value in kW can be obtained.

a  b 

Figure 4.16. a. Control Panel b. Network analyzer

4.2.5. Thermocouple Calibrator

The heat consumed by the electrical heater and the heat gained by the hot air is compared for each experiment. The results are expected to be similar. But for every experiment there are significant difference between the two values. The heat losses to the surroundings from the system surfaces causes this difference. For every experiment, the temperature of each surface are measured by the network analyzer device and then the losses were calculated.

Figure 4.17. The Temperature Calibrator

CHAPTER 5

EXPERIMENTAL PROCEDURE AND HEAT TRANSFER CALCULATIONS

In this thesis, enhancement of heat transfer in a solar air heater by using porous medium is experimentally investigated. A laboratory simulation model is constructed and tested in different conditions and configurations to achieve a significant enhancement in heat transfer.

5.1. Experimental Procedure

All the experiments begin at 09:00 a.m. and end at 05:00 p.m. or 08:00 p.m. The computer and the assistant program of the data logger are kept open during the experiments to collect and save the data. Firstly, the on-off switch located on the control panel, is set to the "on" position to give the system energy. Than to start the air flow, the switch of the fan is switched to "1-on" position (Figure 5.1). With this action the fan is ready to blow and the final task is to manipulate the capacity of the fan between 0 to 100 % with the capacity button.

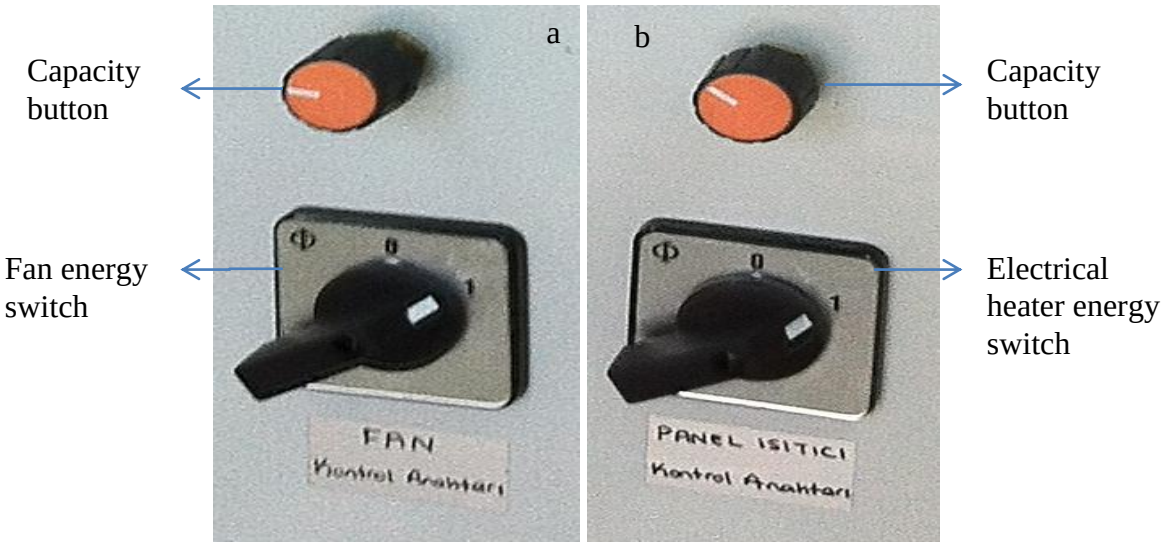

Figure 5.1. The capacity and energy buttons of a. the fan b. the electrical heater

The same procedure is followed for the panel electrical heater. The energy is provided by adjusting the energy switch and then the capacities are again adjusted by capacity button.

The electrical heater works with the same capacity for all experiments. It is adjusted to a position where the air outlet temperature is close to 55°C and this was not changed until the end of experimental period. The energy provided to the electrical heater to achieve the desired flux is measured by a network analyzer device.

5.2. Heat Transfer Calculations

The heat gained from the hot air, heat consumed by the electrical heater, heat losses to the surroundings, mean velocity and temperature values calculated for each experiment. The equations and the method of calculations are described briefly in this section.

5.2.1. Calculation of Heat Transfer Rate and Heat Losses

The heat gained by the hot air is calculated for every experiment. It is expected that the heat consumed by the heater and the heat gained from the hot air will have almost similar values. The differences between these two values occur because of the heat losses from the sides of the system to the surroundings.

$$Q_{gained} = m * C_p * (T_{mean,outlet} - T_{mean,inlet}) \quad \text{(From the hot air)} \qquad (5.1)$$

To calculate the heat loss, the temperatures of each side of the collector are measured and heat loss for each side is calculated individually. The Qloss calculations were performed for the lateral sides, the top side and the underside separately.

- For the lateral side calculations, the Churchill and Chu correlations were used;

For laminar flow

$$\overline{Nu_L} = 0,68 + \frac{0,670 * Ra_L^{1/4}}{[1+(0,492/Pr)^{9/16}]^{4/9}} \qquad (5.2)$$

For turbulent flow

$$\overline{Nu_L} = \left\{0,825 + \frac{0,387 * Ra_L^{1/6}}{[1+(0,492/Pr)^{9/16}]^{8/27}}\right\}^2 \qquad (5.3)$$

- For the top and bottom side calculations;

[For top surface $\overline{Nu_L} = 0,54 * Ra_L^{1/4}$ (10^4<Ra$^{1/4}$<10^7) (5.4)

[For top surface $\overline{Nu_L} = 0,15 * Ra_L^{1/3}$ (10^7<Ra$^{1/4}$<10^{11}) (5.5)

[For bottom surface $\overline{Nu_L} = 0,27 * Ra_L^{1/4}$ (10^5<Ra$^{1/4}$<10^{10}) (5.6)

- For all of these calculations Rayleigh number is necessary;

$$Ra_L = Gr_L * Pr = \frac{g * \beta * (T_s - T_\infty) * L^3}{v * \alpha} \quad (5.7)$$

By using each Nusselt number, the heat transfer coefficient for each surface is calculated. The heat loss from each surface calculated using the equation.

$$Q = h * A * \Delta T \quad (5.8)$$

$$Q_{loss} = Q_{loss,top} + Q_{loss,bottom} + Q_{loss,lateral} \quad (5.9)$$

5.2.2. Calculation of Mean Velocity

During the experiments the velocity values are taken from the ten holes that were opened above the flow straightening duct. Five of the holes are opened at the inlet section while as the rest of are opened at the exit section of the system. An average velocity value is calculated for each experiment according to the formulas below:

$$V_{average} = \frac{\Delta A * (V_1 + V_2 + V_3 + \cdots + V_n)}{A_{total}} \quad (5.10)$$

where ΔA is the area that the velocity measurement was taken for each value.

The mass flow rate value for each experiment is calculated using the equation below;

$$\dot{m} = \rho * V_{average} * A_{cross\ sectional} \quad (5.11)$$

As a general look; at the beginning of this study, reference experiments were conducted with a clear channel. When the reference data were recorded and the necessary graphs were drawn, experiments with porous media were carried out. The porous material was located in the collector at different porosities. One porous material is at a thickness of 7 mm. So 7 layer of porous material fills the collector. Initially, 1 layer of porous material was located and tested in the collector. This was increased in stages, by one, up to 7 layers, all stages were tested. The results are shown and discussed in the results section.

5.2.3. Calculation of Mean Temperature

The inlet and exit temperature data are collected from the ten holes which the velocity data are also taken. A total number of 30 temperature values are collected from each five holes for inlet and exit temperatures. By using the equation given below an average temperature values is calculated for inlet and exit sides. The calculated average temperature values are used in other calculations.

$$T_{mean} = \frac{\int \rho * u * C_v * T * dA}{\dot{m} * C_v} \tag{5.12}$$

A example view of points that; which data is collected from where;

$u_{1,1}, T_{1,1}, A_{1,1}$	$u_{1,2}, T_{1,2}, A_{1,2}$	…	…	$u_{1,m}, T_{1,m}, A_{1,m}$
$u_{2,1}, T_{2,1}, A_{2,1}$	…	…	…	…
…	…	…	…	…
…	…	…	…	…
…	…	…	…	…
$u_{n,1}, T_{n,1}, A_{n,1}$	…	…	…	$u_{n,m}, T_{n,m}, A_{n,m}$

$$T_{mean} = \frac{(u_{1,1} * T_{1,1} * A_{1,1}) + (u_{1,2} * T_{1,2} * A_{1,2}) + \cdots .... + (u_{n,m} * T_{n,m} * A_{n,m})}{(u_{1,1} * A_{1,1}) + (u_{1,2} * A_{1,2}) + \cdots .... + (u_{n,m} * A_{n,m})} \tag{5.13}$$

CHAPTER 6

PROBLEMS OF EXPERIMENTAL SETUP

Many problems occurred during the experimental period. Most of them were solved by trying other methods. A brief explanation of each problem faced is given below.

First of all, the temperature profile was not uniform as expected and there were oscillations in the graphs that were drawn. To understand the reason for the oscillations the some methods were tried such as;

In the first trials the capacity of the heater was adjusted. Firstly, the capacity of the electrical heater was increased step by step to the 50 % range. While the fan was working at 20% capacity (the capacity button of the fan was at a position illustrated in Figure 6.1.c), the electrical heater worked to 1/8 of it capacity at first and this is increased in intervals of 1/8, as seen from Figure 71.

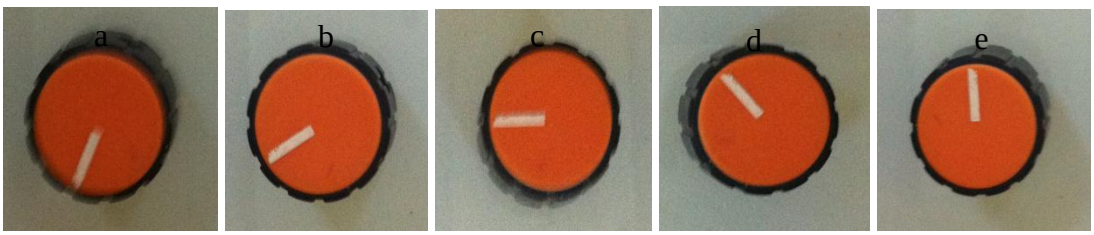

Figure 6.1. The capacity ratio values are; a.0%, b.12.5%, c.25%, d.37.5%, e.50%

The adjustment of the capacity button was not changed until the temperature values became steady in every thermocouple. The variation of the temperatures in each thermocouple is controlled by the software of the data logger which was installed on the computer. It was seen that this method has no significant effect on the temperature results.

- Secondly, the locations of thermocouples were changed to ensure that they have not broken down. The location of each thermocouple was changed and it was shown that none of them had broken down.
- Then, the air velocity was decreased because at high velocity values the flow could be turbulent and this affects the temperature results. Also a flow laminarizator

was added to the duct that was located just before the solar collector. These two approaches made the results much better.

- As a last revision, the software of the electrical heater that supplies heat to the solar collector was changed. The electrical heater consists of two resistances each 7, 5 kW with a total value of 15 kW. These two resistances work with P.I.D control *(proportional-integral-derivative-controller-a PID is a feedback controller which calculates an "error" value as the difference between a measured process variable and a desired set point. The controller attempts to minimize the error by adjusting the process control inputs.*) and generates a discontinuous voltage. The system was intermittent with a time interval of 120 seconds. After the modification this time interval was reduced to 1 second. This modification improved the results significantly and the data taken became more stable.

The second problem involved the collection of data relating to the electrical heaters energy consumption. 3 different data measurement devices were tried for this task. The brief explanation of each device is given below;

- A **multimeter** *(multimeter is a rectangular box shaped device that shows the voltage, ampere and the power of the electrical heater)* and a **powermeter** *(powermeter helps to measure the consumed power manually. The device has two probes and by connecting these probes to the cables that connects the electrical heater with the line that supports electricity to the system, the power could be seen on the screen)* were used for the same purpose. They both measure the power that the panel electrical heater consumes during the experiments. But because of the discontinuous working of the electrical heaters which was caused by the P.I.D control, these devices were unable to measure the heat value correctly.

As explained in Section 4.2.4 above, this problem was solved by using a network analyzer device to measure the data in kWh units.

a  b 

Figure 6.2. a. The multimeter, b.The powermeter

The system's last problem occurred while trying to measure the pressure drop due to various porosities. 4 Different devices were used to measure the pressure drop data but none of them worked

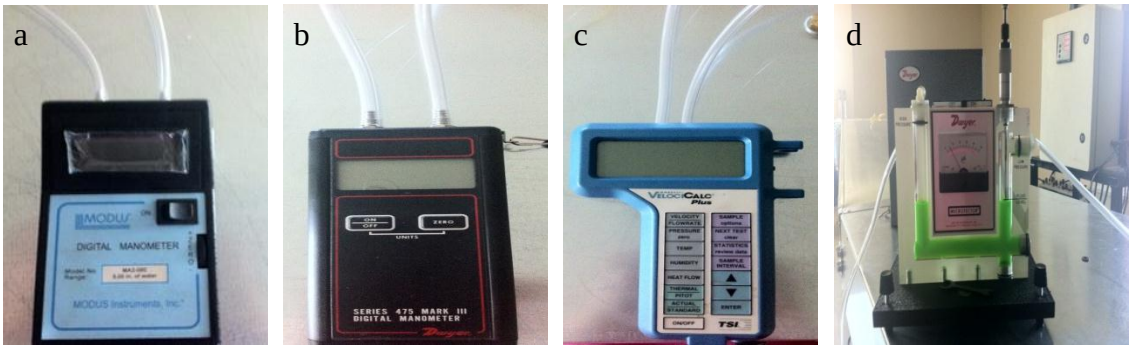

Digital Manometer:	*Digital Manometer:*	*Velocity Calculator:*	*Microtector:*
This is a sensitive digital manometer. But it failed to register any results. The min. value that this device can measure is 0, 25 Pa.	This shows the differential pressure between two points in inch W.C. and in Pa. The min. value that this device can measure is 0, 1 Pa.	This device also takes pressure data. Butit also failed to regşster results. The min. value that this device can measure is 0, 1 Pa.	This is the most sensitive device of the 4 but it also failed to register any results. The min. value that this device can measure is 0, 06 Pa.

Figure 6.3. a. Digital Manometer, b.Digital Manometer c.Velocity Calc. d. Microtector

None of these devices gave any value because the drop in pressure is very small and out of their measurement ranges. The clear channel pressure drop was calculated according to the friction losses. The result for the clear channel was 0,027 Pa (0, 00275 mmWC). Because of this, this thesis does not include the pressure drop value.

CHAPTER 7

RESULTS AND DISCUSSION

The heat transfer enhancement of a solar air heater using porous material was investigated in this study. The reference experiments were performed with the constructed experimental setup described in previous chapters. The temperature data along the length and width of the collector was plotted and is given below.

8 experimental results will be discussed in this section. The collector was tested while it was clear and assisted with 1,2,3,4,5,6,7 layers of porous material. The graphs for each experiment were drawn for each five thermocouples which were located on the same line. For clarity, each five thermocouples were named as shown in Figure 7.1 below:

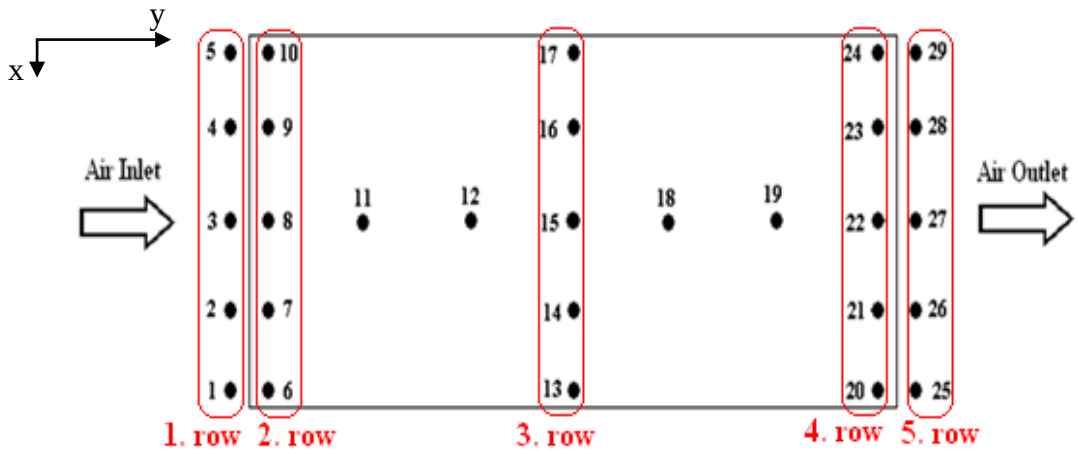

Figure 7.1. Location of Thermocouples along the collector

Depending on the data collected all necessary plots are drawn to compare the results accurately. All the collected data are given separately in the Appendices section of the thesis.

7.1. Heat Balance for Performed Experiments

The heat balances for each experiment performed with the equations that are given in Chapter 5. The heat gained by the heated air that flows inside the channel is

calculated. And then, the heat consumed to obtain this heated air is measured with the network analyzer device. There are significant heat losses to the surrounding from the top, bottom and lateral sides of the collector. These losses are calculated for each experiment too.

$$Qconsumed = Qgain + Qloss \tag{7.1}$$

Because, these calculations based on an experimental setup, an error value occurs for every experiment between 21-36%.

7.2. Change of Velocity Profile

The velocity data is collected for each 8 experiments (clear, 1 layer assisted, 2 layer assisted….7 layer assisted). The mean velocity and mass flow rate for each 8 experiment are 0.189 m/s and 0.0055 kg, respectively. Based on the collected data, each velocity profile is plotted. The effect of porous layer on the velocity distribution in the channel is observed and the plots for clear channel, 4 layer porous assisted (semi-filled) and 7 layers porous assisted (fulfilled) are given below.

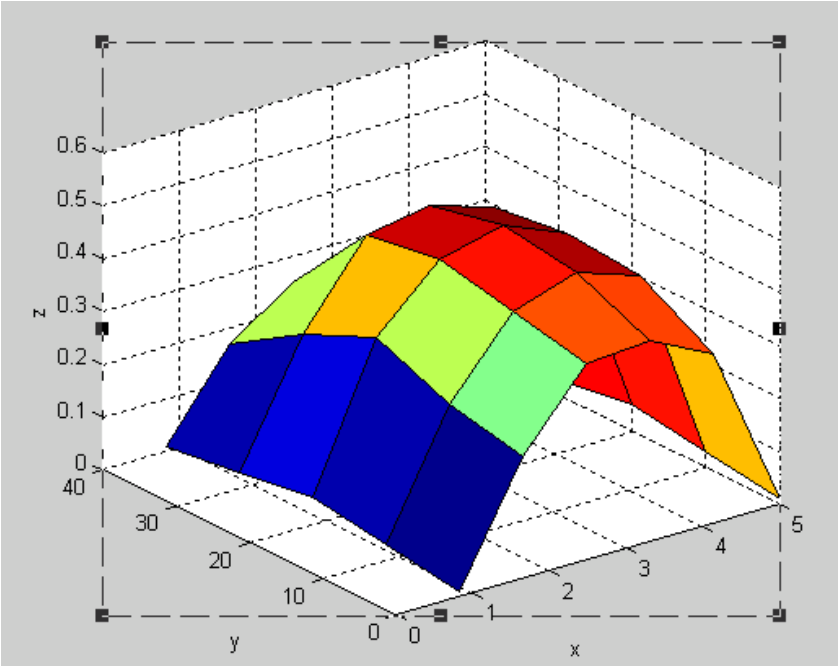

Figure 7.2. The velocity profile for clear channel

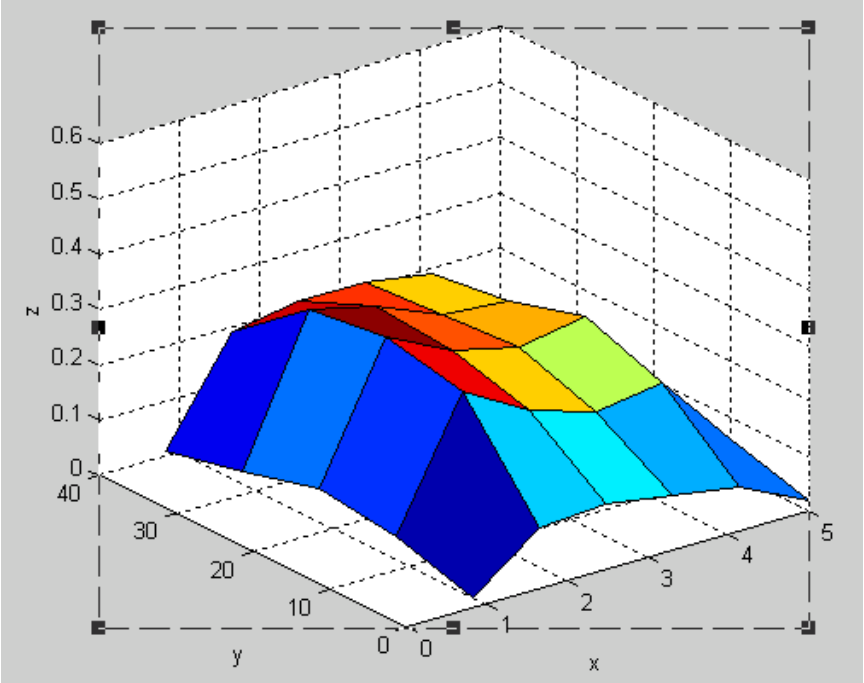

Figure 7.3. The velocity profile for 4 layers porous assisted (semi-filled) channel

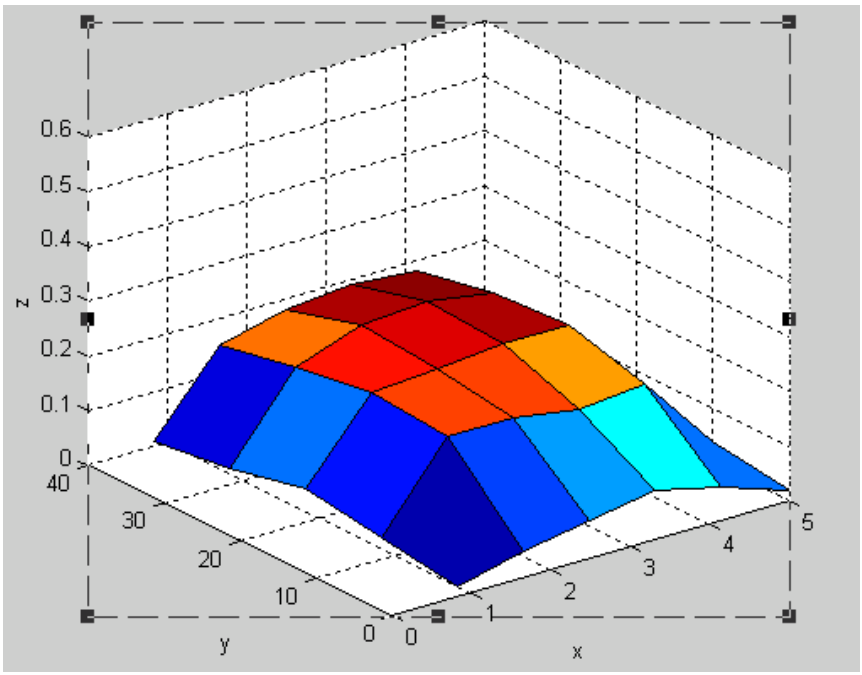

Figure 7.4. The velocity profile for 7 layers porous assisted (fulfilled) channel

As it can be seen from the plots clearly, the porous layers ruin the velocity distribution in the channel. In the first plot; air flows freely in the clear channel. It has the minimum velocity values at the top and at the bottom of the collector while as reaches its maximum velocity value at the centerline of the collector as expected. In the second plot, the channel is semi-filled with porous material. As a result of those porous

layers which fill the half of the channel, the flow is turbulent and its values are decreased. On the other hand, the second half of the channel which is not filled with porous layers has a similar velocity profile with the clear channel. And finally, in the third plot, the channel is fully filled with porous layers. These porous layers composed a resistance to the flow of air in the channel. So the velocity of air is decreased a lot totally.

7.3. Changes of Inlet and Outlet Temperatures

The temperature data is collected longitudinally and transversely for each 8 experiments (clear, 1 layer assisted, 2 layer assisted….7 layer assisted). The inlet and outlet temperature values are plotted and given for clear channel, 4 layers porous assisted (semi-filled) channel and 7 layers porous assisted (fulfilled) channel. In the graphs the inlet temperatures are represented with the blue dots while as the outlet temperatures are represented with the red dots. The average inlet temperatures for these 3 cases are 28, 5°, 28, 6° and 28, 5°C while as the average outlet temperatures are 55,34°, 56,5° and 56,67°C respectively. The outlet temperatures were increased for each case about 27-28°C. But adding porous layers in the flow channel of air have no significant effect on the outlet temperature of air.

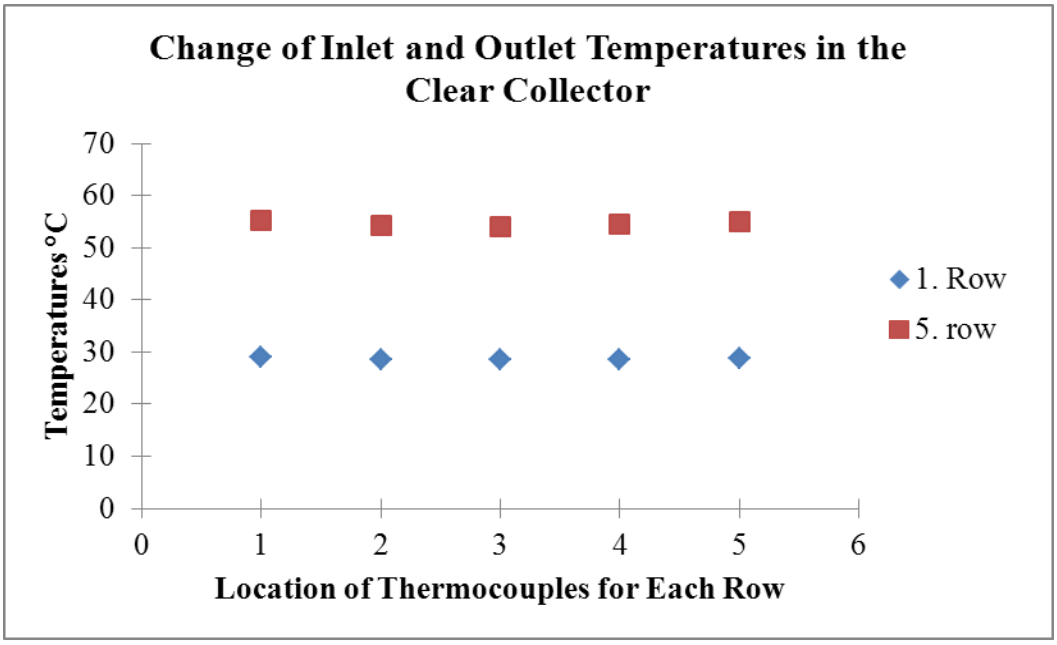

Figure 7.5. The change of Inlet and Outlet Temperatures of Air for Clear Channel

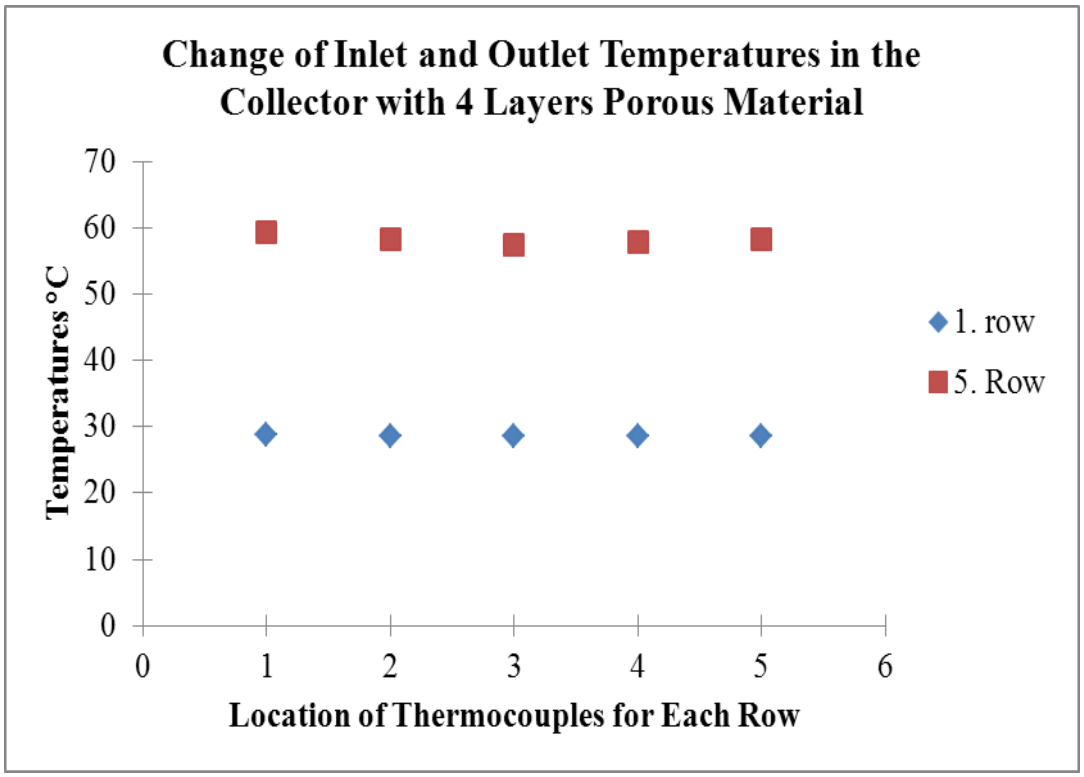

Figure 7.6. The change of Inlet and Outlet Temperatures of Air for 4 Layers Porous Assisted (semi-filled) Channel

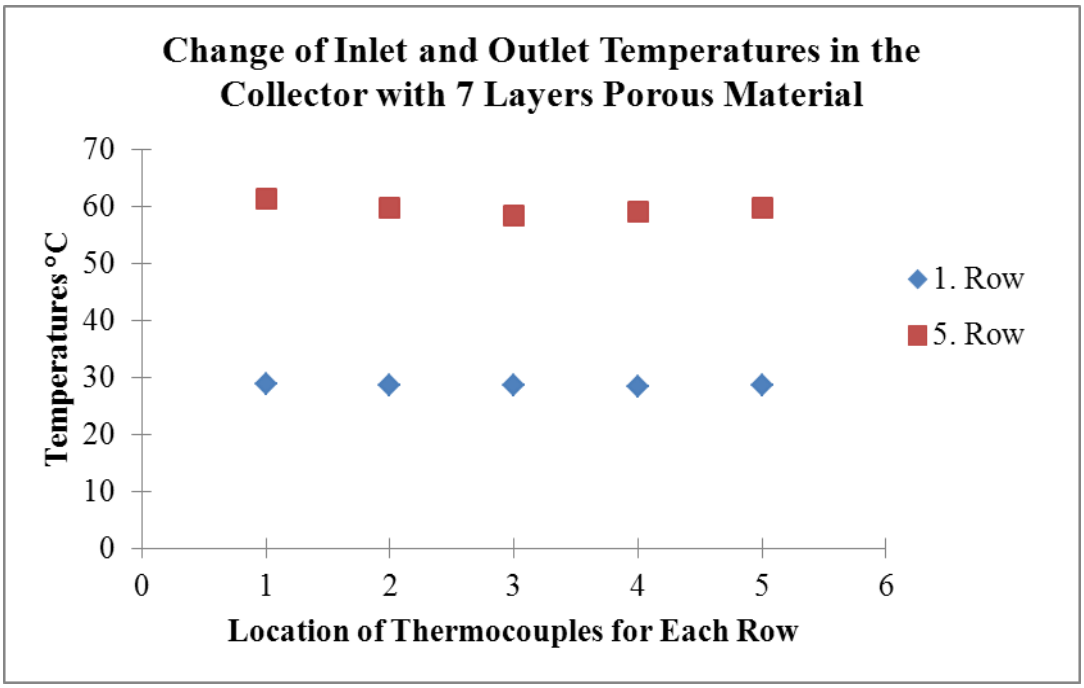

Figure 7.7. The change of Inlet and Outlet Temperatures of Air for 7 Layers Porous Assisted (fulfilled) Channel

7.4. Change of Temperature Profiles in the Collector

7.4.1. Transverse Temperature Profiles

Based on the collected data during all experiments, the temperature profiles of air along the collector are plotted. Air enters the collector and as it flows through the channel its temperature rises due to the constant heat flux from the bottom side. The plots for the clear channel, for 4 layers porous assisted (semi-filled) and for 7 layers porous assisted (full-filled) channels are given below. The values which are taken transversely from the collector are plotted verses to the location of thermocouples. In all these three cases the temperature values are increased as air flows through the exit of channel. As the porous layer number increase inside the collector, these layers create a resistance to air flow. Because of this resistance the velocity of air decreases. Due to the decreasing velocity the temperature values increases a little bit in high porous channels.

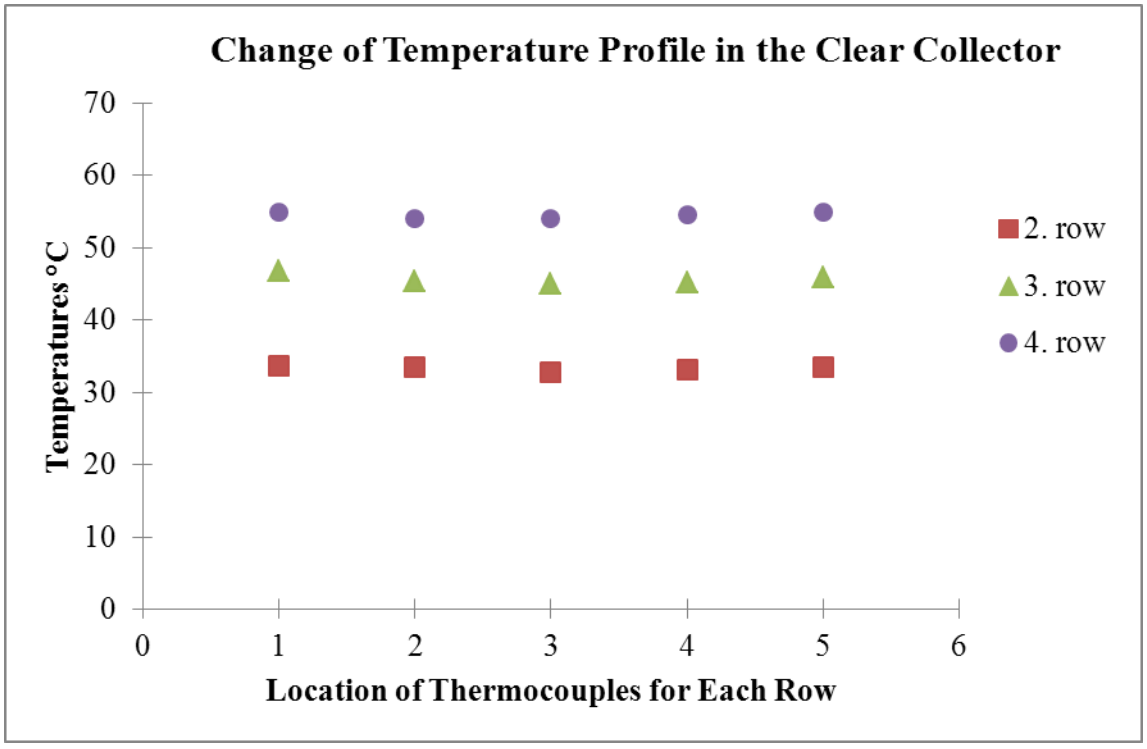

Figure 7.8. The change of Temperature Profile of Air for Clear Channel

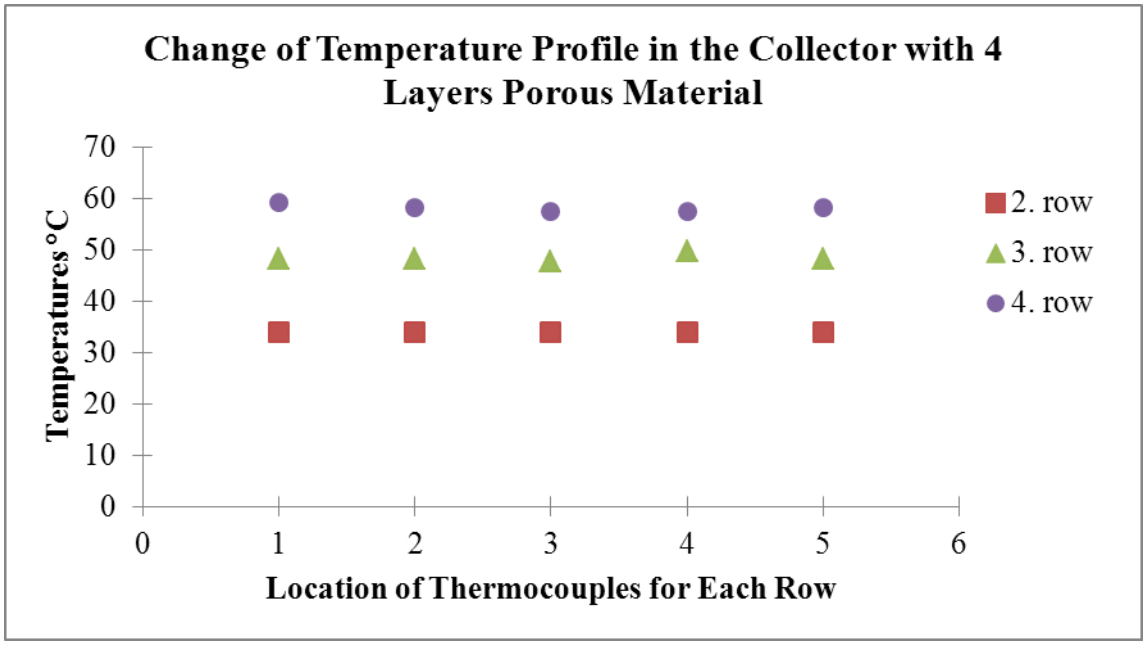

Figure 7.9. The change of Temperature Profile of Air for 4 Layers Porous Assisted (semi-filled) Channel

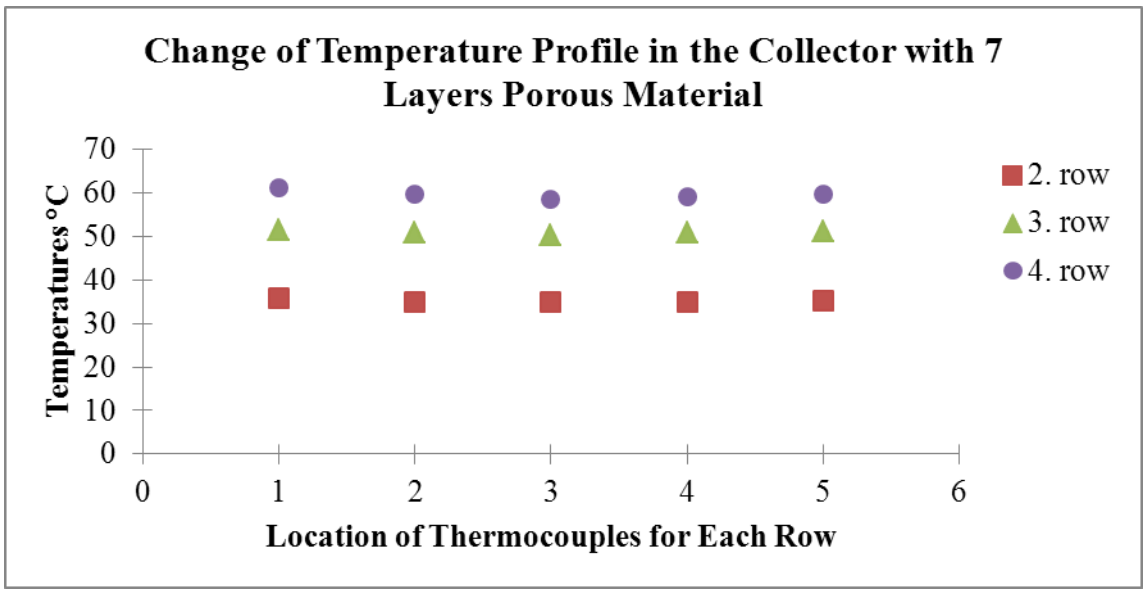

Figure 7.10. The change of Temperature Profile of Air for 7 Layers Porous Assisted (fulfilled) Channel

7.4.2. Longitudinal Temperature Profile

The longitudinal temperature profiles are plotted for these set of experiments, too. The temperature change of air between the inlet and the exit of the collector is observed with these plots. Air enters the collector at similar temperatures for each

experiment and its temperature rises as it get closer to the exit. But after the 4th layer of porous material, the temperature difference decreases for every thermocouple and the slope of the trend line decreases.

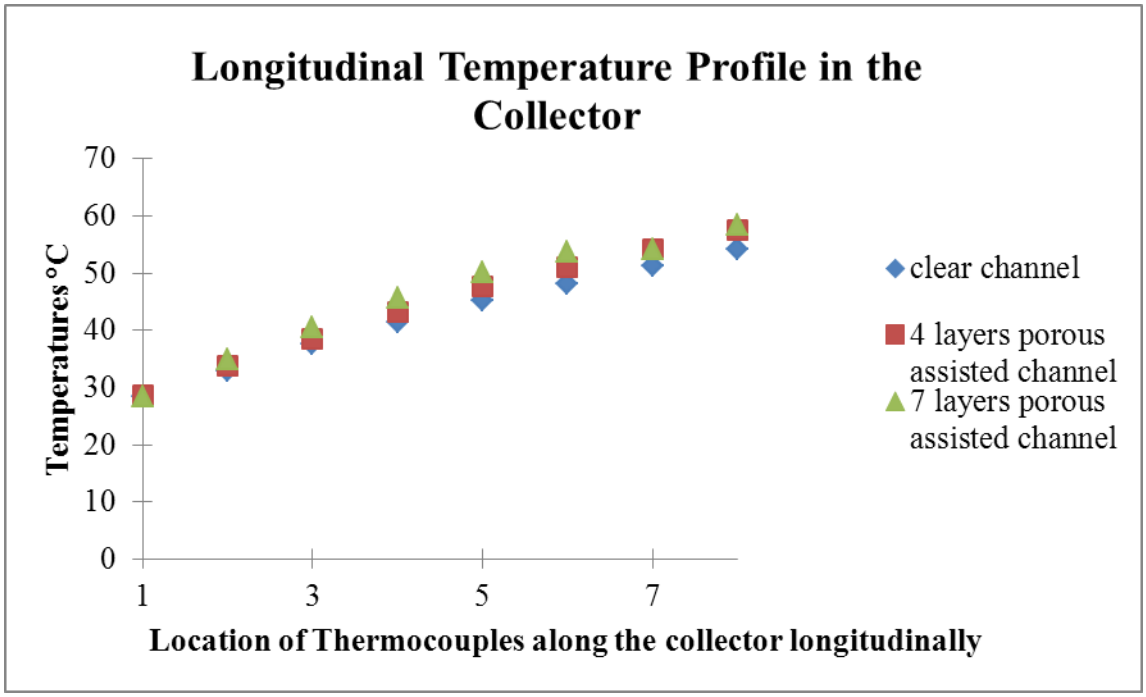

Figure 7.11. The Longitudinal Temperature Profile

7.5. Change of Absorber Surface Temperature

The absorber temperature data measured from five different points on plate. For each 8 experiments (clear and 1 to 7 porous layers assisted) the temperature values verses location of thermocouples graph is drawn over and over and given below. The blue dots at the upper side of the plot represents the clear channels' plate temperatures, while as the red triangle shaped dots at the bottom side of the graph represents the plate temperatures for the fulfilled channel. So it can be seen clearly from these dots that, the absorber plate temperature values decreases as the porous layer number increases. The maximum absorber plate temperature value for clear channel is 116, 8°C. This thermocouple value decreased to 82, 3°C by adding 7 layers of porous material inside the collector. All values for these five thermocouples are decreased from clear channel to full filled channel.

When the flow channel is clear, the absorber plate temperature is at very high values. While air flows inside the channel, its bottom side contacts with this high temperature absorber plate. But at the upper sides of the channel depth; the temperature values decreases suddenly. As a result of this non-uniform temperature distribution inside the channel, the temperature distribution of the air becomes non-uniform, too. The porous layers which are added to the flow channel prevent this non-uniform temperature distribution inside. The temperature of the absorber plate, transferred to the porous layers by conduction. So the temperature values decreases uniformly along the depth of the channel. Finally, the porous layers which are located on the way of air flow make the temperature distribution uniform.

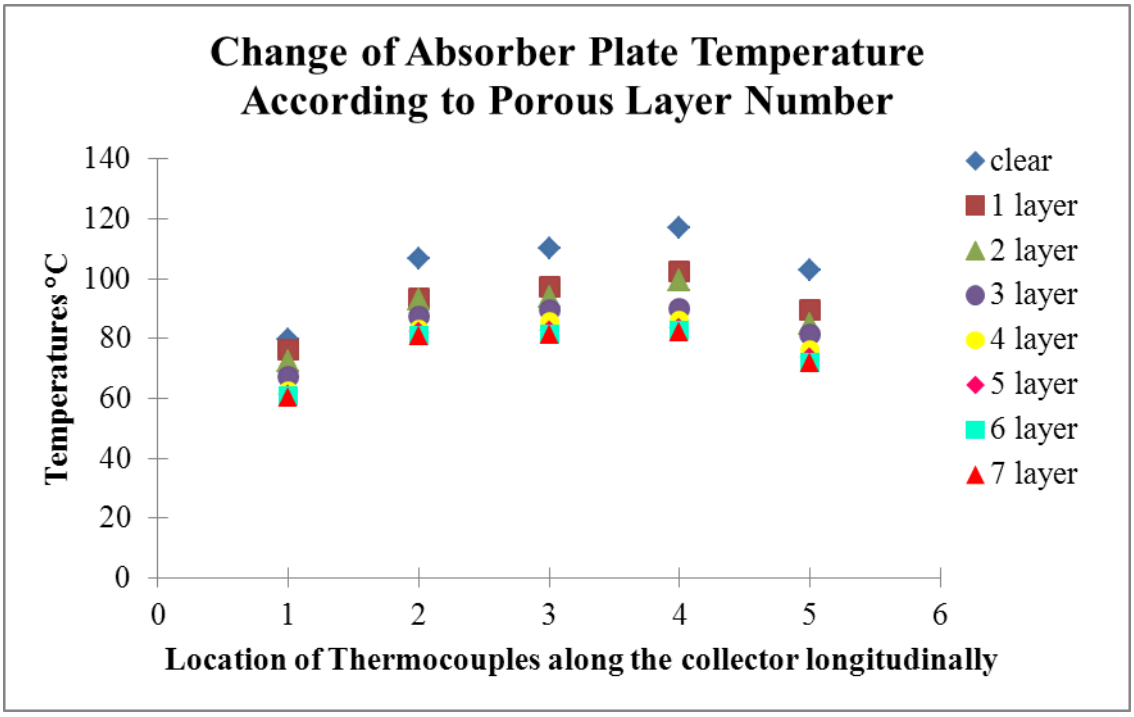

Figure 7.12. The Change of Absorber Plate Temperature According to Porous Layer Number

CHAPTER 8

CONCLUSIONS

The enhancement of heat transfer in a solar air heater collector by using porous medium is investigated in this thesis. A solar air heater is designed and constructed for this thesis. A set of experiments are conducted and the results are discussed in Chapter 7. At the end of this thesis, according to the results of 1 clear and 7 porous layer assisted channel (a total of 8 experiments) experiment; it was concluded that;

- The porous layers made no significant temperature enhancement on the exit temperature of air. Air enters the collector at similar temperatures for each 8 experiments and at the end of each experiment the exit temperatures are similar, too. The clear channel and fulfilled channel exit temperatures are 55, 34 °and 55, 67°C, respectively.
- The most important result is that the absorber surface temperature decreased as the porous layers added inside the flow channel. Firstly, the setup was experimented while it is clear. In this condition, the absorber temperature is at very high values and the temperature distributed non-uniformly along the depth of the channel. By adding porous layers the absorber temperature is decreased significantly. This makes the temperature distribution inside the channel more uniform.
- Another benefit of reduced surface temperature is it decreases the heat loss between the surface and surroundings. High absorber surface temperature losses much heat to the surroundings from the bottom of constructed setup. But when the temperature distributed uniformly inside the channel, the absorber temperature decreases therefore the heat loss decreases.
- The porous layers ruin the velocity profile inside the collector. The porous layers created a resistance to air flow. So, from the location of the first porous layer to the seventh layer inside the channel, the velocity decreases and its profile damaged as it strikes to the porous layers. As the velocity decreases due to the increasing porous layers, the temperature values should be increased in these conditions. But the temperature values that are used in the heat transfer

calculations are estimated with the mean temperature equations. So the exit temperatures did not increase according to the increasing porous layers.

- In spite of the insulation material that wrapped out the whole system, there are remarkable heat losses from the sides of the system to the surroundings. The heat transfer calculations are made for every 8 experiment. The heat gain and the heat consumed are expected to be same. But between these values there is a significant difference. This difference occurs because of the heat losses from the system to the surroundings. The system is insulated from all sides but the losses could not reduce to zero, though. But with the increasing porous layers, the losses decreased when compared to the losses with clear channel.

After all results examined, it is obvious that the use of porous material inside a solar air heater has a positive effect on the system.

REFERENCES

Aharwal, K.R., B.K. Gandhi and J.S. Saini (2008) "Experimental Investigation on Heat-Transfer Enhancement due to a Gap in an Inclined Continuous Rib Arrangement in a Rectangular Duct of a Solar Air Heater." *Renewable Energy* 33:585-596.

Aharwal, K.R., B.K. Gandhi and J.S. Saini (2009) "Heat Transfer and Friction Characteristics of Solar Air Heater Ducts Having Integral Inclıned Dıscrete Ribs on Absorber Plate." *International Journal of Heat and Mass Transfer* 52:5970-5977.

Akpınar, E.K. and F. Koçyigit (2010) "Energy and Exergy Analysis of a New Flat-Plate Solar Air Heater Having Different Obstacles on Absorber Plates" *Applied Energy.*

Aldabbagh, L.B.Y., F. Egelioglu and M Ilkan (2010) "Single and Double Pass Solar Air Heaters with Wire Mesh as Packing Bed" *Energy* 35:3783:3787.

AL-Kamil, M.T. and Al-Ghareeb A.A (1996) "Effect of Thermal Radiation Inside Solar Air Heaters" *Energy Conversation Management* 38(14):1451-1458.

Alta, D., E. Bilgili, C. Ertekin and O. Yaldız (2010) "Experimental Investigation of Three Different Solar Air Heaters: Energy and Exergy Analyses" *Applied Energy.*

Alvarez, G., J. Arce, L. Lira and M.R. Heras (2004) " Thermal Performance of an Air Solar Collector with an Absorber Plate Made of Recycable ALuminium Cans" *Solar Energy* 77:107-113.

Bhagoria, J.L., J.S. Saini and S.C. Solanki (2002) "Heat Transfer Coefficient and Fricition Factor Correlaltions for Rectangular Solar Air Heater Duct Having Transverse Wedge Shaped Rib Roughness on the Absorber Plate" *Renewable Energy* 25:341-369.

Bopche, S.B. and M.S. Tandale (2009) "Experimental Investigations on Heat Transfer and Frictional Characteristics of a Turbulator Roughened Solar Air Heater Duct" *International Journal of Heat and Mass Transfer* 52:2834-2848.

Enibe, S.O. (2002) "Performance of a Natural Circulation Solar Air Heating System with Phase Change Material Energy Storage" *Renewable Energy* 27: 69-86.

Esen, H. (2008) "Experimental Energy and Exergy Analysis of a Double-Flow Solar Air Heater Having Different Obstacles on Absorber Plates" *Building and Environment* 43: 1046-1054.

Forson, F.K., M.A.A. Nazha and H. Rajakaruna (2003) "Experimental and Simulation Studies on a Single Pass, Double Duct Solar Air Heater" *Energy Conservation and Management* 44:1209-1227.

Gao, W., W. Lin, T. Liu and C. Xia (2007) "Analytical and Experimental Studies on the Thermal Performance of Cross-Corrugated and Flat-Plate Solar Air Heaters" *Applied Energy* 84: 425-441.

Hachemi, A. (1999) "Comperative study on the Thermal Performances of Solar Air Heater Collectors with Selective and Nonselective Absorber-Plate" *Renewable Energy* 17: 103-112.

Hans. V.S., R.P. Saini and J.S. Saini (2010) "Heat Transfer and Friction Factor Correlations for a Solar Air Heater Duct Roughened Artificially with Multiple V-Ribs" *Solar Energy* 84:898-911.

Hermann, W. A. (2006). "Quantifying global energy resoruces" *Energy* 31(12) : 1685-1702

Ho, C.D., H.M. Yeh and R.C. Wang. (2005). "Heat-transfer Enhancement in Double-Pass Flat-Plate Solar Air Heaters with Recycle" *Energy* 30:2796-2817.

Ho, C.D., H.M. Yeh, T.W. Cheng, T.C. Chen and R.C. Wang (2009) "The Influences of Recycle on Performance of Baffled Double-Pass Flat-Plate Solar Air Heaters with Internal Fins Attached." *Applied Energy* 86:1470-1478.

Jaurker, A.R., J.S. Saini and B.K. Gandhi (2006) "Hat Transfer and Friction Characteristics of Rectangular Solar Air Heater Duct Using Rib-Grooved Artificial Roughness." *Solar Energy* 80:895-907.

Karim, M.A. and M.N.A. Hawlader (2004) "Development of Solar Air Collectors for Drying Applications" *Energy Conversation and Management* 45:329-344.

Karmare, S.V. and A.N. Tikekar (2009) "Experimental Investigation of Optimum Thermahydraulic Performance of Solar Air Heaters with Metal Rib Grits Roughness" *Solar Energy* 83: 6-13.

Karwa, R., S.C. Solanki and J.S. Saini (2001) "Thermo-Hydraulic Performance of Solar Air Heaters Having Integral Chamfered Rib Roughness on Absorber Plates" *Energy* 26:161-176.

Kiatsiriroat, T., W. Jiatrakul and A. Nuntaphan. (2007). " Experimental Study on Heat Transfer Enhancement in Solar Air Heater by Electric Field" *Heat Transfer Engineering* 28(1):38-41.

Koyuncu, T (2006) "Performance of Various Designs of Solar Air Heaters for Crop Drying Applications" *Renewable Energy* 31:1073:1088.

Kumar, A., J.L. Bhagoria and R.M. Sarviya (2009) "Heat Transfer and Friction Correlations for Artificially Roughened Solar Air Heater Duct with Discrete W-Shaped Ribs" *Energy Conservation and Managemen*t 50:2106-2117.

Kurtbaş, I. and A. Durmus (2004) "Efficiency and Exergy Analysis of a New Novel Solar Air Heater" *Renewable Energy* 29: 1489-1501.

Layek, A., J.S. Saini and S.C. Solanki (2009) "Effect of Chamfering on Heat Transfer and Friction Characteristics of Solar Air Heater Having Absorber Plate Roughened with Compound Turbulators" *Renewable Energy* 34:1292-1298.

Madhlopa, A., S.A. Jones and J.D. K. Saka (2002) "A Solar Air Heater with Composite-Absorber Systems for Food Dehydration" *Renewable Energy* 27: 27-37.

Mıdıllı, A., H. Olgun and T. Ayhan (1999) "Experimental Studies on Mushroom and Pollen Drying" *International Journal of Energy Research* 23:1143-1152.

Mohsen-Languri, E., H. Taherian, R. Masoodi and J.R. Reisel (2009) "An Energy and Exergy Study of a Solar Thermal Air Collector." *Thermal Science* 13(1): 205-216

Momin, A.M.E., J. S. Saini and S.C. Solanki (2002) "Heat Transfer and Friction in Solar Air Heater Duct With V-Shaped Rib Roughness on Absorber Plate." *International Journal of Heat and Mass Transfer* 45: 3383-3396.

Morton, O. (2006). "Solar Energy:A nee day Dawning." *Nature* 443 :19-22.

Moummi, N., S. Youcef-Ali, A. Moummi and J.Y. Desmons (2004) "Energy Analysis of Solar Air Collector with Rows of fins" *Renewable Energy* 29: 2053-2064.

Omojaro, A.P. and L.B.Y. Aldabbagh (2010) "Experimental Performance of Single and Double Pass Solar Air Heater with Fins and Steel Wire Mesh Absorber" *Applied Energy* 87:3759-3765.

Othman, M.Y., B. Yatim, K. Sopian and M.N. A. Bakar (2006) "Double Pass Photovoltaic-Thermal Solar Collector" *Journal of Energy Engineering* 132(3): 121-126.

Ozgen, F., M. Esen and H. Esen (2009) "Experimental Investigation of Thermal Performance of a Double-Flow Solar Air Heater Having Aluminium Cans" *Renewable Energy* 34:2391-2398.

Ozturk, H.H. and Y. Demirel (2004). " Exergy-Based Performance Analysis of Packed-Bed Solar Air Heaters" *Internatioanl Journal of Energy Research* 28:423-432.

Pakdaman, M. F., A. Lashkari, H. B. Tabrizi and R. Hosseini (2011) "Performance Eevaluation of a Natural-Convection Solar Air-Heater with a Rectangular-Finned Absorber Plate" *Energy Conservation and Management* 52: 1215-1225.

Peng, D., X. Zhang, H. Dong and K. Lv (2010). "Performance Study of a Novel Solar Collector" *Applied Thermal Engineering* 30:2594-2601.

Potdukhe, P.A. and S.B. Thombre (2008) "Development of a New Type of Solar Dryer:Its Mathematical Modelling and Experimental Evaluaition" *International Journal of Energy Research* 32:765-782.

Prasad, S.B., J.S. Saini and K.M. Singh (2009) "Investigation of Heat Transfer and Friction Characteristics of Packed Bed Solar Air Heater Using Wire Mesh as Packing Material" *Solar Energy* 83:773-783.

Ramani, B.M., A. Gupta and R. Kumar (2010). " Performance of a Double Pass Solar Air Collector" *Solar Energy* 84:1929-1937.

Sahu, M.M. and J.L. Bhagoria (2005) "Augmentation of Heat Transfer Coefficient by Using 90° Broken Transverse Ribs on Absorber Plate Of Solar Air Heater" *Renewable Energy* 30: 2057-2073.

Smil, V. (2006). "Organisation for Economic Co-operation and Development." *Energy of the Crossroads:* 12

Sopian, K., M.A. Alghoul, E. M. Alfegi, M.Y. Sulaiman and E.A. Musa (2009). "Evaluation of thermal efficiency of double pass-solar collector with porous-nonporous media." *Renewable Energy* 34:640-645.

Togrul, I.T., D.Pehlivan and C. Akosman (2004) "Development and Testing of a Solar Air-Heater with Conical Concentrator." *Renewable Energy* 29:263-275.

Varshney, I. and J.S. Saini (1998). " Heat Transfer and Friction Factor Correlations for Rectangular Solar Air Heater Duct Packed with Wire Mesh Screen Matrices" *Solar Eneregy* 62(4):255-262.

Yeh, H.M., C.D.Ho and J.Z. Hou (2002) "Collector Efficiency of Double-Flow Solar Air Heater with Fins Attached" *Energy* 27: 715-727.

APPENDIX A

TEMPERATURE DATA OF ALL EXPERIMENTS

- The velocity and temperature distributions inside the channel are collected from five holes which are opened on the top side of the system. For clarity, a schematic view of the data measurement holes is given first.

First hole	Second hole	Third hole	Fourth hole	Five hole
1. Data	1. data	…	…	…
1. Data	2. data	…	…	…
3. Data	…	…	…	…
4. Data	…	…	…	…
5. data	…	…	…	…
6. data	…	…	…	…

- The absorber plate temperatures are measured with the five thermocouples which are located on the absorber plate.

- The measured temperature (°C) data for each clear channel;

56,2	55,9	55,1	55,6	56,1
55,8	55,3	54,6	55,4	55,8
55,5	54,7	54,2	54,8	55,3
54,2	53,3	53,1	54	53,1
55,6	54,6	54,5	55,3	55,7
56	56	55,2	55,6	56,4

- The measured temperatuee (°C) data for each 1 layer porous assisted channel;

57	56,3	56,1	56,3	56
56,9	56,2	55,9	56,1	54,7
56,2	55	54,6	55,6	55,2
56,1	54,9	54,1	55,3	55
56,7	55,6	54,7	55,9	54,7

57,1	56,2	56,2	56,2	55,4

- The measured temperature (°C) data for each 2 layer porous assisted channel;

58,6	56,5	56,1	56,8	56,4
57,7	56,1	55,9	56,2	56,2
57,2	55,5	55,2	56	56,1
57,3	55	54,8	55,1	56
57,4	55,8	55,4	55,9	56,4
58,2	56,3	56	56,8	57,1

- The measured temperature (°C) data for each 3 layer porous assisted channel;

61,1	56,2	56,2	56,9	56,6
60,5	55,9	55,8	55,9	56,3
58,9	56,9	56,5	56,6	56
58,5	54,9	55,2	55,7	56,2
59,7	55,9	55,8	55,2	56
61,7	57,4	56,2	57,7	60,3

- The measured temperature (°C) data for each 4 layer porous assisted channel;

63,2	56,6	56,2	57,2	58,2
61,3	55,6	55,8	55,9	57,3
61	56,9	56,6	56,5	57,1
61,8	57,1	56,4	56,8	57
62,4	56,8	56,2	56,4	57,6
63,1	57,4	57,1	57,5	58,1

- The measured temperature (°C) data for each 5 layer porous assisted channel;

64,1	57,3	56,3	61,3	61,7
62,6	56,6	55,3	55	58,4
61,2	57,3	55,8	54,8	57,5
59,7	57,5	56,2	55,9	57,1
61,1	57,8	56	56,4	56,9
63,9	59,1	56,3	61,8	62,1

- The measured temperature (°C) data for each 6 layer porous assisted channel;

64,6	57,6	56,85	60	62,2
63,8	56,5	56,5	58,3	60,9
62,1	57,3	56,7	56,5	58,6
59,1	57,6	55,8	57,3	57,9
61,8	57	56,2	57,5	57,8
64,4	57,6	57,4	61,1	62,6

- The temperature (°C) .data for each 7 layer porous assisted channel;

64,2	58,5	59,4	60,3	63,9
63,9	56,9	56,8	57,4	61,5
63,1	56,6	56,2	56,3	58,9
59,4	56,7	56,1	56	58,3
63,8	56,6	55,9	55,8	58,2
64,7	58,2	59,6	60,8	62,4

APPENDIX B

VELOCITY DATA OF ALL EXPERIMENTS

- The measured velocity (m/s) data for each clear channel;

0.01	0,03	0,05	0,03	0,01
0,12	0,23	0,27	0,24	0,18
0,15	0,33	0,36	0,31	0,24
0,16	0,38	0,42	0,37	0,25
0,14	0,33	0,40	0,32	0,21
0,01	0,03	0,05	0,03	0,01

- The measured velocity (m/s) data for each 1 layer porous assisted channel;

0,01	0,03	0,05	0,03	0,01
0,12	0,24	0,26	0,25	0,19
0,15	0,32	0,40	0,35	0,26
0,16	0,36	0,43	0,39	0,24
0,12	0,31	0,40	0,31	0,19
0,01	0,03	0,05	0,03	0,01

- The measured velocity (m/s) data for each 2 layer porous assisted channel;

0,01	0,03	0,05	0,03	0,01
0,13	0,20	0,24	0,20	0,19
0,17	0,32	0,35	0,21	0,23
0,15	0,35	0,42	0,36	0,24
0,11	0,30	0,36	0,29	0,18
0,01	0,03	0,05	0,03	0,01

- The measured velocity (m/s) data for each 3 layer porous assisted channel;

0,01	0,04	0,07	0,03	0,01
0,12	0,17	0,25	0,26	0,23
0,16	0,25	0,40	0,39	0,30
0,13	0,28	0,37	0,35	0,25
0,09	0,27	0,28	0,33	0,21
0,01	0,04	0,07	0,03	0,01

- The measured velocity (m/s) data for each 4 layer porous assisted channel;

0,02	0,06	0,08	0,04	0,01
0,11	0,29	0,32	0,30	0,19
0,12	0,22	0,26	0,27	0,21
0,10	0,18	0,23	0,22	0,21
0,08	0,20	0,25	0,21	0,19
0,02	0,06	0,08	0,04	0,01

- The measured velocity (m/s) data for each 5 layer porous assisted channel;

0,05	0,13	0,16	0,12	0,04
0,08	0,24	0,26	0,23	0,19
0,09	0,20	0,24	0,25	0,20
0,10	0,19	0,22	0,22	0,18
0,08	0,18	0,23	0,21	0,18
0,05	0,03	0,16	0,22	0,04

- The measured velocity (m/s) data for each 6 layer porous assisted channel;

0,04	0,10	0,15	0,13	0,03
0,06	0,21	0,22	0,20	0,16
0,08	0,18	0,21	0,23	0,19
0,10	0,17	0,23	0,22	0,18
0,09	0,18	0,23	0,21	0,18
0,04	0,10	0,15	0,13	0,03

- The measured velocity (m/s) data for each 7 layer porous assisted channel;

0,02	0,04	0,06	0,03	0,01
0,05	0,19	0,20	0,18	0,15
0,07	0,19	0,21	0,22	0,18
0,09	0,17	0,22	0,23	0,19
0,06	0,18	0,22	0,21	0,18
0,02	0,04	0,06	0,03	0,01

APPENDIX C

ABSORBER PLATE TEMPERATURE DATA OF ALL EXPERIMENTS

- The absorber plate temperatures (°C) for each eight experiments.

	1.point	2. point	3. point	4. point	5. point
clear	79,8	106,8	110,2	116,8	102,9
1 layer	76,3	93,5	97,4	102,5	89,5
2 layer	72,5	92,9	93,8	99,3	84,9
3 layer	67,1	87,5	89,5	90,1	81,3
4 layer	62,4	83,3	85,8	86,3	76,3
5 layer	61,3	82,3	82,8	83,6	73,8
6 layer	60,7	81	81,3	82,8	72,1
7 layer	60,5	81,1	81,2	82,3	71,8